Mixtures of ultracold Bose gases in one dimension

A Quantum Monte-Carlo study

Luca Parisi

Department of Physics, University of Trento
Supervisor: S. Giorgini
May 3, 2019

Contents

Introduction

The quantum many problem is a very challenging problem which arise in many different sub-fields in physics. For instance understanding the properties of nuclei , predicting the phase diagram of strongly correlated solids and understanding the structure of neutrons stars are all problems which require a solution of a quantum many body problem.
The many problem is particularly challenging when correlations play a key role and mean field theories cannot be applied. Testing many-body theories against experiments is however difficult as most of these systems are either dirty or cannot easily be controlled in the laboratory. Recently , the realization of ultra-cold quantum gases of both bosons and fermions has made possible the implementation of non trivial quantum many-body hamiltonians in the laboratory, allowing for the investigation of fundamental quantum many-body physics, such as superfluidity, Anderson localization, superfluid to Mott transition in optical lattices and much more. Unfortunately in three dimensions reaching regimes where correlations become important is hindered by instabilities towards collapse of the gas. However, these instabilities are not present in one dimensional systems, even for very strong interactions. While any real experiment is done in three dimensions, it is possible to confine the gas in very narrow quasi-one dimensional tubes , even in the strongly correlated regime[1], which are very well described by one-dimensional models. Recently it has also become possible to realize ultra-cold quantum gases of different species [2], either by using two different atoms or two different energy levels of the same atom, with different scattering properties. In these thesis we consider a mixture of Bose gases with contact interactions in one dimension. For the sake of simplicity we will study systems with equal masses and equal intra-species coupling and we investigate the properties of the mixture by varying intensity of both intra-species and inter-species coupling strength g and $\tilde{g}$, focusing on how correlations change the properties of the system. In this work we will only consider repulsive intra-species interactions ($g > 0$). Both attractive and repulsive inter-species interactions will be considered, corresponding respectively to positive and negative values of $\tilde{g}$.

In one dimension the system is entirely determined by only two parameters $\gamma = \frac{mg}{\hbar^2 n}$ and $\eta = \frac{m\tilde{g}}{\hbar^2 n}$ characterizing respectively the strength of intra-species and inter-species interactions. Mean-field theories are valid for small values of γ and η, which can be obtained either at weak couplings or high densities, while at large values of the coupling strength g tunneling between particles is suppressed and in the limit of infinite repulsion the atoms become impenetrable. While no exact analytical solutions are known in higher dimensions, exact solutions can be found in one-dimensional systems in some limiting regimes. In the case of a single component the model is known as the Lieb-Liniger model[5] which can be solved exactly using Bethe Ansatz techniques (BA)[6]. In the limit of infinite repulsion one realizes the Tonks- Girardeau gas (TG)[7] where one can prove that all static properties are equal to those of a free spinless Fermi gas, as the particle impenetrability plays the role of an effective Pauli principle. An analytical solution is also available in mixtures in the limit of very strong intra-species repulsion and arbitrary inter-species interaction , as the system can be mapped to the Yang-Gaudin model[6, 8, 9] , describing a gas of spin 1/2 fermions with contact interactions. For finite repulsion strength, however, no analytical solutions are known and one must resort to numerical techniques. In particular we use essentially exact zero-temperature Quantum Monte-Carlo techniques, which are able to tackle the strong correlations present in these systems.

We first investigate the problem of a very imbalanced mixture, composed of just one particle of one component interacting with a large number of particles of the second component. This impurity problem has attracted quite some interest in recent years because it represents a model of a particle interacting with a bath which contains many degrees of freedom, the so called "polaron" problem [10], a popular model in condensed matter physics. For instance an electron interacting with the phonons of a ionic cristial can be seen as a Bose polaron problem. While the problem of an impurity in a fermionic bath has attracted much attention both theoretically and experimentally , the problem of a bosonic impurity has not been addressed as thoroughly.

In three dimensions the impurity problem has been investigated theoretically using Quantum Monte Carlo methods [11], perturbation theory[12] , the T-matrix approximation [13], mean field methods[14] and variational methods [15]. The Bose polaron problem has also been investigated experimentally[16, 17], obtaining good agreements with Quantum Monte Carlo simulations [18]. The problem of an impurity in a optical lattice has also been investigated theoretically and experimentally[19].

In one dimension , the properties of the polaron are enriched by the fermionization of the bosonic degrees of freedom and can be solved exactly in the

limit of a Tonks-Girardeau gas [20, 21]. The problem of a bosonic impurity in a one dimensional has also been investigated experimentally, using a mixture of K impurities in a gas of Rb atoms[65]. The properties of an impurity immersed in a Luttinger liquid have also been investigated[23, 24]. Beyond mean field studies of the impurity problem have also been realized in lattice models using the Density Matrix Renormalization group [25], but were never investigated in the continuum. We perform a systematic numerical study of the main static and dynamic properties of the Bose polaron such as the binding energy, the effective mass and the contact parameter and compare with mean-field results and perturbation theory, in the limit of weak interactions, and with BA results in the limit of infinite intra-species repulsion. We find that the binding energy, defined as the difference of the energy of the gas plus one impurity minus the energy of the gas without the impurity is found to increases monotonically for increasing impurity-bath interaction and saturates in the limit of $\eta \to \infty$ at a value that depends on the intra-species repulsion γ. The dressing of the impurity with the fluctuations of the bath alters the effective mass of the polaron. With increasing interactions we observe an increase in the effective mass of the polaron which becomes very large when the impurity becomes impenetrable, as a moving impurity needs to push all of the atoms of the bath. While for a strongly interacting bath a large effective mass can only be reached for large values of the coupling η , large effective masses can be reached quite sooner in a weakly interacting gas, signaling polaron localization already at moderate impurity-bath interactions. This picture is further confirmed by the contact parameter, the density of the gas at the impurity position, which shows a strong depletion for strongly interacting impurities. For attractive impurity-bath interactions the binding energy is negative. For strong intra-species repulsion, where the gas behaves as a free Fermi gas, and for $\eta \to -\infty$ the impurity becomes strongly bound with just one atom of the bath,as it cannot bind more particles because of the effective Pauli principle. The binding energy approaches the binding energy of the dimer in vacuum and the effective mass becomes twice the mass of the atom. This condition no longer holds for weaker inter-species interaction, and the polaron becomes more deeply bound as one reduces γ , resulting in an increased binding energy and effective mass. Our results where published in Physical Review A [26]. We then turn to the study of balanced mixtures. Mean-field theories predict that two species are miscible only when $\eta < \gamma$: in this regime configurations with neighboring particles of the other component are more energetically favorable. As this picture may be modified by correlations, we perform quantum Monte-Carlo simulations to investigate the miscibility phase diagram up to the strong coupling regime and we find no deviations from the predicted mean field phase diagram. We then investigate

the miscible phase and in particular the so called Andreev-Bashkin effect[27] where quantum fluctuations can create a dissipation-less drag between two interacting superfluids, which has never been observed experimentally . We numerically compute this spin drag and find it to become very large at strong interactions. The knowledge of the magnetic susceptibility and of the spin drag allows us to calculate the speed of spin waves, low-energy modes excited by long wavelength perturbations of the magnetization which are the lowest energy excitations of the system. The results of this study were published in Physical Review Letters [28].
We also investigate the collective excitations of inhomogeneous mixtures trapped by a harmonic confining potential and in particular we extract the breathing and spin-dipole mode frequency , which can be easily measured in experiments.
A gas is a system which energetically prefers to minimize its density, in contrast to a liquid which displays an energy minimum at a nonzero density. Mean-field theory predicts a mixture with attractive inter-species interaction for $|\eta| < \gamma$ and an instability of the gas phase when $|\eta| = \gamma$, where repulsive and attractive interactions cancel each other. Close to this regime the role of quantum fluctuations cannot be neglected , and it has been shown that by adding quantum fluctuations at the lowest perturbative order ,also known as Lee-Huang-Yang corrections (LHY) ,the energy acquires a minimum at a nonzero density, a signature of a liquid phase[29]. This liquid state is peculiar because it can occur at very low densities compared to other known superfluid liquids such as ^{4}He. This description is however valid only for weak interactions and it is unknown if the phase survives at stronger couplings. We perform quantum Monte-Carlo simulations of the system with periodic boundary conditions and find evidence of a phase transition from a liquid to a gas phase at a critical ratio $\frac{\eta}{\gamma} = 0.47(3)$. We also investigate the properties of the liquid up to the critical interaction strength, such as the equilibrium density, the chemical potential,the compressibility as well as correlations and structural properties. We find that while mean field calculations with LHY corrections are able to reproduce the compressibility quite well , they fail to reproduce the chemical potential that differs from QMC predictions already at moderate couplings. In fact perturbative methods cannot describe the formation of dimers at low densities. We find that the one body density matrix decays at large distances as a power law at a rate that becomes large close to the phase transition, which suggests that strong particle correlations are present in this regime. We also observe a linear dependence of the structure factor , both in the density and magnetization channel, which is compatible with the absence of an energy gap. This study was published in Physical Review Letters[30].

This thesis is organized as follows

- Chapter 1: We introduce the theoretical background and tools used in the remainder of the thesis.
- Chapter 2: We introduce the quantum Monte-Carlo method which was used extensively to obtain the results discussed in the later chapters
- Chapter 3: We discuss our results on the study of an impurity immersed in a Bose gas with contact interactions
- Chapter 4: We discuss uniform mixtures with repulsive interactions. In particular we discuss the Andreev-Bashkin effect.
- Chapter 5: We discuss inhomogeneous mixtures trapped by a harmonic potential. In particular we investigate the spin-dipole mode.
- Chapter 6: We discuss mixtures with attractive inter-species interactions. In particular, we describe and characterize the liquid homogeneous phase.

Chapter 1

Many-body physics in one dimension

The many-body problem has always been a difficult problem to tackle and poses a serious challenge for both numerical and analytical approaches, due to the huge dimensionality of the Hilbert space. In one dimension, the problem is usally easier to solve. In fact the Bethe ansatz (BA) technique allows one to solve analytically many non trivial interacting models. Where the BA fails efficient numerical methods exist (such as the Density Matrix Renormalization Group) that give access to both static and dynamical properties. For this reason the 1D problem has been and still is often considered as a mere toy model. However the physics of low-dimensional dystems is strikingly different from three dimensional physics and is interesting in its own right.

The peculiar properties of one-dimensional systems are mainly due to the particular topology: all particles are aligned in a row and cannot avoid each other. The main consequence is that correlations between particles are enhanced and quasi-particle excitations quickly decay in collective excitations. This leads to the failure of many models that are successful in higher dimensions such as the Landau liquid theory for fermions. These models need to be interchanged with different models especially tailored for one spatial dimension, such as the Luttinger liquid model. We of course live in a 3D world but nowadays it is possible to realize experiments in very confined geometries, that can be very well approximated by one dimensional models. In particular it is possible to realize clean and tunable ultracold quantum gases in arbitrary geometries, offering an ideal test bed for quantum many body problems.

In these chapter we introduce the theoretical concepts that we will be using in the remainder of the thesis. First we will describe the two body problem.

Then we will build on our knowledge of two body interactions to describe several many body theories. First we will describe the mean field and hydrodynamic approach which allow to describe the macroscopic properties of the systems. Then we describe some exactly solvable models, both for bosons and fermions. We will also discuss the Luttinger liquid theory, which takes the place of the Landau Fermi liquid model in one dimension.
Finally we give a brief introduction to ultracold quantum gases and a brief overview of how quasi-1D ultracold quantum gases can be experimentally realized.

1.1 The two body problem

Before describing the rich physics of many-body sistems we focus on the two-body problem[31][32]. The discussion in this section is based on In the center of mass the hamiltonian takes the form

$$H = -\frac{\hbar^2}{2m*}\frac{\partial^2}{\partial_x^2} + V(x) \tag{1.1}$$

where $\frac{1}{m*} = \frac{1}{m1} + \frac{1}{m2}$ is the reduced mass of the two particles with mass m_1 and m_2 ,x is the distance between the two particles and V is the two body interaction potential, which we assume to be real and local.

Scattering in the continuum

Let us look for solutions in the scattering continuum. The solution, at distances larger than the range of the potential takes the form

$$f(x) = \sin(kx + \delta(k)) \tag{1.2}$$

where $\hbar k = \sqrt{(2m^*E)}$ and E is the energy. The effect of the potential is to add a momentum-dependent phase shift. In the limit of very low scattering energy $k \to 0$, the scattering no longer depends on the details of the potential. The phase shift becomes universal. It depends on one parameter only, called the scattering length defined as

$$a = -\lim_{k\to 0}\frac{\delta(k)}{k} \tag{1.3}$$

In this universal regime, where we neglect high-momentum collisions, we are free to substitue the interaction potential with any other potential as long as

it reproduces the same scattering length. This alternative effective potential is called a pseudo-potential. For instance we can choose to use a zero-range contact pseudo-potential , obtaining the hamiltonian

$$H = -\frac{\hbar^2}{2m^*}\frac{\partial^2}{\partial_x^2} + g\delta(x) \tag{1.4}$$

By simple substitution of the general wavefunction 1.2 into the hamiltonian we find an expression for the phase shift

$$\tan\delta(k) = \frac{\hbar^2 k}{m^* g} \tag{1.5}$$

from which we can extract the relation between the scattering length and the coupling g

$$a = -\frac{\hbar^2}{m^* g} \tag{1.6}$$

We point out that the scattering length is of the opposite sign with respect to the coupling constant . Repulsive interactions lead to a negative scattering length, while attractive interactions correspond to a positive scattering length. Moreover the absolute value of the scattering length decreases with increasing strength of the coupling. Weakly interacting particles have a large absolute scattering length, while strongly interacting particles have a very small scattering length.

Bound states

Potentials with an attractive part may support bound states. There is a relation between the phase shifts in the continuum and bound states. For positive scattering length one can find a bound state with energy

$$\epsilon = -\frac{\hbar^2}{2m^* a^2} \tag{1.7}$$

In the case of a contact interaction, if the coupling g is positive the scattering length is negative and no bound states exist. For negative coupling, the scattering length is positive and the hamiltonian supports one bound state. We can look for a solution of the form

$$f(x) = e^{-kx} \tag{1.8}$$

One can readily check that the function $f(x)$ describes an eigenstate of the hamiltonian with energy

$$\epsilon = -\frac{\hbar^2 k^2}{2m^*} \tag{1.9}$$

By comparing with equation 1.7 we get

$$k = \frac{1}{a} \tag{1.10}$$

1.2 Correlation functions

Let us pass from the simple two body problem to the problem of many interacting particles. Because of interactions , different particles will not be independent and become correlated. Correlation functions play an important role in many-body physics. Here we define several correlation functions which will play a key role in later sections.

One Body Density Matrix

The one body density matrix (OBDM) is defined as

$$\rho(x, x') = \left\langle \hat{\Psi}^\dagger(x)\hat{\Psi}(x') \right\rangle \tag{1.11}$$

where $\hat{\Psi}(x)$ is the field operator[33], which destroys one particle at the spatial position x. The $\langle\cdot\rangle$ denotes the average over the ground state of the system.The diagonal elements of the matrix yield the density function

$$n(x) = \left\langle \Psi^\dagger(x)\Psi(x) \right\rangle \tag{1.12}$$

In a translationally invariant system the one body density matrix depends only on the difference $x - x'$ and one can write

$$\rho(x) = \left\langle \hat{\Psi}^\dagger(x)\hat{\Psi}(0) \right\rangle \tag{1.13}$$

The OBDM is equal to the Fourier transform of the momentum distribution

$$n(p) = \left\langle \hat{\Psi}^\dagger(p)\hat{\Psi}(p) \right\rangle \tag{1.14}$$

where $\Psi(p)$ is the field operator in the momentum representation, which destroys a particle with momentum p.
It is well known that a macroscopic number of bosons can occupy the state with momentum $p = 0$. This peculiare phase of matter is called a Bose Einstein Condensate (BEC). In a BEC the momentum distribution takes the form of a Dirac delta peaked at zero momentum plus a regular component

$$n(p) = N_0\delta(p) + \tilde{n}_0(p) \tag{1.15}$$

where N_0 is the number of particles condensed in the zero-momentum state. By taking the Fourier transform one can easily prove that

$$\frac{N_0}{L} = \lim_{x\to\infty} \rho(x) \tag{1.16}$$

where L is the length of the box. Thus the asymptotic limit of the OBDM can characterize the onset of Bose Einstein condensation.

Pair Correlation

The pair correlation represents the probability to find a particle at distance x from another particle. In a translationally invariant system the pair correlation can be written as

$$g(x) = \frac{1}{n^2} \left\langle \hat{\Psi}^\dagger(x)\hat{\Psi}^\dagger(0)\hat{\Psi}(0)\hat{\Psi}(x) \right\rangle \tag{1.17}$$

At large distances particles become uncorrelated and the pair correlation saturates to one.

1.2.1 Structure factor

The structure factor can be defined as

$$S(k) = \frac{1}{N} \left\langle \mid \rho(k) \mid^2 \right\rangle \tag{1.18}$$

where $\rho(k) = \sum_{i=1}^{N} e^{ikx_i} = \int e^{ikx_i} n(x)$ is the Fourier transform of the density operator. It is related by a Fourier transform to the pair correlation function

$$S(k) = 1 + n \int e^{ikx}(g(x) - 1)dx \tag{1.19}$$

where $n = N/L$ is the density of the system, N is the number of particles and L is the length of the box. The static structure factor gives us information on the response of the system to a perturbation in the density with wavenumber k.

1.3 The Bogoliubov approximation

After discussing the two-body problem we can turn to the study of the many body problem. The hamiltonian is then given by

$$H = \int dx \frac{\hbar^2}{2m} \frac{\partial\hat{\psi}^\dagger(x)}{\partial_x} \frac{\partial\hat{\psi}(x)}{\partial_x} + \int dx \int dx' \hat{\psi}^\dagger(x)\hat{\psi}^\dagger(x')V(x-x')\hat{\psi}(x)\hat{\psi}(x') \tag{1.20}$$

where $\hat{\psi}(x)$ is the field annihilation operator and $V(x)$ is the two-body interaction potential. We can now substitute the Fourier representation of the field operator

$$\psi(x) = \frac{1}{\sqrt{L}} \sum_k c_k e^{ikx} \tag{1.21}$$

in the hamiltonian. The Fourier-space hamiltonian can then be written

$$H = \sum_k a_k^\dagger a_k \frac{k^2}{2m} + \frac{1}{2L} \sum_{k1,k2,q} a_{k1+q}^\dagger a_{k2-q}^\dagger V(q) a_{k1} a_{k2} \tag{1.22}$$

where the operator a_k destroys a particle with momentum k and $V(q)$ is the Fourier transform of the potential. However, we saw that at low energies the details of the potential do not matter and we can substitue the potential $V(q)$ with an effective short-range potential that reproduces the scattering length of the original potential. In particular, we can use a contact pseudo-potential with coupling g.

$$H = \sum_k a_k^\dagger a_k \frac{k^2}{2m} + \frac{g}{2L} \sum_{k1,k2,q} a_{k1+q}^\dagger a_{k2-q}^\dagger a_{k1} a_{k2} \tag{1.23}$$

If we neglect interactions, in the ground state all atoms will be in the state with $k = 0$. Let us suppose that the interaction potential is so weak that only a tiny fraction of atoms will populate states with higher energies. This is equivalent to assuming Bose Einstein Condensation with a large condensate fraction. At the zeroth order we can neglect the role of excited states and assume that all atoms are in the $k = 0$ state. Thus we can neglect all a_k in the hamiltonian with $k \neq 0$ and subsitute the operator a_0 with the number $\sqrt{N}$, neglecting the quantum fluctuations around the lowest state. Thus we reduce the hamiltonian to

$$E = \frac{gN^2}{2L} \tag{1.24}$$

where the kinetic energy has been entirely neglected . We can expand to the next leading order

$$H = \frac{g}{2L} a_0^\dagger a_0^\dagger a_0 a_0 + \sum_k \frac{k^2}{2m} a_k^\dagger a_k + \frac{g}{2L} \sum_k \left(4 a_0^\dagger a_k^\dagger a_0 a_k + a_k^\dagger a_{-k}^\dagger a_0 a_0 + a_0^\dagger a_0^\dagger a_k a_{-k} \right) \tag{1.25}$$

Once again we neglect fluctuations of the $k = 0$ state , by making the substitution $a_0 \to \sqrt{N_0}$ where N_0 is the occupancy of the $k = 0$ state.

$$H = \frac{gN_0^2}{2L} + \sum_k \frac{k^2}{2m} a_k^\dagger a_k + \frac{gN_0}{2L} \sum_k \left(4 a_k^\dagger a_k + a_k^\dagger a_k^\dagger + a_k a_k \right) \tag{1.26}$$

However N_0 is no longer equal to the number of particles N, as we are not entirely neglecting the population of higher excited states . We can substitute the relation $N_0 = N - \sum_k a_k^\dagger a_k$ in the hamiltonian 1.26 and obtain

$$H = \frac{gN^2}{2L} + \sum_k \frac{k^2}{2m} a_k^\dagger a_k + \frac{gN}{2L} \sum_k \left(2a_k^\dagger a_k + a_k^\dagger a_k^\dagger + a_k a_k \right) \tag{1.27}$$

The hamiltonian is quadratic in a_k and can be diagonalized using the Bogoliubov transformation

$$\hat{a}_k = u_k \hat{b}_k + v_k^* \hat{b}_{-k}^\dagger \tag{1.28}$$

where u_k and v_k are some free parameters and b_k is a new destruction operator. In order for b_k to satisfy the bosonic commutation relation $[b_k, b_k^\dagger] = 1$ the parameters u_k and v_k must satisfy the condition $|u_k|^2 - |v_k|^2 = 1$. We can substitute the transformation 1.28 in the hamiltonian and choose the parameters u_k and v_k in order to eliminate the off-diagonal elements $b_k^\dagger b_k^\dagger$ and $b_k b_k$ from the hamiltonian. This condition yields

$$\frac{gn}{2}(|u_k|^2 + |v_k|^2) + \left(\frac{k^2}{2m} + gn \right) u_k v_k = 0 \tag{1.29}$$

After some algebra one obtains the expression for u_k, v_k

$$u_k, v_k = \pm \left(\frac{\frac{k^2}{2m} + gn}{2\epsilon(k)} \right)^{\frac{1}{2}} \tag{1.30}$$

with

$$\epsilon_k = \left[\frac{gn}{m} k^2 + \left(\frac{k^2}{2m} \right)^2 \right]^{\frac{1}{2}} \tag{1.31}$$

The hamiltonian can be rewritten as

$$H = E_0 + \sum_k \epsilon(k) b_k^\dagger b_k \tag{1.32}$$

which is the hamiltonian of a gas of free bosonic particles with energy dispersion $\epsilon(k)$, shifted by a constant energy

$$E_0 = g\frac{N^2}{2L} + \frac{1}{2} \sum_k \left[\epsilon(k) - gn - \frac{k^2}{2m} \right] \tag{1.33}$$

Performing the integral yields

$$\frac{E_0}{L} = \frac{1}{2} gn^2 - \frac{2}{3\pi} g^{3/2} n^{3/2} \tag{1.34}$$

The state with no Bogoliubov excitations is the ground state and its energy is simply given by E_0 .
The whole Bogoliubov theory relies on the assumption that a BEC gas is present. Unfortunately it can be proven that in 1D at any finite value of the interactions, Bose Einstein Condensation cannot take place[31] . This theorem is compatible with the predictions of the Luttinger liquid theory which predicts at zero temperature an algebraic decay of the correlation functions, as describe later in chapter. However this decay is only algebraic and one-body correlations decays to zero only at very large distances . Thus the properties of these systems do not differ much from a system with actual Bose-Einstein condensation. While we cannot have an actual BEC , we can have a quasi-BEC which is well described by the Bogoliubov theory, as we will see in the remainder of this chapter.

1.4 The Gross-Pitaevskii equation

The Bogoliubov theory can only be applied to homogeneous systems. In non-homogenous systems one needs to resort to a different theory.
Let us write the Heisenberg equation for the field operator $\hat{\Psi}(x)$ [33], which destroys a particle at position x. The equation takes the form

$$i\hbar\frac{\partial}{\partial t}\hat{\Psi} = [H, \hat{\Psi}] \tag{1.35}$$

Let us suppose to already have exchanged the real interactions with a contact-like pseudo potential with coupling g. Then the hamiltonian in second quantization takes the form

$$H = \int dx \frac{\hbar^2}{2m}\frac{\partial\hat{\psi}^\dagger(x)}{\partial_x}\frac{\partial\hat{\psi}(x)}{\partial_x} + g\int dx\hat{\psi}^\dagger(x)\hat{\psi}^\dagger(x)\hat{\psi}(x)\hat{\psi}(x) + \int dx U(x)\hat{\psi}^\dagger(x)\hat{\psi}(x) \tag{1.36}$$

where $U(x)$ is an external potential. Trough substitution of the hamiltonian in the Heisenberg equation we get

$$i\hbar\frac{\partial}{\partial t}\hat{\Psi}(x,t) = \left\{-\frac{\hbar^2}{2m}\frac{\partial}{\partial_x^2} + g\hat{\Psi}^\dagger(x,t)\hat{\Psi}(x,t) + U(x)\right\}\hat{\Psi}(x,t) \tag{1.37}$$

However this equation is not in closed form. If we neglect quantum fluctuations, we can approximate the field operator $\hat{\Psi}(x)$ by a classical complex field $\Psi(x)$, equal to the average value of the field operator $\left\langle\hat{\Psi}(x)\right\rangle$. Replacing the field operator by a classical field implies that all atoms condense in one

macroscopic state with wavefunction $\Psi(X)$. The GP equation then takes the form

$$i\hbar\frac{\partial}{\partial t}\Psi(x,t) = \left\{-\frac{\hbar^2}{2m}\frac{\partial}{\partial_x^2} + g|\Psi(x,t)|^2 + U(x)\right\}\Psi(x,t) \tag{1.38}$$

Notice that the operator $\hat{\Psi}(x,t)$ destroys a particle and the average $\langle\Psi(x,t)\rangle$ on any state with a well defined number of particles will be zero. However in the limit of a very large number of particles we can assume that removing or adding a single particle will not modify much the macroscopic state and thus we may assume that the two states are the same , instead of being orthogonal.
The Gross-Pitaevskii equation is a time-dependent equation , describing the evolution of the condensate wavefunction. However, we may be interested on stationary solutions. The condensate wavefunction can be written as

$$\Psi(x,t) = \left\langle\hat{\Psi}(x,t)\right\rangle \tag{1.39}$$

$$= \left\langle e^{i\frac{t}{\hbar}H}\hat{\Psi}(x)e^{-i\frac{t}{\hbar}H}\right\rangle \tag{1.40}$$

Let us suppose to take the average on the lowest eigen-state of the hamiltonian with N particles. As the field operator destroys one particle, the resulting average must be zero as states width different particle numbers are orthogonal to each other. However in the large N limit one may neglect the difference between the condensate wavefunction with N and N-1 particles. Applying the evolution operators respectively on the left and the right one may write the approximate expression

$$\Psi(x,t) \approx \left\langle\hat{\Psi}(x)\right\rangle e^{-\frac{i}{\hbar}[E(N)-E(N-1)]t} = \Psi(x)e^{-\frac{i}{\hbar}\mu t} \tag{1.41}$$

where $\mu = E(N+1)-E(N)$ is the chemical potential of the system. Plugging the expression 1.41 into the GP equation, one gets the stationary GP equation

$$\left(-\frac{\hbar}{2m}\frac{\partial^2}{\partial_x^2} + g|\Psi(x)|^2 + U(x)\right)\Psi = \mu\Psi \tag{1.42}$$

The stationary GP equation is similar to a Schrodinger equation, but with an added nonlinear term arising from mean-field interactions and involves the chemical potential instead of the energy. The GP equation can also be obtained from the minimization of the energy functional

$$E = \int dx\left\{\frac{\hbar^2}{2m}\partial_x\Psi(x)\partial_x\Psi(x)^* + \frac{g}{2}|\Psi(x)|^4\right\} \tag{1.43}$$

under the constraint that the norm of the wavefunction $\int dx|\Psi(x)|^2$ is equal to the number of particles N .
The GP equation is able to treat non-homogeneous systems and is applicable in the limit of weak interactions, where quantum fluctuations are negligible.

1.5 Superfluid Hydrodynamics

Let us consider the equation for the field operator

$$i\hbar\frac{\partial}{\partial t}\hat{\Psi}(x,t) = \left\{-\frac{\hbar^2}{2m}\frac{\partial}{\partial_x^2} + \int \hat{\Psi}^\dagger(x',t)V(x'-x)\hat{\Psi}(x',t)\right\}\hat{\Psi}(x,t) \quad (1.44)$$

Let us suppose that the superfluid is moving with some velocity v . In a moving frame of reference where the fluid is at rest, assuming Galileian invariance, the solution takes the form

$$\hat{\Psi}(x,t) = \hat{\Psi}_0(x-vt)e^{iS(x,t)} \quad (1.45)$$

where $\Psi_0(x)$ is the stationary solution in the system at rest and $\phi(x,t)$ is an additional phase factor that depends on the velocity of the fluid

$$S(x,t) = \frac{1}{\hbar}\left[mvx - \left(\frac{1}{2}mv^2 + \mu\right)t\right] \quad (1.46)$$

Let us now consider the average value $\langle\Psi\rangle_0 = \sqrt{n}e^{iS(x)}$, where n can be seen as the density of the superfluid. The superfluid velocity can instead be written as

$$v_s = \frac{\hbar}{m}\partial_x S(x) = \partial_x\phi(x) \quad (1.47)$$

where $\phi(x) = \frac{\hbar}{m}S(x)$. We now define the superfluid order parameter as $\rho = nm$. The superfluid fraction must satistify the continuity equation

$$\frac{\partial\rho}{\partial_t} + div(v_s\rho) = 0 \quad (1.48)$$

while the phase of the order parameter must satisfy the equation

$$m\partial_t\phi = -\left(\frac{1}{2}mv_s^2 + \mu\right) \quad (1.49)$$

Notice that both ρ and the phase ϕ are not operators, and that $\hbar$ dropped out from the equations. The hydrodynamic equations can be though of as

classical equations describing a quantum fluid. They can also be obtained from the Hamilton equation of the classical hamiltonian

$$H = \int dx \left(\frac{\rho}{2} (\partial_x \phi)^2 + e(\rho) \right) \tag{1.50}$$

The first term represents the kinetic energy arising from the flow while the second term $e(\rho)$ is the energy per unit volume of the uniform system at rest. This hydrodynamic theory can be interptred as a classical theory, describing a quantum system. The classical hamiltonian can be promoted to a quantum hamiltonian by imposing the bosonic commutation relations

$$[\phi(x), \rho(x')] = \delta(x - x') \tag{1.51}$$

The hamiltonian then becomes

$$H = \int dx \left[\partial_x \hat{\phi} \frac{\hat{\rho}}{2} \partial_x \hat{\phi} + e(\hat{\rho}) \right] \tag{1.52}$$

We can now expand the density operator around its average ground state value

$$\hat{\rho} = \rho + \delta\hat{\rho} \tag{1.53}$$

We can substitute expression 1.53 into the hamiltonian and by keeping all terms up to the second order we get

$$H = \int dx \left[\frac{1}{2} \rho (\partial_x \hat{\phi})^2 + \frac{c^2}{2} \frac{(\delta\hat{\rho})^2}{\rho} \right] \tag{1.54}$$

where

$$mc^2 = n \frac{\partial}{\partial_n} \mu \tag{1.55}$$

The hamiltonian 1.54 corresponds to independent oscillations and its excited states are phonons with linear dispersion $\hbar\omega(k) = ck$, where c is the speed of sound.

1.6 The Luttinger liquid model

We mentioned that the absence of quasi-particle excitations in one dimension leads to the failure of the Fermi liquid theory. The one dimensional geometry forces us to look for a different model , which does not rely on quasiparticle excitations, but on collective excitations instead : the Luttinger liquid theory. Let us first consider a very simple system : non-interacting one-dimensional

fermions.
The hamiltonian contains only the kinetic energy

$$H = -\frac{\hbar^2}{2m}\sum_{i=1}^{N}\frac{\partial^2}{\partial_{x_i}^2} \tag{1.56}$$

which in second quantization takes the form

$$H = \sum_k \epsilon(k)\left(c_k^\dagger c_k\right) \tag{1.57}$$

where $\epsilon(k) = \frac{k^2}{2m}$ is the free-particle dispersion and c_k destroys a particle with momentum k. We can then expand the free-particle energy dispersion around the Fermi surface. In one dimension the Fermi surface is made by only two momentums : k_F and $-k_F$. The energy dispersion up to the first order is given by

$$\epsilon(k) \approx \frac{k_F^2}{2m} + \hbar v_F(\pm k - k_F) \tag{1.58}$$

where the sign +(-) represents right(left) moving particles. The expansion is only valid around the Fermi energy, but if we assume that only low-energy excitations are important we can approximate the free particle spectrum with the expanded spectrum 1.58 in the whole momentum range. Than the hamiltonian, neglecting a constant shift, becomes

$$H = \sum_{d=\pm}\sum_k \hbar v_F(dk - k_F)c_{k_d}^\dagger c_{k_d} \tag{1.59}$$

where $c_\pm$ is the operator that destroys a right(left) moving particle.

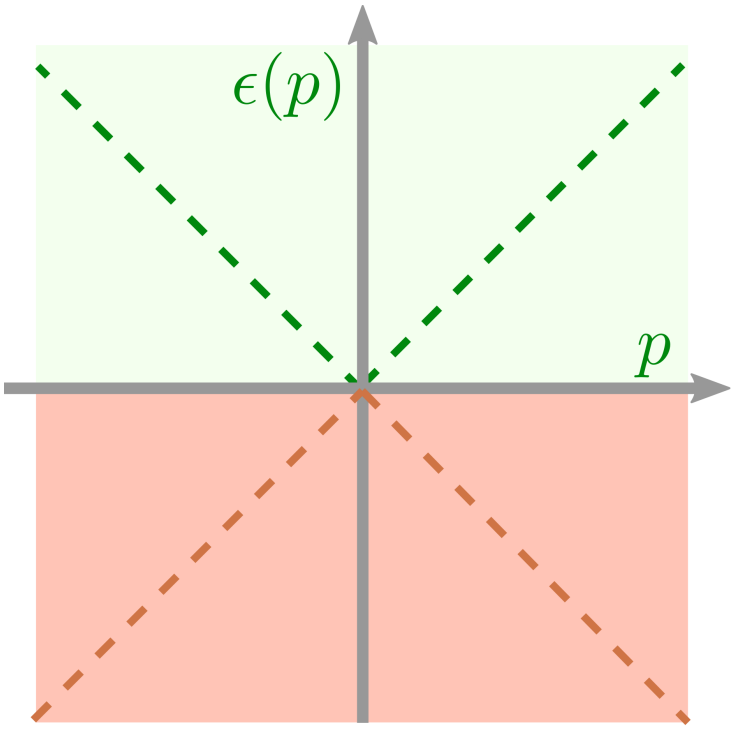

Figure 1.1: A sketch of the linear energy dispersion. States with momentum lower than the fermi moentum are all occupied. The two green dashed lines represents the energy dispersion for right and left moving particles

We can now recast the hamiltonian in real space introducing the field operators for the right and left moving particles

$$\begin{aligned} \psi_R &= \tfrac{1}{\sqrt{L}} \textstyle\sum_k c_{k,+} e^{-i(k-k_F)x} \\ \psi_L &= \tfrac{1}{\sqrt{L}} \textstyle\sum_k c_{k,-} e^{i(k+k_F)x} \end{aligned} \tag{1.60}$$

By inserting equations 1.60 into the hamiltonian 1.58 we arrive at

$$H = -i\hbar v_F \int \left[dx \psi_R^\dagger \frac{\partial \psi_R}{\partial x} - \psi_L^\dagger \frac{\partial \psi_L}{\partial x} \right] \tag{1.61}$$

which can be solved using the bosonization technique. This technique consists in mapping the original fermionic fields to conjugate bosonic fields. Let us first define the right and left density $\rho_R = \psi_R^\dagger \psi_R$ and $\rho_L = \psi_L^\dagger \psi_L$. We can define the fields $\phi(x)$ and $\Pi(x)$ in termes of right and left density as

$$\begin{aligned} \partial_x \phi(x) &= -\pi \left(\rho_R(x) + \rho_L(x) \right) \\ \Pi(x) &= \rho_R(x) - \rho_L(x) \end{aligned} \tag{1.62}$$

which can be shown to satisfy the bosonic commuation relations

$$[\phi(x), \Pi(y)] = \delta(x - y) \tag{1.63}$$

In terms of these new fields the hamiltonian can be rewritten as

$$H = \frac{\hbar}{2} v_F \int dx \left[\pi \Pi(x)^2 + \frac{1}{\pi} \left(\partial_x \phi \right)^2 \right] \tag{1.64}$$

By linearizing the excitation spectrum we managed to map the original fermionic hamiltonian to a bosonic hamiltonian, neglecting high-energy excitations. This model is usually called the Tomonaga-Luttiger model. However Haldane showed that the same treatment can be generalized also to interacting bosonic and fermionic gapless models provided that high-energy modes do not play a significant role. This generalized model can be written as

$$H = \frac{\hbar}{2} c \int dx \left[K \pi \Pi(x)^2 + \frac{1}{\pi K} \left(\partial_x \phi \right)^2 \right] \tag{1.65}$$

which depends on the parameter c, with the dimension of a velocity, and the dimensionless parameter K, also called the Luttinger parameter. In the special case $c = v_F$ and $K = 1$ on recovers the Tomonaga-Luttiger model. These parameters are not universal and depend on the details of the interaction and are inputs of the model. However, once the values of these two parameters are known for some one dimensional hamiltonian, its low-energy properties can be recovered using the hamiltonian 1.65. The Luttinger parameter can be related to the compressibility κ of the system trough the relation

$$\kappa = \frac{K}{\hbar c \pi} \tag{1.66}$$

The Luttinger parameter controls the long range behavior of correlation functions.
For instance let us consider the OBDM

$$\rho(x) = \left\langle \Psi(x)^\dagger \Psi(0) \right\rangle \tag{1.67}$$

At large distances the OBDM is predicted to decay algebraically [34] as

$$\rho(x) \propto x^{-1/(2K)} \tag{1.68}$$

The Luttinger parameter fixes the rate of the decay and thus represents a measure of the strength of correlations in the system.

1.7 Exactly solvable models

The discovery of the Bethe ansatz technique has allowed to tackle analitically many non-trivial problems in one spatial dimension. Here we present two such models. One is the Lieb-Liniger model[5], which describes a system of bosons with contact like interactions. The second is the Yang-Gaudin [8, 9] model, which describe a system of spinful fermions with contact interactions.

1.7.1 The Lieb-Liniger model

The Lieb-Liniger model[5, 6] is a specific microscopic model of bosons interacting via a short-range potential with coupling strength g.

$$H = -\frac{\hbar^2}{2m}\sum_i \frac{\partial^2}{\partial_{x_i}^2} + g\sum_{i<j}\delta(x_i - x_j) \tag{1.69}$$

While this hamiltonian is far from trivial and cannot be solved in higher dimensions, in one dimension the system allows an exact semi-analytical solution using the Bethe-Ansatz technique [35]. The ground-state energy of the model in the thermodynamic limit is given by

$$\frac{E_0(\gamma)}{N} = \frac{\hbar^2}{2m}n^2 e(\gamma) \tag{1.70}$$

where E_0 is the ground state energy, N is the number of particles and e(γ) is a dimensionless function of the dimensionless parameter

$$\gamma = \frac{mg}{\hbar^2 n} \tag{1.71}$$

that characterizes the strength of the interaction. It is interesting to notice that the whole equation of state only depends on the single parameter γ proportional to the ratio of the coupling constant and the density. In the weak coupling regime γ is small as the coupling g is small. However, the same regime can be achieved at higher values of the coupling but with higher densities. In contrast to systems in higher dimensions, decreasing the density does not reduce the role of interactions but instead increases it. The function $e(\gamma)$ can be obtained by solving the system of integral equations

$$g_\lambda(x) = \frac{1}{2\pi} + \frac{1}{\pi}\int_{-1}^{1} g_\lambda(y)\frac{\lambda}{\lambda^2 + (x-y)^2}dy \tag{1.72}$$

$$\gamma = \lambda\left(\int_{-1}^{1} g_\lambda(x)dx\right)^{-1} \tag{1.73}$$

for the unkown parameter λ and the unkown function $g_\lambda(x)$. Then the energy can be obtained from

$$e(\gamma) = \frac{\gamma^3}{\lambda^3} \int_{-1}^{1} g_\lambda(x) x^2 dx \tag{1.74}$$

While no analytical solutions are known, they can be easily solved numerically, for instance using a self-consistent recursive procedure. When

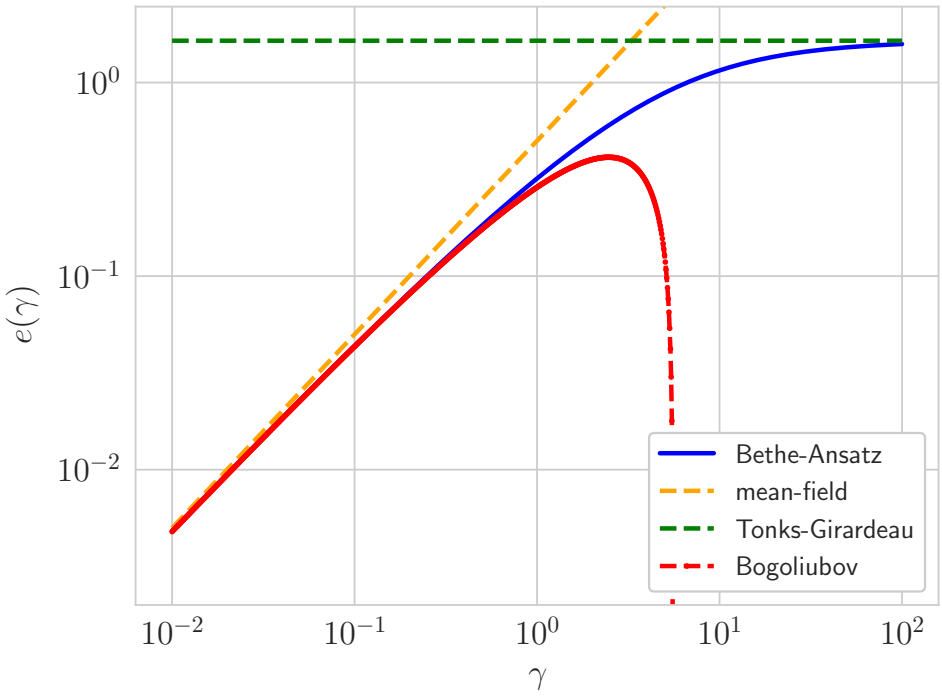

Figure 1.2: The energy per particle versus γ. The solide blue line represents the numerical solutions of the BA equations compared with results from mean field theory(dashed orange),Bogoliubov theory (red dashed line) and the energy of a free Fermi gas (green dashed line)

$\gamma \ll 1$ interactions are weak and particles can easily exchange positions via quantum tunneling and mean-field theory is valid. In figure 1.2 we compare the solution of the Bethe Ansatz equations with mean-field theory and Bogoliubov theory. The agreement of Bogoliubov theory is very good up to $\gamma \approx 1$, despite mean-field theory not being strictly valid as Bose-Einstein condensation does not occur. At larger values of γ the energy saturates to a constant value. In this regime the coupling strength is so large that quantum

tunneling between particles is no longer possible and the particles become impenetrable. We can think of a gas of impenetrable bosons with short-range interactions as a gas of non interacting particles with the constraint that two particles cannot occupy the same position. This constraint plays the role of an effective Pauli principle , making the gas behave essentially as a gas of free Fermions. In fact, this mapping between the Lieb-Liniger gas in the limit $\gamma \to \infty$ with a gas of free spinless fermions has been rigorously proved. In this limit the system is also called Tonks-Girardeau gas (TG) . It is possible to show that the many-body wavefunction of the TG gas and the many-body wavefunction of a free spinless Fermi gas have the same modulus and differ only for a sign factor which accounts for the different symmetry under particle exchange [36].

$$\psi_{TG} = |\psi_F| \tag{1.75}$$

This condition implies that the energy and mean value of any local observable will be the same for the two systems. Notice that the mapping is not valid for non local observables. An example of a non local observable is the momentum distribution , which is obtained from the Fourier transform of the off-diagonal one body density matrix. The boson mapping is not valid for this observable , which differs significantly for a Tonks-Girardeau gas and a spinless free Fermi gas[37]. Figure 1.2 clearly shows that as $\gamma \to \infty$ the energy approaches the energy of a non-interacting gas of spinless fermions.

$$\frac{E}{N} = \frac{e_F}{3} \tag{1.76}$$

where e_F is the Fermi energy of a non-interacting spinless Fermi gas.

$$e_F = \frac{\hbar^2 \pi^2 n^2}{2m} \tag{1.77}$$

The mapping does not extend to non local observables. For instance, the momentum distribution of a free spinless Fermi gas is very different from the one of a bosonic TG gas.

1.7.2 The Yang-Gaudin model

So far we only dealt with bosons. We will now discuss a model of spinful fermions with short-range interactions.

$$H = -\frac{\hbar^2}{2m} \sum_{\sigma=\uparrow\downarrow} \sum_i \frac{\partial^2}{\partial_{x_i^\sigma}^2} + g \sum_{i<j} \delta(x_i^\uparrow - x_j^\downarrow) \tag{1.78}$$

The hamiltonian 1.78 only involves interactions between particles with different spins, with coupling g. Adding a contact interaction between particles with the same spin would not affect the system because the Pauli principle prevents particles of the same spin to occupy the same position in space. The hamiltonian is SU(2) symmetric . It can be solved exactly using the Bethe Ansatz both for a finite number of particles and directly in the thermodynamic limit [38, 129, 6]. In the latter case the Bethe Ansatz equations reduce to a system of coupled integral equations, which we describe below.

Repulsive interactions

We first study the case $g > 0$. The BA solution takes the form of a system of integral equations

$$\rho_1 = \frac{1}{2\pi} + \int_{-A_2}^{A_2} K_1(k-k')\rho_2(k')dk' \tag{1.79}$$

$$\rho_2 = \int_{-A_1}^{A_1} K_1(k-k')\rho_1(k')dk' - \int_{-A_2}^{A_2} K_2(k-k')\rho_2(k')dk' \tag{1.80}$$

$$K_l(x) = \frac{1}{2\pi}\frac{lc}{(lc/2)^2 + x^2} \tag{1.81}$$

with the conditions

$$\frac{N}{L} = \int_{-A_1}^{A_1} \rho_1(k)dk \tag{1.82}$$

$$\frac{N_\downarrow}{L} = \int_{-A_2}^{A_2} \rho_2(k)dk \tag{1.83}$$

$$\frac{E}{L} = \int_{-A_1}^{A_1} k^2\rho_1(k)dk \tag{1.84}$$

where $c = gm/\hbar^2$, E is the ground state energy of the system, L is the length of the system, N is the total number of particles , $N_\uparrow$ is the number of particles with spin up and $N_\downarrow$ the number of particles with spin down . The bounds A_1 and A_2 are unkown and are fixed respectively by the total number of particles and the number of spin down particles. The parameter $\gamma = \frac{mg}{\hbar^2}$ is the same parameter introduced previously. As in the Lieb-Liniger model, the equations do not depend on the coupling g and density n independently but only trough their ratio. This system of equations cannot be solved analitically , but they can be easily solved numerically. Analytic expressions can be obtained in the limit of weak and strong coupling. If $g = 0$ the Yang Gaudin

hamiltonian describes two non-interacting free Fermi gases. Thus the energy is given by

$$E = N_\uparrow \frac{\hbar^2 \pi^2 n_\uparrow^2}{6m} + N_\downarrow \frac{\hbar^2 \pi^2 n_\downarrow^2}{6m} \tag{1.85}$$

If the coupling g is small, we can treat the interactions between particles with up and down spin within the mean field approximation and the energy becomes

$$E = N_\uparrow \frac{\hbar^2 \pi^2 n_\uparrow^2}{6m} + N_\downarrow \frac{\hbar^2 \pi^2 n_\downarrow^2}{6m} + g n_\uparrow n_\downarrow L \tag{1.86}$$

which is linear in the coupling g. As one increases g the energy increases and in the limit of very strong coupling spin up and down particles become impenetrable. Similarly to the case of a TG gas described in the previous section, the impenetrability plays the role of an effective Pauli principle between the two different spin components and the system can be mapped to a spin polarized Fermi gas with energy

$$E = (N_\uparrow + N_\downarrow) \frac{\hbar^2 \pi^2 \left(n_\uparrow + n_\downarrow\right)^2}{6m} \tag{1.87}$$

Attractive interactions

We now turn to the case $g < 0$. Also in this case the model can be solved and the solution takes the form of a system of coupled integral equations.

$$\rho_1(k) = \frac{1}{2\pi} + \int_{-A_2}^{A_2} K_1(k - k')\rho_2(k')dk' \tag{1.88}$$

$$\rho_2(k) = \frac{1}{\pi} + \int_{-A_1}^{A_1} K_1(k - k')\rho_1(k')dk' + \int_{-A_2}^{A_2} K_2(k - k')\rho_2(k')dk' \tag{1.89}$$

with the conditions

$$\frac{N}{L} = 2\int_{-A_2}^{A_2} \rho_2(k)dk + \int_{-A_1}^{A_1} \rho_1(k) \tag{1.90}$$

$$\frac{N_\downarrow}{L} = 2\int_{-A_2}^{A_2} \rho_2(k)dk \tag{1.91}$$

The ground state energy is given by

$$\frac{E}{L} = \int_{-A_2}^{A_2} (2k^2 - \frac{\gamma^2}{2})\rho_2(k)dk + \int_{-A_1}^{A_1} k^2 \rho_1(k)dk \tag{1.92}$$

K_1 and K_2 are the same as defined above. For weak interactions the ground-state energy is still given by 1.84. Two particles interacting with an attractive contact interaction will form a bound state with energy

$$\epsilon_b = -\frac{\hbar^2}{m|a|^2} \tag{1.93}$$

where $a = -\frac{\hbar^2}{2mg}$ is the scattering length. The contribution of the binding energy is small when the coupling is small but when the coupling becomes large the main contribution to the total energy comes from ϵ_b. Let us consider the case of a balanced mixture, for the sake of simplicity. When the coupling is very large particles of different spin will form bosonic molecules of two different spin states. At low densities, where $\gamma > 0$, one than obtains a Tonks-Girardeau gas of molecules , with twice the mass of the bar atom and density half of the total density of the Yang-Gausin gas . The energy can then be written as the sum of the binding energy of the molecules and the energy of the Tonks-Girardeau gas[6].

$$\frac{E}{N} = -\frac{1}{2}\epsilon_b + \frac{\hbar^2\pi^2 n^2}{12m} \tag{1.94}$$

1.8 Ultracold quantum gases

So far we discussed some general theoretical models. While one dimensional models can be implemented in a variety of platforms, we will here discuss only one physical system of experimental relevance : dilute trapped atomic gases cooled down to extremely low temperatures (few μK). These systems are usually very dilute , with the distance between particles much larger than the range of the interactions. Thermal energy is so small that most collisions only involve the s orbitals and higher energy states can be neglected. Interactions in ultracold quantum gases can be modeled by contact interactions with high accuracy and one can easily compare experiments with theory once the value of the scattering length is known, without the need to determine any other parameter.

Despite being macroscopic objects (typically a few μm in size) they are inherently quantum. One of the most spectacular effects of the quantum nature of bosonic gases is the phenomenon of Bose Einstein condensation (BEC). The theoretical prediction of BEC was made already at the beginning of the last century but the first experimental observations can only much later. A first form of Bose Einstein condensation was first experimentally realized with the realization of liquid ^{4}He [40]. However liquid helium is a strongly interacting

system where the role of interactions cannot be neglected[31]. This system exhibits properties very different from the original theory of a free Bose gas proposed by Bose ed Einstein.
The first observation of a weakly interacting Bose Einstein Condensate was not made until 1995[41, 42]. The main challenge is the extremely low temperature required to achieve Bose-Einstein condensation. Such low temperatures were eventually reached, using two different cooling techniques, laser cooling [43] and evaporative cooling [44].

Stability

Even when the interaction potential at large distances is repulsive, it may support several bound states. If the incident energy is not large enough colliding atoms may not scatter, but instead fall into a bound state, decreasing their energy. As energy must be conserved, the excess energy must be carried away, typically trough a third atom participating in the collision. If the bound state is deep, the excess energy will be large and the third body will acquire enough energy to escape the trap, leading to a drastic reduction of the number of atoms in the condensate. This mechanism of *three body losses* [45] hinders the realization of strongly correlated three dimensional quantum gases, which support deep bound states.
In quasi-one-dimensional systems, because of the restricted topology, it is much less likely for three atoms to be found at the same position and the three body recombination rate is much smaller.
Consequently quantum gases in quasi-one dimensional geometries are much more stable than in less constrained geometries.

1.8.1 Feshbach resonances

Feshback resonances are a useful tool that allows one to experimentally tune the scattering length[46]. As atoms have several internal states, the interaction potential may depend on the internal states of the colliding atoms and several scattering channels are possible. If the collision energy is resonant with a bound state in a certain channel , we say that the channel is closed. Conversely, if the collisional energy is resonant with one of the states in the continuum we say that the channel is open. The Feshbach resonance happens when one couples resonantly an open and closed channel. Experimentally the coupling can be made applying an external magnetic field . The dependence of the scattering length on the magnetic field can be approximately written

as[46]

$$a_B = a_0 \left(1 - \frac{\Delta B}{B - B_0}\right) \tag{1.95}$$

where B_0 is the magnetic field at resonance , ΔB is the width of the transition and a_0 is the off-resonant scattering length.

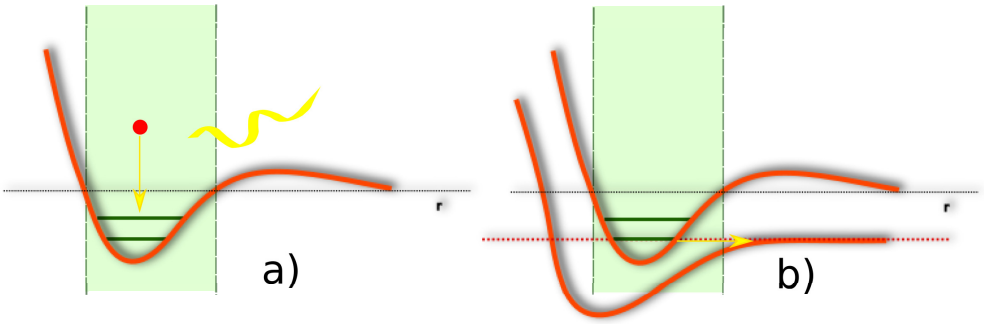

Figure 1.3: a) Illustration of three body losses. Two atoms form a bound state by releasing energy that heats the condensate b) Illustration of a Feshbach Resonance. The collisional energy is resonant with a bound state in the closed channel and the continuum in the open channel

1.8.2 One dimensional traps

Quantum gases have been produced in a variety of geometries. It is possible to realize isotropic, elongated cigar-like and flat pancake-like traps. It is also possible to trap atoms in tight optical lattices.
For instance it is possible to trap atoms in a two dimensional trapping lattice, with a shallow harmonic trapping in the remaining direction. Atoms will be trapped in the shape of many elongated tubes. If the lattice is deep enough , different tubes will not interacting with each other. When taking measurements, one performs an average over all the elongated tubes.

Such a geometry is very close to the geometry of a one-dimensional system, however , as we live in a three-dimensional world , it will not be entirely one-dimensional. This leads us to the question of which systems can actually be described by a one-dimensional model. It turns out that the approximation can be very good when the transverse confinement is strong enough. In case of a harmonic anisotropic trapping potential

$$U(x) = \frac{1}{2} m(w_x^2 x^2 + w_\perp^2 (y^2 + z^2)) \tag{1.96}$$

Figure 1.4: Cartoon representing an array of 1D tubes , created using a 2D optical lattice

the 1D regime can be reached when the transverse trapping is much larger then the longitudinal trapping frequency and the typical scales of the system, i.e. when

$$\hbar\omega_\perp \gg \mu, k_B T \tag{1.97}$$

where μ is the chemical potential and T is the temperature. In this regime one can prove that in the transverse direction the density profile takes the form of a gaussian whose size is given by the transverse harmonic length

$$a_\perp = \sqrt{\frac{\hbar}{m\omega_\perp}} \tag{1.98}$$

The longitudinal direction instead can be well described by a one-dimensional theory with an effective scattering length [47].

$$\frac{1}{a_{1D}} = -\frac{a_{3D}}{a_\perp^2}\frac{1}{1 - A\frac{a_{3D}}{a_\perp}} \tag{1.99}$$

where $A = \zeta(1/2)\sqrt{2} \approx 1.0326$ and $\zeta(x)$ is Riemann's zeta function. Notice that the relation 1.99 provides an additional mechanism to tune the 1D scattering length by tuning the transverse confinement , besides Feshbach resonances used to tune the 3D scattering length.
The presence of confinement induced resonances and the suppression of three body losses allows one to reach strongly interacting regimes ($a_{1D} \ll 1$).
A hallmark achievement in this direction was the experimental realization of the TG gas[48]. Since this achievement many experiments have probed interacting quasi-1D gases with short range interactions, obtaining results in very good agreement with the Lieb-Liniger theory[49, 50, 51].

Chapter 2

Quantum Monte-Carlo

In this chapter we describe the main numerical technique used in this work. Quantum Monte-Carlo techniques have long been the method of choice to study ground-state properties of large strongly correlated systems because of its favorable polynomial scaling with the size of the system and high accuracy. In dimensions higher than one, it is often the only method able to accurately tackle correlations in large systems. In one dimension the Density Renormalization Group (DMRG) method is another viable choice. However, most DMRG algorithms are limited to lattice systems and extrapolation to the continuum can be difficult. In this thesis we use two different flavors of quantum Monte-Carlo, the Variational Monte-Carlo (VMC) and the Diffusion Monte-Carlo (DMC). The VMC method samples an ansatz of the many-body wavefunction and is as accurate as the wavefunction ansatz. The DMC method instead samples the imaginary time evolution of the system to project out the true ground-state of the system with arbitrary accuracy. We will first review the basic of all Monte-Carlo based methods. Then we will describe the variational Monte-Carlo algorithm (VMC), which uses the metropolis method to sample the wavefunction ansatz. Then we describe an alternative algorithm, the Smart Variational Monte-Carlo (SVMC) . SVMC also samples the ansatz wavefunction by sampling a markovian diffusion process in imaginary time. We will then discuss how to optimize the wavefunction by minimizing the energy. Finally we will describe the DMC method. For a more in depth discussion one may consult [52, 53].

2.1 Preliminaries

In nature many events are stochastic and different measurements can yield different results. For instance, the result of the throw of a dice or the outcome

of the measurement of the position of a quantum particle. A variable that can take several values is called a random variable. In the case of the throw of a dice the variable can only take one of six discrete values. A sequence of throws yields a sequence of random values, called a random sequence $s = s_1, s_2..s_N$. If the dice is fair, all outcomes are equally likely. However, if the dice is loaded a few outcomes may be more frequent than others and we can define the probability of a certain value i as

$$p(i) = f_i/N \tag{2.1}$$

where i is the possible outcome of a throw ,f_i is the number of occurrences of the result i in a sequence of N throws. As each throw must yield a number between 1 and 6 the sum of the probabilities of all possible outcomes must sum to one

$$\sum_i p_i = 1 \tag{2.2}$$

In the case of the measurement of a quantum particle the possible outcomes are infinite, but we can still define the probability to observe a particle in a small position interval δx_i

$$p_i = p(x_i)\delta x_i \tag{2.3}$$

where $p(x_i)$ is equal to the square of the wavefunction of the particle. In the limit of $\delta_{x_i} \to 0$ $p(x_i)$ becomes a continuous function and is called a probability distribution function (pdf). As the sum of the probabilities to find the particle in any interval must sum to one the pdf must satisfy the normalization condition

$$\int dx p(x) dx = 1 \tag{2.4}$$

We may be interested on the mean position of the particle, or any observable $\hat{O}$ that depends on the position of the particle

$$\langle O \rangle = \frac{\int dx O(x) p(x) dx}{\int dx p(x) dx} \tag{2.5}$$

Another interesting property is the variance of the observable

$$\sigma_O^2 = \langle O^2 \rangle - \langle O \rangle^2 \tag{2.6}$$

In the case of a particle in a harmonic potential we know that the distribution of the particle is simply given by a gaussian. The gaussian pdf is defined as

$$p(x) = \frac{1}{\sqrt{2\pi\sigma}} \exp - \frac{(x-\mu)^2}{2\sigma^2}) \tag{2.7}$$

where μ is the average value of the distribution and σ its variance. In this case the integral 2.5 is very easy to perform. However, we want to perform the integration numerically. One approach is to divide the real space in many intervals and then sum the observable values multiplied by the pdf over all possible intervals. However this method becomes daunting when the dimensionality increases and soon becomes unfeasible. Another approach is to create a sequence of particle positions $X = \{x_1, x_2...x_N\}$ distributed according to the *pdf* $p(x)$. The mean value is given by

$$\langle O \rangle = \frac{\sum_{i=1}^{N} O(x_i)}{N} \tag{2.8}$$

It can be proven that this approach is more efficient when the dimensionality of the integral is greater than 4. This approach relies on the possibility to generate particle positions according to the distribution $p(x)$. In our case the distribution function is very sample: it is just a gaussian. Random numbers may be sampled efficiently from a gaussian distribution using the Box-Muller algorithm. The algorithm consists in

- Generate two random numbers u_1,u_2 between 0 and 1 with uniform probabilities.
- Then we set

$$y_1 = \sqrt{-2\log(u_1)}\cos 2\pi u_1 \tag{2.9}$$

$$y_2 = \sqrt{-2\log(u_2)}\cos 2\pi u_2 \tag{2.10}$$

  It can be shown that y_1 and y_2 are distributed according to a gaussian distribution with mean 0 and variance 1.

- We can make the substitution $y \to \sigma y + \mu$ to obtain a variable still distributed according to a gaussian but with mean μ and variance σ.

In general we may have to deal with a distribution much more complicated than a simple gaussian. Thus we need a method to generate random numbers according to some arbitrary distribution $f(x)$. One such algorithm exists: the Metropolis-Hasting algorithm.

2.1.1 The Metropolis algorithm

Let us first consider a random sequence

$$x = \{x_1, x_2...x_N\} \tag{2.11}$$

The random numbers are not independent and the probability to obtain a certain value x may depend on all previous elements of the sequence. Given a certain sequence the transition probability to obtain the value x at the next step may be rewritten as

$$\Gamma(x_i = x|x_{i-1}....x_0) \tag{2.12}$$

A **Markov process** is a sequence of random numbers where the probability to obtain a certain value at step i depends on the value of the previous step only

$$\Gamma(x_i = x|x_{i-1}...x_0) \equiv \Gamma(x_i, x_{i-1}) \tag{2.13}$$

Defining a transition probability $\Gamma(x, x')$ is sufficient to define the stochastic process. The probability density of obtaining a certain value at a certain step can then be obtained by integrating over all possible values times the probability to obtain the value at the previous step times the transition probability from the previous to current value

$$p_i(x) = \int dx' p_{i-1}(x')\Gamma(x, x') \tag{2.14}$$

The process can be called **stationary** when the distribution $p_i(x)$ is the same for all steps after some step i_{min}

$$p_i(x) \equiv p(x) \quad \forall i > i_{min} \tag{2.15}$$

A sufficient but not necessary condition for a Markov process to be stationary is the **detailed balance** condition

$$p(x)\Gamma(x, x') = p(x')\Gamma(x', x) \tag{2.16}$$

The equation 2.16 indicates that the probability of a transition from a value x to another value x' is the same as the backward transition.
Our goal is to sample the stationary distribution $p(x)$. As we cannot sample directly $p(x)$ which may be too complicated, we can define a Markov process with transition probability $\Gamma(x, x')$. We may start from a random value and sample the next value from the transition probability Γ. We iterate for several steps and after a certain amount of steps the condition 2.16 ensures that values will be distributed according to the targeted probability distribution $p(x)$. The difficulty lies in finding a transition probability $\Gamma(x, x')$ that we can sample and satisfies the detailed balance condition. We can decompose the transition probability as

$$\Gamma(x, x') = T(x, x')A(x, x') \tag{2.17}$$

where $T(x, x')$ is an arbitrary transition probability and $A(x, x')$ is an acceptance probability$A(x, x')$. We can sample transitions from the distribution T but we do not accept all transitions. If a transition is rejected the new value will be the same as the current value. This acceptance probability is chosen in order to satisfy the detailed balance condition 2.16. In particular we choose

$$A(x, x') = min\left(1, \frac{p(x')T(x', x)}{p(x)T(x, x')}\right) \tag{2.18}$$

This choice of the acceptance probability distribution ensures that the Markov process will converge to the targeted distribution function $p(x)$ for any choice of $T(x, x')$. As the choice of T no longer matters, we may choose a Gaussian distribution.

$$T(x, x') = \frac{1}{\sqrt{2\pi\sigma}} \exp -\frac{(x - x')^2}{2\sigma^2} \tag{2.19}$$

We notice that this choice of probability is symmetric : the probability to perform a move is equal to the probability of the opposite move. In this case the expression for the acceptance probability becomes even simpler

$$A(x, x') = min\left(1, \frac{p(x')}{p(x)}\right) \tag{2.20}$$

The variance is a free parameter of the Markov process and will not affect the equilibrium distribution. However it does affect the efficiency of the sampling. In fact, a large variance will allow to explore more configurations , however the acceptance ratio is likely to be very small and most moves will be rejected and thus "wasted". A small variance is not desirable either, as most moves will be accepted but the space of all possible values is explored very slowly. In order to choose an optimal variance we can look at the acceptance ratio r, equal to the ratio of number of accepted moves and the total number of moves. For an efficient simulation the mean value of the ratio should lie in the range $r \approx 30 - 70\%$. In summary to sample an arbitrary distribution function $p(x)$ all we need to do is

1. Start from an initial value x_0.

2. Sample a new value x' according to a gaussian distribution using the Box-Muller algorithm centered on the current value x and arbitrary variance.

3. If $p(x') > p(x)$ accept the move. Otherwise generate a uniform random number $r \in (0, 1)$. If $p(x')/p(x) > r$ accept the move otherwise the move is rejected.

4. If the move was accepted set the new value equal to x' otherwise set the new value equal to the current one. Go back to step 2.

After a certain number of steps, the detailed balance conditions ensures that the sequence of values $\{x_i\}$ will be distributed according to the distribution $p(x)$. Notice that the algorithm only depends on the ratio $p(x)/p(x')$. Thus the algorithm remains the same if we multiply the distribution function by a constant. In other words, we do not need to worry about the normalization and we may use an unnormalized distribution whose integral does not sum to one.

2.2 Importance sampling

Suppose we want to measure the average

$$\langle O \rangle = \frac{\int dx p(x) O(x)}{\int dx p(x)} \tag{2.21}$$

with respect to some observable O and some probability distribution $p(x)$. The denominator takes into account that the distribution may not be normalized.
We may perform the interagral using the Monte-Carlo method, i.e. sampling the random variable from the distribution $p(x)$. However, the distribution may be difficult to sample. In that case, we may want to draw samples from another distribution $f(x)$, easier to sample. We note that the average 2.23 may be rewritten as

$$\langle O \rangle = \frac{\int dx f(x) \frac{p(x)}{f(x)} O(x)}{\int dx f(x) \frac{p(x)}{f(x)}} = \tag{2.22}$$

$$= \frac{\int dx f(x) w(x) O(x)}{\int dx f(x) w(x)} \tag{2.23}$$

which can be interpreted as a weighted average of the observable O with weight $w(x) = p(x)/f(x)$ and probability distribution $f(x)$. Thus we can perform the original average 2.23 by averaging over a different distribution, simpler to sample, with the benefit of a much more efficient sampling. However, this distribution change comes at a cost : we need to perform a weighted average instead of a normal average. As long as the two distributions are similar, the weight will not flucutuate much during the sampling and does not hurt the efficiency of the simulation. However if the two distributions are

very different the weight will fluctuate wildly during the sampling, and may assume both very small and large values. However, only random variables with an associated large weight will actually contribute to the average, while configurations with small weight only have a negligible role. Of all sampled configurations only a few will actually matter, which in practice means that the effective number of samples is much smaller than the number of samples drawn from the distribution $f(x)$, harming the efficiency of the simulation. In practice one can earn efficiency using importance sampling only if the two distributions are similar. In this case the ratio will not fluctuate much and the simulation will remain efficient. A useful parameter to characterize the efficiency of the simulation is the effective weight $w_{\text{eff}}(x)$.

$$w_{\text{eff}}(x) = \frac{\left\langle \frac{p(x)}{f(x)} \right\rangle^2}{\left\langle \left(\frac{p(x)}{f(x)} \right)^2 \right\rangle} \tag{2.24}$$

The effective weight is a number between 0 and 1. An effective weight of 1 indicates a constant weight and maximum efficiency, while a small effective ratio indicates a wildly fluctuating weight and very low efficiency.

2.3 Variational Monte-Carlo (VMC)

Let us consider the problem of solving the quantum hamiltonian of N interacting particles

$$H = -\frac{\hbar^2}{2m} \sum_i \frac{\partial^2}{\partial^2_{x_i^\sigma}} + V(x_1, x_2..., x_N) \tag{2.25}$$

Suppose we want to measure the mean value of some observable $\hat{O}$ in its ground-state. We may not know the exact ground-state wavefunction , but we may have a good ansatz for the wavefunction $\Psi(x_1, x_2, ...x_N)$. The average of the observable O is

$$\langle O \rangle_\Psi = \frac{\int dX \Psi^*(X) \langle X | O | \Psi \rangle}{\int dX |\Psi(X)|^2} \tag{2.26}$$

where we denote with $X = \{x_1, x_2, ...x_N\}$ the collection of the N particle coordinates. Notice that the expression in the denominator is required as the wavefunction may not be normalized. This expression may be rewritten as

$$\langle O \rangle_\Psi = \frac{\int dX |\Psi(X)|^2 \frac{\langle X|O|\Psi\rangle}{\Psi(X)}}{\int dX |\Psi(X)|^2} \tag{2.27}$$

We can now interpret the integral as an average over the distribution function $\frac{|\Psi(x)|^2}{\int dx|\Psi(X)|^2}$ of the local operator $O_L(X) = \frac{\langle X|O|\Psi\rangle}{\Psi(X)}$.We saw how to use the Metropolis algorithm to sample an arbitrary function $p(x)$. However x can be any object of any configuration space and need not to be restricted to $x \in \Re$. In particular we can use the Metropolis algorithm, described in the previous section, to generate many-particle configurations X with probability density $p(X) = |\Psi(X)|^2$. A tyipical VMC simulation constists in

1. Start from a random configuration $X = \{x_1, x_2...x_N\}$

2. Generate N random distances $\{d_i\}$ from a gaussian distribution $N(0, \sigma)\}$

3. Generate a new configuration X' by displacing each particle of the sampled distance d_i

$$X' = \{x_i + d_i\} \quad d_i \in N(0, 1) \tag{2.28}$$

4. Compute the ratio of the wavefunction computed in the old and new configurations

$$p = \frac{|\Psi(X')|^2}{|\Psi(X)|^2} \tag{2.29}$$

5. If $p > 1$ accept the new configuration. Otherwise generate a random number r with uniform probability between zero and 1. If $r < p$ accept the new configuration, otherwise the configuration is rejected.

6. If the move is accepted set $X \to X'$, otherwise keep the current configuration. Go back to step 2.

After a few iterations, the Metropolis algorithm will generate configurations distributed according to the square of the wavefunction and one can begin to accumulate the average of the observables we are interested in.

2.4 Trial Wavefunctions

The success of VMC stems from the quality of the ansatz wavefunction. Fortunately for many systems some very good ansatz for the ground-state wavefunction are known. A good wavefunction needs not only to be accurate, but should also be computationally efficient, i.e. the evaluation of the wavefunction should scale polynomially with the size of the system. Luckily

for bosons, a very good approximation to the wavefunction is given by the form

$$\Psi(X) = \Psi_{1B}(X)\Psi_{2B}(X)\Psi_{3B}(X) \tag{2.30}$$

$$\Psi_{1B}(X) = \prod_i \phi_i(x_i) \tag{2.31}$$

$$\Psi_{2B}(X) = \prod_{i<j} f(x_i - x_j) \tag{2.32}$$

$$\Psi_{3B}(X) = \prod_{i<j<k} g(x_i - x_j, x_i - x_k) \tag{2.33}$$

$$\tag{2.34}$$

where $X = \{x_1...x_N\}$ represents the many-body spatial configuration of the system and ϕ, f, g are arbitrary one dimensional functions, which characterize respectively one-body,two-body and three-body correlations. If the system is translationally symmetric, for instance in the case of a homogeneous system, the one-body term no longer plays a role.
The second product in the wavefunction over all particle pairs is essential to reproduce the correlations in the system. It was famously introduced by Jastrow[54] , as an ansatz for solving the many body problem which has proven to be quite successful[52, 55]. For instance it has been successfully used to describe liquid Helium and it is able to describe the ground state of the Lieb-Lieniger model with very high accuracy[56]. The third product over all triples includes explicitly three-body correlations. The term Ψ_{2B} is already able to describe three body and higher order correlations mediated by two body interactions and often this last term often provides only a small correction and can often be neglected [56, 55]. An useful approximate representation is given by the form

$$\Psi_{3B} = exp\left\{\lambda_T \sum_i \left(\sum_j \xi(x_i - x_j)\right)^2\right\} \tag{2.35}$$

where ξ is some arbitrary function and λ_T is a variational parameter.Three body correlations are described by the sum over three indices contained in the exponent of equation 2.35. This representation is useful because one only needs to determine a one dimensional function $\xi(x)$ instead of a two dimensional wavefunction g(x,y). This form is more convenient as one needs to parametrize just a one dimensional function instead of the two dimensional function $g(x, y)$.
The ansatz $\Psi(X)$ for the wavefunction can also be justified from the generalized Feynman-Kacs formula and many-body perturbation theory [57]. One

may choose any functional form for the two-body correlation function f , as long as it satisfies the so called **cusp condition**. At small inter-species distances the wavefunction is dominated by two-body physics and correlations with other particles do not play a significant role. Thus the two-body correlation function should be chosen such to match the two-body solution $u_2(x)$ in the limit of vanishing inter-species distance.

$$f(x) \propto u_2(x) \tag{2.36}$$

Another important requirement is that the wavefunction should satisfy the main symmetries of the hamiltonian and the boundary conditions. For instance it is easy to verify that the proposed many-body wavefunction is symmetric under particle exchange, as required by the wavefunction of a bosonic system. In general the wavefunction is not normalized. However we have already seen that in a VMC simulation we do not require the wavefunction to be normalized.

2.5 Wavefunction Optimization

As the choice of the correlator f, g, ϕ is free we may choose these correlators in order to minimize the energy of the variational wavefunction. More generally speaking , our wavefunction may depend on P parameters. Let us denote these parameters as the vector $\alpha = (\alpha_1, ..., \alpha_P)^T$. Then one needs to find the parameters which minimize the average energy.

$$E(\alpha) = \frac{\langle \Psi_\alpha \,|\, H \,|\, \Psi_\alpha \rangle}{\langle \Psi_\alpha \,|\, \Psi_\alpha \rangle} \tag{2.37}$$

The energy can be estimated in a VMC simulation as

$$E(\alpha) = \frac{\int dX |\Psi_\alpha(X)|^2 e_l(X))}{\int dX |\Psi_\alpha(X)|^2} = \langle e_l(X) \rangle \tag{2.38}$$

where $e_l(X) = \frac{H\Psi(X)_\alpha}{\Psi_\alpha(X)}$ is the local energy and $\Psi_\alpha(X) = \langle X \,|\, \Psi_\alpha \rangle$ is the wavefunction. One method to minimize $\Psi_\alpha(X)$ consists in running several simulations for several values of the first parameter α_1 while keeping constant all the others. Once chosen an optimal α_1 one then proceeds to optimize , one by one, all other parameters. However this procedure is inefficient and may easily end up in a local minimum instead of the global minimum of the parameter space. In order to overcome this problem one needs to optimize all parameters at once. The simplest method is to use the stochastic gradient algorithm. According to this algorithm one performs a random walk

in parameter space. For each parameter α_i one can estimate the gradient of the energy g given by

$$g_i = \frac{\partial}{\partial_{\alpha_i}} E(\alpha) \tag{2.39}$$

The gradient is estimated during a regular Variational Monte Carlo simulation. When enough statistics has been accumulated, one performs a move in parameter space in the opposite direction of the gradient.

$$\alpha_i \rightarrow \alpha_i - \Delta g_i \tag{2.40}$$

Suppose we change the multidimensional wavefunction parameter a little. If the displacement is not too large we can expand the variational state around the current parameter α_0

$$|\Psi_\alpha\rangle = |\Psi_0\rangle + \sum_{i=1}^{P} |\Psi_i\rangle \, \delta\alpha_i \tag{2.41}$$

where

$$|\Psi_0\rangle = |\Psi_{\alpha_0}\rangle \tag{2.42}$$

$$|\Psi_i\rangle = \frac{\partial \, |\Psi_\alpha\rangle}{\partial \alpha_i} \tag{2.43}$$

However Ψ_α is not normalized. Let us denote by $\overline{\Psi}_\alpha$ the normalized wavefunction.

$$\left|\overline{\Psi}_\alpha\right\rangle = \frac{|\Psi_\alpha\rangle}{\sqrt{\langle \Psi_\alpha \,|\, \Psi_\alpha \rangle}} \tag{2.44}$$

One can then reduce the possible parameter space by only searching parameters that do not alter the normalization. Then one needs to find the minimum of the associated Lagrange functional by solving

$$\nabla_\alpha \{ E(\alpha) + E_{\text{lin}} \left\langle \overline{\Psi}_\alpha \,\middle|\, \overline{\Psi}_\alpha \right\rangle \} = 0 \tag{2.45}$$

where E_{lin} is a Lagrange multiplier. One can then substitute the linear expansion for the wavefunction in expression 2.45 and obtain

$$\delta\alpha = -\Delta S^{-1} g \tag{2.46}$$

where $\Delta = \frac{1}{2E_{\text{lim}}}$ and $\delta\alpha = (\delta\alpha_1, ...\delta\alpha_M)^T$ represents the direction in parameter space that minimizes the energy and S is a $P \times P$ square matrix whose matrix elements are given by

$$S_{i,j} = \left\langle \overline{\Psi}_i \,\middle|\, \overline{\Psi}_j \right\rangle \tag{2.47}$$

where $\left|\overline{\Psi}_i\right\rangle = \partial_{\alpha_i}\left|\overline{\Psi}\right\rangle$. This method is known as stochastic reconfiguration[59]. This procedure is then iterated many times until one converges to the minimum energy. Δ is a free hyper-parameter of the optimization procedure. It needs to be small enough in order for the simulation to be stable. However choosing a small Δ implies that a large number of iterations are required to converge to the minimum energy.
Another iterative method is the so called linear method[60]. The linear method is similar to the stochastic gradient approximation, where we exchange $E(\alpha)$ with $\left\langle\overline{\Psi}_\alpha\right| H \left|\overline{\Psi}_\alpha\right\rangle$. Then one needs to solve

$$\nabla_\alpha \left\{\left\langle\overline{\Psi}_\alpha\right| H \left|\overline{\Psi}_\alpha\right\rangle - E_{\text{lin}} \left\langle\overline{\Psi}_\alpha \middle| \overline{\Psi}_\alpha\right\rangle\right\} = 0 \tag{2.48}$$

After some manipulations one obtains

$$\begin{pmatrix} e & g^T \\ g & \mathcal{H} \end{pmatrix} \begin{pmatrix} 1 \\ \delta\alpha \end{pmatrix} = E_{\text{lin}} \begin{pmatrix} 1 & 0 \\ 0 & S \end{pmatrix} \tag{2.49}$$

where $\mathcal{H}$ is a $P \times P$ matrix with matrix elements

$$\mathcal{H}_{i,j} = \left\langle\overline{\Psi}_i\right| H \left|\overline{\Psi}_j\right\rangle \tag{2.50}$$

The equation can be recast as

$$\overline{H}\delta\overline{\alpha} = E_{\text{lim}}\overline{S}\delta\overline{\alpha} \tag{2.51}$$

where $\overline{H}$ and $\overline{S}$ are extended $(P+1) \times (P+1)$ matrices and $\delta\overline{\alpha}$ is the extended vector $\delta\alpha = (1, \delta\alpha_1, \delta\alpha_2 ... \delta\alpha_P)^T$. Finding a solution to equation 2.49 is equivalent to finding the generalized eigenvalues of the matrix $\overline{H}$ with the overlap matrix $\overline{S}$. This is a standard problem in linear algebra and can be efficiently solved using routines available in linear algebra libraries , such as Lapack.
The matrix elements can be estimated during a usual variational Monte-Carlo run. Once enough statistics has been accumulated , one can build the matrices $\overline{H}$ and $\overline{S}$ and solve the generalized eigenvalue problem, to obtain the vector $\delta\alpha$ which minimizes the energy E_{lim}. We can then make the substitution $\alpha \to \alpha + \delta\alpha$. The new parameter configuration should have a smaller energy but may not be a minimum, unless the optimal wavefunction depends linearly on the parameters and the linear expansion is valid for any value of $\delta\alpha$. In this case the linear method yields the optimal solution in just one step. As most wavefunctions are not linear in the parameters the procedure outlined above needs to be iterated several times until the energy converges to the minimum value. The estimators for the matrix $\overline{S}$ can be written[60] as

$$\overline{S}_{00} = 1 \tag{2.52}$$

$$\overline{S}_{i0} = 0 \quad \overline{S}_{0j} = 0 \tag{2.53}$$

$$\overline{S}_{i,j} = \left\langle \frac{\Psi_i(X)}{\Psi_0(X)} \frac{\Psi_j(X)}{\Psi_0(X)} \right\rangle - \left\langle \frac{\Psi_i(X)}{\Psi_0(X)} \right\rangle \left\langle \frac{\Psi_j(X)}{\Psi_0(X)} \right\rangle \tag{2.54}$$

where the brackets denote the statistical average over the unnormalized wavefunction $\Psi_0(X)$. The $\overline{H}$ matrix elements can be written[60] as

$$\overline{H}_{00} = \langle e_l(X) \rangle \tag{2.55}$$

$$\overline{H}_{i0} = \left\langle \frac{\Psi_i(X)}{\Psi_0(X)} e_l(X) \right\rangle - \left\langle \frac{\Psi_i(X)}{\Psi_0(X)} \right\rangle \langle e_l(X) \rangle \tag{2.56}$$

$$\overline{H}_{0j} = \left[\left\langle \frac{\Psi_j(X)}{\Psi_0(X)} e_l(X) \right\rangle - \left\langle \frac{\Psi_j(X)}{\Psi_0(X)} \right\rangle \langle e_l(X) \rangle \right] + \langle e_j(X) \rangle \tag{2.57}$$

$$\begin{aligned} \overline{H}_{ij} = & \left[\left\langle \frac{\Psi_i(X)}{\Psi_0(X)} \frac{\Psi_j(X)}{\Psi_0(X)} e_l(X) \right\rangle - \left\langle \frac{\Psi_i(X)}{\Psi_0(X)} \right\rangle \left\langle \frac{\Psi_j(X)}{\Psi_0(X)} e_l(X) \right\rangle \right] - \\ & \left[+ \left\langle \frac{\Psi_j(X)}{\Psi_0(X)} \right\rangle \left\langle \frac{\Psi_i(X)}{\Psi_0(X)} e_l(X) \right\rangle - \left\langle \frac{\Psi_i(X)}{\Psi_0(X)} \right\rangle \left\langle \frac{\Psi_j(X)}{\Psi_0(X)} \right\rangle \langle e_l(X) \rangle \right] + \\ & \left[\left\langle \frac{\Psi_i(X)}{\Psi_0(X)} e_j(X) \right\rangle - \left\langle \frac{\Psi_i(X)}{\Psi_0(X)} \right\rangle \left\langle \frac{\Psi_i(X)}{\Psi_0(X)} \right\rangle \langle e_j(X) \rangle \right] \end{aligned} \tag{2.58}$$

where

$$e_j(x) = \partial_{\alpha_j} e_l(X) = \frac{\Psi_j(X)}{\Psi_0(X)} \left(\frac{H\Psi_j(X)}{\Psi_j(X)} - e_l(X) \right) \tag{2.59}$$

is the derivative of the local energy with respect to the parameter α_j. Note that the matrix elements involve the evaluation of terms which can be written as covariances of appropriate operators. This choice of estimators allows one to reduce the statistical error on the matrix elements. The element H_{11} is equal to the local energy. The remainder of the first row of the $\overline{H}$ matrix is an estimate of half the energy gradient . Similarly the first column, besides the first element, is an estimate of half the energy gradient.
However the row and column estimators are not the same. Actually we may note that this definition of the hamiltonian matrix $\overline{H}$ does not appear to be symmetric at all, even though the matrix $\overline{H}$ is supposed to be hermitian. It can actually be shown that for large enough statistics the matrix is symmetric[60], however when the averages are accumulated with a finite number of samples, as in any Monte-Carlo simulation, the matrix may not be symmetric. It has been shown that such an asymmetric choice of the hamiltonian matrix estimator is in general less noisy than the symmetric

estimator[60], and thus more convenient when estimated during a Monte-Carlo simulation.
However this choice raises a stability issue. In fact the matrix $\overline{H}$, estimated in a VMC simulation with a finite number of steps, is no longer symmetric and a solution to the generalized eigen-value problem is not guaranteed. An other stability issue stems from the fact that the generalized eigenvalue equation is only valid for small displacements in the parameter space. However the lowest eigenvector may not be small at all and be outside the realm of validity of the linear expansion . To regularize the problem we may add a constant δ to the diagonal elements of the matrix $\overline{H}$, except the first element. Adding the constant may yield a matrix with real eigenvalues and in general tends to reduce the amplitude of the eigenvector, thus solving both our stability issues. As the optimal value of the shift δ is not known one can try several values of δ , obtaining several parameter variations . For each new parameter one can perform a short VMC run to estimate the energies of each new parameter. Then one selects the parameter which yields the lowest energy.

2.6 Smart Variational Monte-Carlo (SVMC)

We explore here an alternative approach to the problem of sampling the wavefunction. The main concept consists in sampling an auxiliary process whose stationary distribution is equal to the distribution we want to sample. We can choose as an auxiliary process a diffusion process, modeled by a Fokker-Plank equation

$$\partial_\tau f(X,\tau) = D\sum_{i=1}^{N} \nabla_i(\nabla_i - F_i(X))f(X,\tau) \tag{2.60}$$

where D is a diffusion constant, driving the speed of the diffusion, while $F_i(X)$ represents the forces acting on the particles, governing the drift of the particles. We want this process to converge in the large time limit to our target distribution, the square of our many-body wavefunction $\Psi(R)$. Once the stationary regime is reached the function $f(R,\tau)$ will no longer depend on time and we can set the time derivative to zero, obtaining the condition for the stationary distribution

$$D\sum_{i=1}^{N}\left[\nabla_i^2 f(X,\infty) - \nabla_i F_i(X) f(X,\infty) - F_i(X)\nabla_i f(X,\infty)\right] = 0 \tag{2.61}$$

We want to obtain $f(X,\infty) = \frac{\Psi^2(X)}{\int dX \Psi(X)^2}$. We note that if we substitute the targeted distribution $f(X,\infty)$ in equation 2.61 and choose the force

$$F_i(x) = 2\nabla_i \log \Psi(X) \tag{2.62}$$

then the equation 2.61 is satisfied. Our problem of sampling $\Psi(X)^2$ is then recast to the problem of sampling $f(R,\tau)$. This can be accomplished by rewriting $f(R,\tau)$ under the form of a markov process, i.e. we want to obtain the distribution at time τ from the distribution at an earlier time step, for instance the initial time $\tau = 0$. Thus we can write

$$f(X,\tau') = \int dX' G(X,X',\tau'-\tau) f(X',\tau) \tag{2.63}$$

where $G(X,X',\delta\tau)$ is the **Green's Function**. The Green's function represents the probability to observe the configuration X' after a time $\delta\tau$ if the current configuration is X. The convolution of the Green's function and the probability distribution propagates the earlier distribution at time τ to the later distribution at time $\tau+\delta\tau$. For this reason the Green's function is also called a propagator. In order for the Fokker-Plank equation to be satisfied the Green's function needs to satisfy the equation

$$-\partial_\tau G(X,X',\delta\tau) = D\nabla_X . \left(\nabla_X - F(X)\right) G(X,X',\delta\tau) \tag{2.64}$$

where we indicated with $\nabla_X = (\partial_{x_1}, \partial_{x_2} ..., \partial_{x_N})$, a vector of single particle derivatives. If $\delta\tau = 0$ the Green's function is not propagating anything and must satisfy

$$G(X,X',0) = \delta(X-X') \tag{2.65}$$

Formally the solution can be then be written as

$$G(X,X',\delta\tau) = e^{D\delta\tau\nabla^2 - D\delta\tau\nabla_X F(X)} \delta(X-X')) \tag{2.66}$$

The exponent of the exponential is made up of the sum of two terms , the Laplacian term describing the diffusion and the force term describing the drift process. We would like to separate the two contributions. It is well known that $e^{A+B} \neq e^A e^B$ if A and B are two operators which do not commute with each other. However one can approximate $e^{A+B} \approx e^A e^B + O([A,B])$ if the commutator $[A,B]$ is small.This approximation is also known as the Trotter approximation . In our case the exponent is proportional to $\delta\tau$ and the Trotter decomposition is certainly valid in the small time step limit $\delta\tau \to 0$.

$$G(X,X',\delta\tau) \approx e^{D\delta\tau\nabla^2} e^{-D\delta\tau\nabla_X F(X)} \delta(X-X')) \tag{2.67}$$

$$= G_{\text{diff}}(X, X', \delta\tau) G_{\text{drift}}(X, X', \delta\tau) \tag{2.68}$$

which is the product of two different Green's functions,G_{diff} , describing the diffusion process and G_{drift}, describing the drift process. First let us consider the drift process

$$G_{\text{drift}}(X, X', \delta\tau) = e^{-D\delta\tau\nabla_X F(X)}\delta(X - X') \tag{2.69}$$

It can be shown that the propagator can be rewritten as

$$G_{\text{drift}}(X, X', \tau) = \delta(X' - X(\tau)) \tag{2.70}$$

Where $R(\tau)$ obeys the equation

$$\frac{dR}{d\tau} = F(R)R(\tau) \tag{2.71}$$

with the initial condition $R(0) = R$.
In practice it means that if the initial configuration is X , there is only one possible configuration at a later time τ, obtained by solving the drift equation 2.71.

An exact solution also exists for the diffusive Green's function $G_{\text{diff}}(X, X')$.

$$G_{\text{diff}}(X, X', \tau) = e^{D\delta\tau\nabla^2}\delta(X - x') \tag{2.72}$$

The solution is given by

$$G_{\text{diff}}(X, X', \tau) = \frac{e^{-\frac{(X-X')^2}{4D\tau}}}{(4\pi D\tau)^{N/2}} \tag{2.73}$$

which is simply a gaussian distribution with variance $2D\tau$. While in a drift process there is only one possible configuration at each given time, in a purely diffusive process at any time there are infinite possible configurations distributed according to a gaussian.
The approximation 2.68 is only valid for a very small time step. The Green's function at large times is in general not known. However we can substitute equation 2.63 for $f(X, \tau)$ several times

$$f(X, \tau) = \begin{array}{l} \int dX_1 dX_2 ... dX_M G(X, X_M, \delta\tau) G(X_M, X_{M-1}, \delta\tau) ... \\ G(X_1, X_0, \delta\tau) f(X_0, 0) \end{array} \tag{2.74}$$

with $\tau = M\delta\tau$. As long as the time step is sufficiently small, we can use the approximation 2.68 for each Green's function.

Note that each propagator describes the probability for the process to transition from a state X to a state X' and only depends on the configuration at the current time. Interpreting the Green functions as probabilities, we can sample the Green's function to obtain the configuration at a later time $\tau + \delta\tau$. We can repeat this process many times. Thus we have defined a Markov process which , after some time will become stationary and the stationary distribution is equal to our target distribution : the wavefunction we wished to sample. The algorithm can be summarized in the following steps :

1. Start from an initial configuration X_0.
2. Perform a **drift step**. In the small time step limit , one just sets
$$X \to X + D\delta\tau F(X) \tag{2.75}$$
where
$$F(X) = \partial_X \log \Psi(X) \tag{2.76}$$
3. Sample the diffusion process. Set
$$X \to X + \sqrt{2D\delta\tau}\chi \tag{2.77}$$
where χ is a vector of N random numbers distributed according to a standard gaussian, with zero mean and unity variance.
4. Go back to step 2.

After a few iterations, the algorithm will sample configurations distributed according to $\Psi^2(X)$. The algorithm is only valid for very small time steps. A finite step will introduce a bias in the simulation. This bias can however be removed by including a Metropolis step.
We have already defined a Markov process where the transition probability $T(X, X')$ can be written as (at first order approximation in the time step)

$$G(X, X', \delta\tau) = \frac{e^{-\frac{(X-X'+DF(X))^2}{4D\delta\tau}}}{(4\pi D\delta\tau)^{N/2}} \tag{2.78}$$

The acceptance ratio of the Metropolis algorithm then becomes

$$A(X, X') = min\left(1, \frac{G(X', X)\Psi^2(X')}{G(X, X')\Psi^2(X)}\right) \tag{2.79}$$

Note that $G(X, X')$ is not symmetric because of the presence of the drift step . The acceptance ratio can then be rewritten as

$$A(X, X') = min\left(1, e^{Q(X,X')}\frac{\Psi^2(X')}{\Psi^2(X)}\right) \tag{2.80}$$

where

$$Q(X, X', \delta\tau) = \frac{F(X) + F(X')}{2}.\left(D\delta\tau\frac{[F(X) - F(X')]}{2} - X' - X\right) \quad (2.81)$$

Adding a Metropolis acceptance step in the SVMC algorithm the bias due to the finite time step vanishes. Thus we can adjust the time step in order to have an optimal acceptance ratio , in the range $30 - 70\%$. Typically the optimal time step is much larger than the one required by a SVMC algorithm without an acceptance-rejection step.

2.7 Estimators

Once we are able to generate configurations from the square of the wavefunction $|\Psi(x)|^2$ we can begin to measure observables. The average of a certain observable is given by equation 2.27 , wich requires an expression for the local observable

$$O_l(X) = \frac{\langle X|\, O\,|\Psi\rangle}{\Psi(X)} \quad (2.82)$$

We will now describe estimators for some of the most common observables of interest in many-body physics

2.7.1 Energy

One the most important observables is the energy. The corresponding local energy estimator is then given by

$$\begin{aligned} e_l(X) &= \frac{\langle X\,|\,H\,|\,\Psi\rangle}{\Psi(X)} \\ &= \frac{\left\langle X\left|-\frac{\hbar^2}{2m}\sum_i \frac{\partial^2}{\partial x_i^2} + V(X)\right|\Psi\right\rangle}{\Psi(X)} \end{aligned} \quad (2.83)$$

where V(X) is a local interaction potential. Suppose that the wavefunction obeys the Jastrow form

$$\Psi = \prod_{i<j} f(x_i - x_j) \quad (2.84)$$

Then the drift force becomes

$$F_i(X) = 2\partial_X \Psi(X) = \sum_{j\neq i} \partial_x \log f(x)\Big|_{x=|x_i - x_j|} sign(x_i - x_j) \quad (2.85)$$

and the local energy can be written as

$$e_l(X) = -\frac{\hbar^2}{2m}\left(\sum_{i\neq j}\frac{\partial^2}{\partial x^2}\log f(x)\Big|_{x=|x_i-x_j|} sign(x_i-x_j) + \frac{1}{4}\sum_i F_i(X)^2\right) + V(x) \tag{2.86}$$

Notice that evaluating the local estimator for the energy requires $O(N^2)$ operations, where N is the number of particles.

2.7.2 Pair correlation

We already discussed the pair correlation

$$g(x) = \frac{1}{n^2}\left\langle \Psi^\dagger(x)\Psi^\dagger(0)\Psi(x)\Psi(0)\right\rangle \tag{2.87}$$

which represents the probability to find a particle at distance x from another particle. The pair correlation can also be written as

$$g(x) = V\left(1-\frac{1}{N}\right)\int dX \frac{|\Psi(X)|^2}{\int dX|\Psi(X)|^2}\delta(x-|x_i-x_j|) \tag{2.88}$$

The pair correlation function can be easily estimated by computing an histogram of relative distances between two particles , accumulated over all sampled configurations and all possible particle pairs. At large distances correlations between particles vanish and the pair correlation function saturates to a constant value, equal to one, by an appropriate choice of the normalization factor.

2.7.3 Static Structure Factor

The structure factor can be written as

$$S(k) = \frac{1}{N}\int dX \frac{|\Psi(X)|^2}{\int dX|\Psi(X)|^2}\sum_{i,j} e^{ik(x_i-x_j)} \tag{2.89}$$

$$= \frac{1}{N}\left\langle \sum_{i,j} e^{ik(x_i-x_j)}\right\rangle \tag{2.90}$$

$$= \frac{1}{N}\left\langle \left|\sum_i e^{ikx_i}\right|^2\right\rangle \tag{2.91}$$

Note that in evaluating the structure factor, the momentum k must be compatible with the periodic boundary conditions, i.e. it must satisfy $k = n2\pi/L$

where L is the length of the box. The structure factor can also be obtained indirectly from the Fourier transform of the pair correlation.

$$S(k) = 1 + n \int dx e^{ikx} \left[g(x) - 1 \right] \tag{2.92}$$

However the direct evaluation is less sensitive to finite-size effects.

2.7.4 Off diagonal one-Body density matrix (OBDM)

The One-body density matrix is defined as

$$\rho(x) = \left\langle \Psi^{\dagger}(x)\Psi(0) \right\rangle \tag{2.93}$$

While all the other observables introduced so far where local, the OBDM is not. In terms of the wavefunction the OBDM can be rewritten as

$$\rho(x) = \int dX \frac{|\Psi(X)|^2}{\int dX |\Psi(X)|^2} \frac{\Psi(x_1 + x, x_2, ...)}{\Psi(x_1, ..., x_n)} \tag{2.94}$$

An efficient estimator may be designed by averaging the ratio $\frac{\Psi(x_1+x,x_2,...)}{\Psi(x_1,...,x_n)}$ over all the particles , for different values of the distance x. To increase the efficiency of the estimator, one may choose the distances x randomly from a uniform distribution between zero and half the box length.

2.8 Diffusion Monte-Carlo (DMC)

Diffusion Monte-Carlo is another Monte-Carlo technique , related to the VMC algorithm. While VMC is not an exact technique as we usually do not know the exact wavefunction the DMC algorithm can yield the ground-state properties of a bosonic hamiltonian with arbitrary accuracy. Let us consider the hamiltonian.

$$H = -\sum_{i=1}^{N} \frac{\hbar^2}{2m} \frac{\partial^2}{\partial_{x_i}^2} + \sum_{i<j} V(x_i - x_j) \tag{2.95}$$

Our goal is to acess the ground-state properties of the hamiltonian H. Let us start from some arbitrary state $|\Psi\rangle$. The state can also be written as a linear combination of eigenstates of the hamiltonian H

$$|\Psi\rangle = \sum_{n} c_n |\Psi_n\rangle \tag{2.96}$$

We also may evolve the state Ψ in imaginary time

$$|\Psi(\tau)\rangle = e^{-\frac{1}{\hbar}H\tau}\,|\Psi\rangle \tag{2.97}$$

which upon substitution of the expansion 2.96 takes the form

$$|\Psi(\tau)\rangle = \sum_n e^{-\frac{1}{\hbar}E_n\tau}\,|\Psi_n\rangle \tag{2.98}$$

where E_n is the energy of the n_{th} excited state. Upon imaginary time evolution each coefficient c_n gets multiplied by an exponential factor $e^{-\frac{1}{\hbar}E_n\tau}$, which becomes exponentially small when $\frac{1}{\hbar}E_n\tau \gg 1$. At long times all excited states become exponentially suppressed. When $\tau \gg \frac{\hbar}{E_1}$, where E_1 is the energy of the first excited state, the contribution to the time evolved state becomes negligible and the time-evolved state is dominated by the lowest energy state

$$|\Psi(\tau)\rangle \propto e^{-\frac{1}{\hbar}E_0\tau}\,|\Psi(0)\rangle \tag{2.99}$$

Evolution in imaginary time is thus able to filter out the ground-state from higher energy states. Methods that perform the time evolution of a state in order to retrieve its lowest energy state component are called **projective methods**.
The DMC algorithm, as many other variants of zero-temperature quantum Monte-Carlo methods, is part of this subclass of methods.
Let us consider the time evolved state in real space representation

$$\Psi(X,\tau) = \langle X|\, e^{-\frac{1}{\hbar}H\tau}\,|\Psi\rangle \tag{2.100}$$

One can insert the identity $I = \int dX'\,|X'\rangle\,\langle X'|$ in the previous expression and obtain

$$\Psi(X,\tau) = \int dX' G(X,X',\tau)\Psi(X') \tag{2.101}$$

where we introduced the Green's function $G(X,X',\tau)$ defined as

$$G(X,X') = \langle X'|\, e^{-\frac{1}{\hbar}H\tau}\,|X\rangle \tag{2.102}$$

The Green's function must also satisfy the equation

$$-\frac{\partial G(X,X',\tau)}{\partial\tau} = \frac{1}{\hbar}HG(X,X',\tau) \tag{2.103}$$

The Green's function describes the probability amplitude to find the system in configuration X' after a certain amount of time τ after a measurement which yielded the particle configuration X. The approach is similar to the

one adopted in SVMC, but with a slightly different form for the propagator. The time evolution operation, for the hamiltonian 2.95 is

$$e^{-\frac{\tau}{\hbar}\left(-\frac{\hbar^2}{2m}\nabla_X^2+V(X)\right)} \tag{2.104}$$

As we did in SVMC , for small time steps we are allowed to break up the exponential in the product of two exponentials

$$e^{-\frac{\tau}{\hbar}\left(-\frac{\hbar^2}{2m}\nabla_X^2+V(X)\right)} \approx e^{\frac{\hbar\tau}{2m}\nabla_X^2}e^{-\frac{\tau}{\hbar}V(X)} + O(\tau^2) \tag{2.105}$$

Inserting another identity between the two time evolution operators one obtains an expression for the Green's function

$$G(X,X') = \int dX'' G_{\text{diff}}(X',X'')G_{int}(X,X'') \tag{2.106}$$

The kinetic part of the break-up gives rise to the Green's function

$$G_{\text{diff}}(X,X',\tau) = e^{D\delta\tau\nabla^2}\delta(X-X') \tag{2.107}$$

where $D = \frac{\hbar\tau}{2m}$. Note that the propagator 2.107 is equivalent to the propagator of a purely diffusive system. We encountered this propagator during the discussion on SVMC and we know that the propagator can be written as

$$G_{\text{diff}}(X,X',\tau) = \frac{e^{-\frac{(X-X')^2}{4D\tau}}}{(4\pi D\tau)^{N/2}} \tag{2.108}$$

The interaction term , if we assume that the potential is local gives

$$G_{\text{int}}(X,X') = e^{-\frac{\tau}{\hbar}V(X)}\delta(X-X') \tag{2.109}$$

Interactions do not change the space configurations, but they multiply the wavefunction by a factor that depends exponentially on the interaction potential.
One can then devise a Markov process, similar to the SVMC Markov process, where we sample from the diffusive Green's function and accumulate at step M the weight $W_{\text{int}}(X_M) = \prod_{j=1}^{M} e^{-\frac{\tau}{\hbar}V(X_j)}$, which depends not only on the current configuration but also on all previous configurations.
Averaging the mean value of some observable now consists in sampling a purely diffusive process and performing a weighted average with the running weigth $W_{\text{int}}(X_M; X_1, X_2...)$. However this is not a Markov process, as the weight depends on the whole history of the Markov chain. It is also likely that the weight will fluctuate a lot during the simulation. And we already

learned when discussing importance sampling that a weight with large fluctuations destroys the efficiency of the simulation.
An alternative method is to try to sample the interacting Green's function. One solution is to create a number of copies of the current configuration X proportional to the weight $W(X) = e^{-\frac{\tau}{\hbar}V(X)}$. We call each copy a *walker* and the process of walker generations branching. After performing the branching we can again evolve in time each walker and perform a branching operation for each walker. When making measurements one averages over all walkers at the current time. This is equivalent to performing measurements with the running weight $W_{\text{int}}(X_M; X_1, X_2...)$. Note that the number of copies of a walker present in the next step may even be zero. When this happen we say that a walker has been killed. The total number of walkers during the simulation may thus both increase and decrease. The average number of walkers thus needs not to keep increasing during the simulation.
We saw that in the large-time limit the wavefunction is proportional to the ground-state multiplied by a factor $e^{-E_0\frac{\tau}{\hbar}}$, which is exponentially small in the large-time limit. To get rid of this coefficient we can multiply the wavefunction by a coefficient $e^{E_0\frac{\tau}{\hbar}}$. Of course , before performing the simulation we do not known the ground-state energy. However we can substitute E_0 with our best approximation for the ground-state energy E_T , by averaging the local energy over all walkers at the current time step. Then we can include this additional weight in the branching weight $W(X) = e^{-(V(x)-E_0)\frac{\tau}{\hbar}}$. However the walker population may occasionally become very large or very small. Such large fluctuations in the number of walkers will hamper the efficiency of the simulation. In order to overcome this problem one can impose that the population of walkers should fluctuate within a certain range. As the number of walkers at each step is controlled by the sum of the weights $W(X)$ over all walkers, one can just introduce a shift in the energy E_T by making the substitution $E_T \to E_T + \delta E_T$ in order to increase or decrease the population of walkers. For instance we may set

$$\delta E_T = \begin{cases} \frac{1}{\delta\tau}\log\frac{\langle N_w\rangle}{N_w+\delta N_w/2} & \text{if} \quad N_w > \langle N_w\rangle + \delta N_w/2 \\ \frac{1}{\delta\tau}\log\frac{\langle N_w\rangle}{N_w-\delta N_w/2} & \text{if} \quad N_w < \langle N_w\rangle - \delta N_w/2 \\ 0 & \langle N_w\rangle - \delta N_w/2 < N_w < \langle N_w\rangle + \delta N_w/2 \end{cases} \tag{2.110}$$

where N_w is the current walker population, $\langle N_w\rangle$ is the desired average number of walkers and δN_w is the width of the allowed population distribution. However this constrain on the walker population imposes a bias to the simulation. The correct sampling of the wavefunction is recovered only when the average number of walkers becomes very large, i.e. in the limit $\langle N_w\rangle \to \infty$.
In summary the DMC algorithm here exposed can be summarized as

1. Start from $N_w(0)$ walkers , distributed according to the initial state wavefunction.

2. Perform the diffusion. Set

$$X_i' \to X_i + \sqrt{2D\delta\tau}\xi_i \tag{2.111}$$

whe ξ_i is a vector of N random numbers drawn from a standard gaussian, with zero mean and unitary variance.

3. Perform the branching for each walker

$$n_i = \text{int}[e^{-\delta\tau\left(\frac{V(X)+V(X')}{2}-E_T\right)} + \xi] \tag{2.112}$$

where ξ is a uniformly generated random number between zero and one.

4. Set the energy E_T equal to the average of the local energy over all the walkers at this time step.

5. Perform the control on the number of walkers. Make the energy shift $E_T \to E_T + \delta E_T$ to control the number of walkers, described by equation 2.110

6. Go back to step 2

The main problem with the algorithm outlined above is that the method is efficient as long as the number of walkers do not fluctuate too much. However, the exponent of the branching factor fluctuates a lot during the simulation , which leads to enormous fluctuations in the walker population.
This problem can be solved by guiding the sampling with an ansatz for the ground-state wavefunction of the hamiltonian.

2.8.1 Importance Sampling

The main idea is not to sample the ground-state wavefunction of the hamiltonian, but the product of the ground-state wavefunction and a guiding wavefunction , to guide the sampling and reduce the fluctuations in the walker population. Instead of trying to sample the true ground-state wavefunction we will be sampling the product of the time evolved wavefunction $\Phi(X,\tau)$ and a time-independent guiding wavefunction $\Psi(X)$.

$$f(X,\tau) = \Psi(X)\Phi(X,\tau) \tag{2.113}$$

Using the expression of $\Phi(X,\tau)$ in terms of its Green's function we get

$$f(X,\tau) = \Psi(X)\Phi(X,\tau) = \int dX'\Psi(X)G(X,X',\tau)\Phi(X',0) \tag{2.114}$$

$$= \int dX'\Psi(X)G(X,X',\tau)\frac{1}{\Psi(X')}f(X',0) \tag{2.115}$$

$$= \int dX'G_{\text{is}}(X,X',\tau)f(X',0) \tag{2.116}$$

where we have defined the importance sampling Green's function

$$G_{\text{T}}(X,X',\tau) = \Psi(X)G(X,X',\tau)\frac{1}{\Psi(X')} \tag{2.117}$$

As for the pure Green's function, an analytical solution can be obtained in the limit of vanishing time step

$$-\frac{\partial G_T(X,X',\tau)}{\partial\tau} = \left(\Psi(X)H\frac{1}{\Psi(X')} - E_T\right)G(X,X',\tau) \tag{2.118}$$

$$= H_{\text{T}}G(X,X',\tau) \tag{2.119}$$

with the effective hamiltonian

$$H_T = -\frac{\hbar^2}{2m}\frac{\partial^2}{\partial_x^2} + \frac{\hbar^2}{2m}\partial_X F(X) + E_L(X) \tag{2.120}$$

where $E_L(X)$ is the local energy and

$$F(X) = 2\partial_X \log\Psi(X) \tag{2.121}$$

is the drift force. The formal solution is given by

$$G(X,X') = e^{-\frac{1}{\hbar}H_T}\delta(X-X') \tag{2.122}$$

In the limit of vanishing time step the Green's function can be computed exactly. At first order the Green's function can be written as

$$G(X,X',\delta\tau) = G_{\text{drift;diff}}(X,X',\delta\tau)W(X,X',\delta\tau) \tag{2.123}$$

where

$$G_{\text{drift;diff}\tau}(X,X',\delta\tau) = \frac{1}{\sqrt{2\pi D\delta\tau}}e^{-\frac{(X-X'-D\tau F(X))^2}{2D\delta\tau}} \tag{2.124}$$

is a gaussian with variance $D = \frac{\hbar^2}{2m}$ shifted by an amount proportional to the drift force F. This diffusion-drift process is equivalent, at first order in

the time step, to the SVMC algorithm. However the full Green's function contains an additional term

$$W(X, X') = e^{-\delta\tau\left(\frac{E_L(X)+E_L(X')}{2}-E_T\right)} \tag{2.125}$$

which we can use as a branching weight, as in the pure DMC algorithm. However, the branching weight involves the local energy instead of the local potential. While the local potential fluctuates a lot between different configurations, the local energy fluctuates mildly provided that the guiding wavefunction remains close to the actual ground-state of the system.
In conclusion, the DMC algorithm with importance sampling consists in a diffusion-drift process identical to the drift-diffusion process of the SVMC algorithm, but with an added branching step , as in pure DMC. However, the branching weight is varying more smoothly. Step by step the DMC algorithm with importance sampling consists in

1. Start from $N_w(0)$ walkers , distributed according to the initial state wavefunction.

2. Perform the diffusion + drift step. Set

$$X_i' \to X_i + \sqrt{2D\delta\tau}\xi_i + \delta\tau F(X) \tag{2.126}$$

   whe ξ_i is a vector of N random numbers drawn from a standard gaussian, with zero mean and unitary variance.

3. Perform the branching for each walker

$$n_i = \text{int}[e^{-\delta\tau\frac{E_L(X)+E_L(X')-E_T)}{2}} + \xi] \tag{2.127}$$

   where ξ is an uniformly generated random number between zero and one.

4. Set the energy E_T equal to the average of the local energy over all the walkers at this time step.

5. Perform the control on the number of walkers. Make the energy shift $E_T \to E_T + \delta E_T$ to control the number of walkers, described by equation 2.110

6. Go back to step 2

An illustration of the branching process can be found in Fig. 2.1.

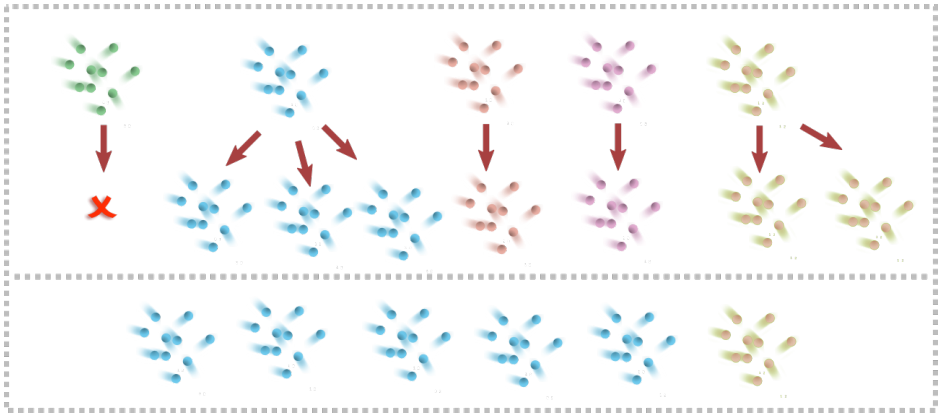

Figure 2.1: Cartoon to represent the evolution of walkers in a branching step. The green walker is killed , blue and orange walkers reproduce while the other walkers are not affected by the branching step. The final row represents a typical configuration after a long time evolution. Notice that most walkers are blue , meaning they all are descendants of the initial blue walker.

2.8.2 Contact interations

Let us suppose we want to simulate a system with contact interactions. As one cannot evaluate numerically a Dirac delta function, we may approximate the delta potential with some other finite-range potential , such as a rectangular potential, and extrapolate to the zero range limit. Alternatively , one may entirely get rid of the potential by imposing the Bethe-Peierls boundary conditions on the ground-state wavefunction. The Bethe-Peierls boundary conditions impose the presence of a discontinuity of the derivative of the wavefunction at vanishing interparticle distance.

$$\left(\frac{\partial}{\partial(x_i - x_j)} \Psi(X) \Big|_{x_i - x_j = 0+} - \frac{\partial}{\partial(x_i - x_j)} \Psi(X) \Big|_{x_i - x_j = 0-} \right) = -\frac{1}{a} \Psi(X) \Big|_{x_i - x_j = 0} \tag{2.128}$$

where a is the scattering length. In a DMC calculation with importance sampling, imposing the boundary conditions 2.128 on the trial wavefunction is equivalent to imposing the boundary conditions on the ground-state wavefunction. If the wavefunction takes the Jastrow form and only two-body interactions are present, the condition 2.128 is satisfied if the two-body

Jastrow function has a discontinuity in the derivative at the origin given by

$$\frac{1}{2}(f'(x=0+) - f'(x=0-)) = -\frac{1}{a}f(x=0) \tag{2.129}$$

Repulsive interactions with periodic boundary conditions

For repulsive interactions a good choice for the jastrow function in a box of length L with periodic boundary conditions is

$$f(x) = \begin{cases} \sin(kx+\delta) & x < X_m \\ \sin(\frac{\pi x}{L})^\beta & X_m < x < L \end{cases} \tag{2.130}$$

with

$$\tan\delta(k) = \frac{\hbar^2}{m^* g} \tag{2.131}$$

The wavefunction is chosen to be equal to the two-body scattering solution up to the matching point X_m. At larger distances the wavefunction is chosen such that in the limit $L \to \infty$ the wavefunction $f(x)$ decays algebraically , as predicted from LL theory, while remaining compatible with periodic boundary conditions for a finite box size L. The parameter β can be chosen as a variational parameter, while the matching point X_m and the wavenumber k are fixed by ensuring the continuity of the wavefunction and its first derivative at the matching point.

Attractive interactions with periodic boundary conditions

For attractive interactions , where the scattering length is positive , one may choose the Jastrow factor

$$h(x) = \begin{cases} e^{-x/a} & x < X_m \\ \sin(\frac{\pi x}{L})^\beta & X_m < x < L \end{cases} \tag{2.132}$$

The function $h(x)$ is equal to the bound state of the two-body problem up to the matching point X_m. At greater distances we assume the same functional form used for repulsive interactions.
Also in this case β is a free variational parameter, while X_m and k are fixed by imposing continuity of the Jastrow term and its first derivative at the matching point X_m.

Repulsive Interactions without periodic boundary conditions

Let us take the limit $L \to \infty$ of a very large box. As $kx \ll 1$ in this limit we can expand the function 2.130 around $kx = 0$ obtaining

$$f(x) = x + a \tag{2.133}$$

We will be using this functional form in simulations without periodic boundary conditions, i.e. in presence of a confining potential.

(2.134)

Attractive Interactions without periodic boundary conditions

For negative coupling, without periodic boundary conditions we can choose the form

$$f(x) = exp\left[-\frac{x}{a}\frac{(\alpha x + p)}{x + p}\right] \tag{2.135}$$

where α and p are variational parameters. In the limit $x \to 0$ one gets the two-body solution. At large distances the fall-off is still exponential , but with a different rate given by α/a.

An example: the Lieb-Liniger gas

We discussed that DMC yields for bosons an exact result only in the limit of small time step and large walker population. In practice one always uses a finite walker population and a finite time step which bias the results of the algorithm. Here we discuss the bias on the energy in function of both the time step and the number of walkers for the typical case of the Lieb-Liniger model with $\gamma = 1$, which corresponds to interactions of intermediate strength.
We use the trial wavefunction

$$\Psi_T(X) = \prod_{i<j} f(x_i - x_j) \tag{2.136}$$

where f is given by equation 2.130 with $X_m = L/2$.
In figure 2.2 we report the energy per particle for several values of the time step and $W = 200$ walkers. The energy clearly increases linearly with decreasing time step and a linear extrapolation yields $E/N = 0.31994(4)$, which is greater than the exact value $(E/N)_{LB} = 0.3195756$. The extrapolated energy differs by just $\approx 2 \cdot 10^{-4}$ at $\delta\tau = 1 \cdot 10^{-3}$.
At this value of the time step, we compute the energy for several values of the average walker population. The results are plotted in figure 2.3 versus the inverse of the average walker population W. A linear extrapolation to an infinite number of walkers yields the value $E/N = 0.31953(5)$, in agreement, within the statistical error, with the BA solution.

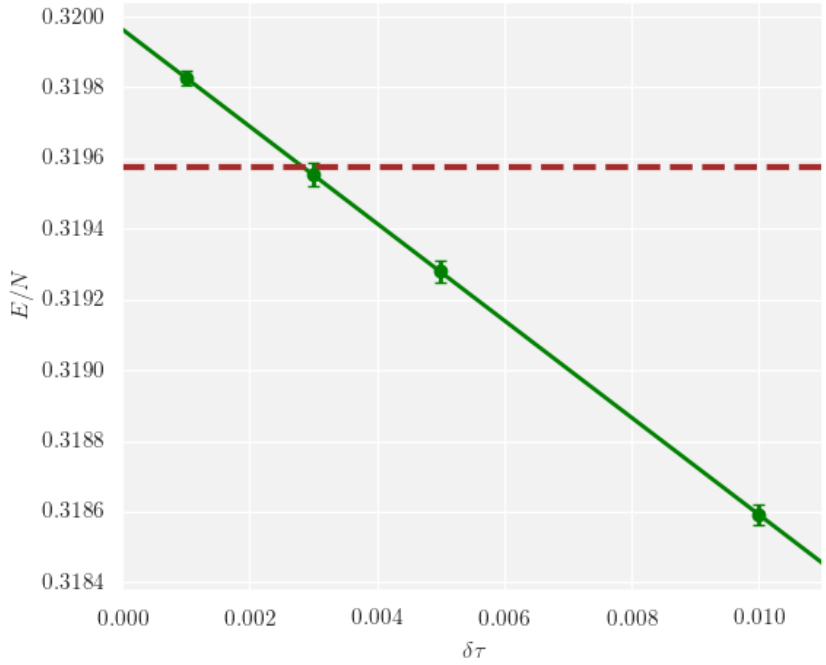

Figure 2.2: Example of time step extrapolation in DMC for the Lieb-Liniger model at $\gamma = 0.1$, with 200 walkers and N=100 particles. The dashed lined marks the exact energy obtained by the BA solution.The energy per particle and the time step are given respectively in units of $\frac{\hbar^2 n^2}{m}$ and $\frac{m}{\hbar n^2}$

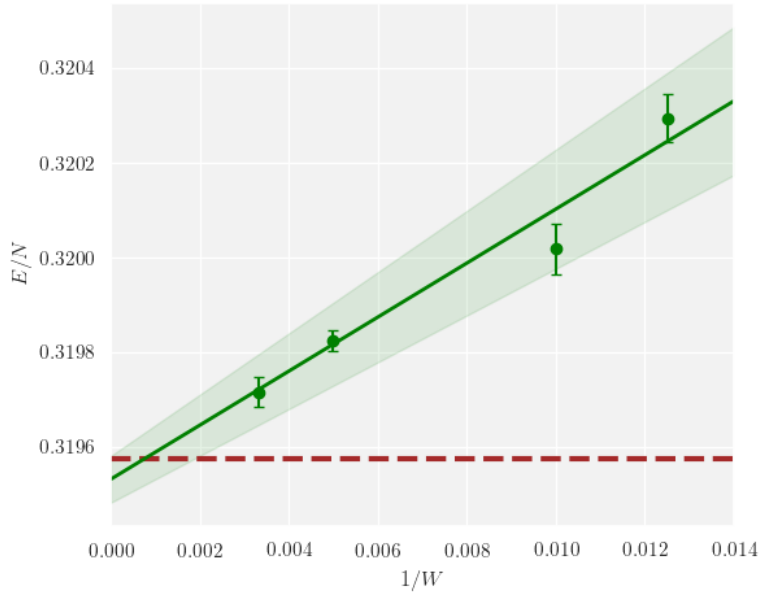

Figure 2.3: Example of extrapolation to infinite walker population in DMC for the Lieb-Liniger model at $\gamma = 0.1$, with time step $\delta\tau = 1e-3$ and N=100 particles. The dashed lined shows the exact energy obtained from the BA solution. The energy per particle and the time step are given respectively in units of $\frac{\hbar^2 n^2}{m}$ and $\frac{m}{\hbar n^2}$

2.8.3 Mixed and pure estimators

One disadvantage of the importance sampling is that we are not sampling the ground-state wavefunction but the product of the ground-state wavefunction $\Phi(X)$ and a guiding wavefunction $\Psi(X)$. Averaging over some local observable O(X) , as we did in SVMC , is equivalent to performing the integral

$$\langle O\rangle = \frac{\int dX \Phi(X)\Psi(X)O(X)}{\int dX \Phi(X)\Psi(X)} \tag{2.137}$$

$$= \frac{\langle\Phi|\, O\,|\Psi\rangle}{\langle\Phi\,|\,\Psi\rangle} \tag{2.138}$$

$$= \langle O\rangle_{\text{mixed}} \tag{2.139}$$

We call this average *mixed average* , which in general differs from the *pure average*

$$\langle O\rangle_{\text{pure}} = \frac{\langle\Phi|\, O\,|\Phi\rangle}{\langle\Phi\,|\,\Phi\rangle} \tag{2.140}$$

A special case where the mixed and pure average are equal is when the observable O commutes with the hamiltonian H. In particular the estimator for the energy is pure. This allows the DMC method to yield energies with arbitrary accuracy.
For observables that do not commute with the hamiltonian we can extrapolate a good approximation for the pure average from the mixed average and the variational average

$$O_{\text{var}} = \frac{\langle\Psi|\, O\,|\Psi\rangle}{\langle\Psi\,|\,\Psi\rangle} \tag{2.141}$$

which can be obtained from a VMC simulation. If the ansatz guiding wavefunction $\Psi(X)$ is close to the ground-state wavefunction of the model $\Phi(X)$ we can expand the ground-state $|\Phi\rangle$ around the guiding state $|\Psi\rangle$.

$$|\Phi\rangle = |\Psi\rangle + |\delta\Psi\rangle \tag{2.142}$$

We can substitute the expansion 2.142 in the mixed and pure estimator

$$O_{\text{mixed}} = O_{\text{var}} + \frac{\langle\Psi|\, O\,|\delta\Psi\rangle}{\langle\Psi\,|\,\delta\Psi\rangle} - O_{\text{var}}\frac{\langle\Psi\,|\,\delta\Psi\rangle}{\langle\Psi\,|\,\Psi\rangle} + O\left(|\delta\Psi\rangle^2\right) \tag{2.143}$$

$$O_{\text{pure}} = O_{\text{mixed}} + \frac{\langle\Psi|\, O\,|\delta\Psi\rangle}{\langle\Psi\,|\,\delta\Psi\rangle} - O_{\text{var}}\frac{\langle\Psi\,|\,\delta\Psi\rangle}{\langle\Psi\,|\,\Psi\rangle} + O\left(|\delta\Psi\rangle^2\right) \tag{2.144}$$

Substracting the two equations we get

$$O_{\text{pure}} = 2O_{\text{mixed}} - O_{\text{var}} + O\left(|\delta\Psi\rangle^2\right) \tag{2.145}$$

Thus if we have a good ansatz for the ground-state wavefunction , we can obtain a very good estimate for the pure estimator.

Forward walking

In some cases the ansatz wavefunction is not able to accurately describe the observable we want to study. In these cases the two estimates O_{mixed} and O_{var} may differ considerably and the linear expansion is not justified. However, it is possible to obtain a pure estimator even for observables that do not commute with the hamiltonian using the forward walking technique.
In a DMC run the mixed estimator can be written as

$$\langle O \rangle = \frac{1}{N_t} \sum_{i=i_{min}}^{N_t} \frac{1}{N_w(\tau_i)} \sum_{j=1}^{N_w(\tau_i)} O(X_{ij}) \tag{2.146}$$

where X_{ij} is the configuration sampled at time i on walker j and one performs an average over all walkers and time steps. In the forward walking technique one performs instead a weighted average

$$\langle O \rangle = \frac{1}{N_t} \sum_{i=i_{min}}^{N_t} \frac{1}{N_w(\tau_i)} \sum_{j=1}^{N_w(\tau_i)} O(X_{ij}) w_{ij} \frac{1}{\sum_{i,j} w_{ij}} \tag{2.147}$$

where the weight $w_{i,j}$ is proportional to the number of descendants of walker j from time $i\delta\tau$ onwards. This estimator is free of bias , with the additional cost of performing a weighted average with weights that depend on the future evolution of each walker.
The weighted average can be easily performed by exploiting the branching mechanism. Each time we make a measurement , the local observed value $O(x_{ij})$ is saved for each walker. At each branching step the walker will inherit the value from the old walker, creating a number of copies of the measurement equal to the number of descendants of the walker. Thus by averaging the stored value over all walkers after n time steps we get an automatic weighted average with weights proportional to the number of descendants after n time steps. If we choose n sufficiently large , one can make the bias of the estimator arbitrarily small. The forward walking algorithm thus consists in

1. Accumulate averages over all measurements stored on walkers n iterations ago

2. On each walker store the local measurement.

3. Perform n_{dec} DMC steps. At each branching step , copy all stored values to descendant walkers. Go back to step 1.

Thus we are able to obtain a measurement for each walker each n_{dec} time steps , after the first n time steps after reaching the stationary distribution.

The forward walking estimator might not look much more expensive than a regular mixed average. However walkers that die before n time steps will not give any contribution to the weighted average. After a sufficiently long time , most walkers will have died and the new population will be made entirely of descendants of just a few walkers (see the illustration in Fig. 2.1). Those few walkers are the only ones to give a contribution to the weighted average. Instead of performing the measurement on all walkers in practice we are only averaging on an effective number of walkers, which typically is much smaller than the actual number of walkers in the simulation. As a result the typical variance of forward walking estimators is much larger then mixed average estimators and require much longer simulation times.

2.8.4 Imaginary time correlations

We have already seen several estimators of ground-state properties. However in DMC we have also access to imaginary time correlations of the form

$$\langle O(t+\tau)O(t)\rangle \tag{2.148}$$

where $O(t)$ is an observable measured at imaginary time t and $O(t+\tau)$ is an observable measured after a certain interval of time τ. Of course, if the system is stationary correlations do not explicitly depend on the initial time t. While correlations in imaginary time do not have a physical interpretation they sometimes can be related to important dynamical properties. This is the cases for an important observable : the superfluid fraction.

2.8.5 Superfluid fraction

Suppose to have two systems : a first system with energy E_0 and a second system with energy E_v moving at velocity v. For both systems we suppose to be in a reference where the walls are at rest. If the system is not superfluid part of the kinetic energy will be converted in excitations , reducing the speed of the flow. At equilbrium the fluid will eventually be at rest. Thus $E_0 = E_v$. However if a fraction of the fluid is superfluid , the superfluid component will not be damped and , even at equilibrium, it will keep flowing with velocity v and the energy will be

$$E_v = E_0 + \frac{1}{2}mv^2\frac{\rho_s}{\rho}N \tag{2.149}$$

where N is the number of atoms of the system and ρ_s/ρ is the *superfluid fraction*. The hamiltonians for the two systems will be

$$H = \sum_{i=1}^{N} \frac{(-\hbar\partial_{x_i})^2}{2m} + V(R) \tag{2.150}$$

$$H_v = \sum_{i=1}^{N} \frac{(-\hbar\partial_{x_i} - mv)^2}{2m} + V(R) \tag{2.151}$$

which give rise to two Green's functions

$$G_v(X, X') = \langle X|\, e^{-(H_v - E_T)\frac{\tau}{\hbar}}\, |X'\rangle \tag{2.152}$$

$$G(X, X') = \langle X|\, e^{-(H - E_T)\frac{\tau}{\hbar}}\, |X'\rangle \tag{2.153}$$

and will have to satisfy the equations

$$-\partial_\tau G(X, X') = (H - E_T)G(X, X') \tag{2.154}$$

and

$$-\partial_\tau G_v(X, X') = (H_v - E_T)G(X, X') \tag{2.155}$$

The Green's function of the moving system differs from the Green's function of the original system by a phase factor

$$G_v(X, X') = e^{i\frac{m}{\hbar}v\sum_i (x_i - x_i')} G_0(X, X') \tag{2.156}$$

This expression can be proven through substitution of expression 2.156 into equation 2.155. Through simple algebra one obtains the equation 2.154 . In a DMC simulation one samples the function $f(X, \tau) = \Psi(X, \tau)\Phi(X, \tau)$, product of the guiding wavefunction $\Psi(X, \tau)$ and the ground-state wavefunction of the hamiltonian H. In terms of the Green's function, $f(X, \tau)$ can be rewritten as

$$f(X, \tau) = \int G_T(X, X') f(X', \tau_0) \tag{2.157}$$

$$= \int \Psi(X) G(X, X') \frac{1}{\Psi(X')} f(X', \tau_0) \tag{2.158}$$

where t_0 is an arbitrary initial time. Similarly in the moving system

$$f_v(X, \tau) = \int \Psi(X) G_v(X, X') \frac{1}{\Psi(X')} f(X', \tau_0) \tag{2.159}$$

$$= \int e^{i\frac{m}{\hbar}v\sum_i (x_i - x_i')} \Psi(X) G(X, X', \tau - \tau_0) \frac{1}{\Psi(X')} f(X', \tau_0) \tag{2.160}$$

$$= \int e^{i\frac{m}{\hbar}v\sum_i(x_i-x_i')} G_T(X, X', \tau - \tau_0) f(X', \tau_0) \tag{2.161}$$

If we choose the initial condition $f_v(X, X') = f(X, X') = \delta(X(\tau_0) - X')$ we get

$$f_v(X, \tau) = e^{i\frac{m}{\hbar}v\sum_i(x_i(\tau)-x_i(\tau_0))} f(X, \tau) \tag{2.162}$$

Now let us consider the ratio

$$\frac{\int dX f_v(X, \tau)}{\int dX f(X, \tau)} = \frac{\int dX e^{i\frac{m}{\hbar}v\sum_i(x_i(\tau)-x_i(\tau_0))} f(X, \tau)}{\int dX f(X, \tau)} \tag{2.163}$$

In the limit $v \to 0$ one may write

$$\frac{\int dX f_v(X, \tau)}{\int dX f(X, \tau)} \approx 1 - \frac{m^2 v^2}{2\hbar^2} \frac{\int dX \left(\sum_i x_i(\tau) - x_i(\tau_0)\right)^2 f(X, \tau)}{\int dX f(X, \tau)} \tag{2.164}$$

$$= 1 - \frac{m^2 v^2}{2\hbar^2 N_w(\tau)} \int dX \left(\sum_i x_i(\tau) - x_i(\tau_0)\right)^2 f(X, \tau) \tag{2.165}$$

where $N_w(\tau)$ is equal to the number of walkers at time τ. On the other hand in the long-time limit the ratio on the left hand is equal to

$$\frac{\int dX f_v(X, \tau)}{\int dX f(X, \tau)} = e^{-\tau(E_v - E_0)} \approx 1 - \delta\tau(E_v - E_0) \tag{2.166}$$

The last step is justified by the assumption that v is small enough that $\tau(E_v - E_0) \ll 1$. Comparing expressions 2.166 and 2.165 and using the definition 2.149 we get an expression for the superfluid fraction

$$\frac{\rho_s}{\rho} = \frac{\hbar^2}{m\tau N_w} \int dX f(X, \tau) W^2(\tau) \tag{2.167}$$

where the quantity

$$W(\tau) = X_{c.m}(\tau_0 + \tau) - X_{c.m.}(\tau_0) \tag{2.168}$$

is called *winding number* and is equal to the displacement of the center of mass $X_{c.m}$ in an imaginary time interval τ. In a simulation with periodic boundary conditions in a box of length L the winding number allows us to determine the number of times the center of mass crosses the boundaries and 'winds around' the length of the box.

Chapter 3

The Bose polaron problem

In this chapter we will be considering the problem of an impurity immersed in a bath of bosonic atoms. We will describe how the properties of the impurity are affected with the bath. This chapter is based on the article [26].

3.1 Introduction

In recent years the problem of an impurity coupled to a quantum bath has received a large attention in the field of ultracold atoms both theoretically and experimentally. In particular, the fermionic version of this problem, *i.e.* when the bath is a spin-polarized Fermi sea, is already a well studied topic with different interesting perspectives addressing the attractive and repulsive branch as well as low dimensions [61]. On the contrary, for the bosonic counterpart corresponding to an impurity immersed in a Bose condensed medium, only very recently there have been experimental studies focusing on the excitation energy and spectral response of the polaron quasiparticle [90, 63]. Previous experiments investigated mainly collisional and dissipation processes involving the bath [64, 65, 66]. On the theoretical side, the Bose polaron problem has been already addressed in a series of studies utilizing different tools such as T-matrix [67] and perturbation [68] approaches, variational wavefunction [69, 70] as well as quantum Monte-Carlo (QMC) methods [86, 96]. Low dimensions, and in particular one-dimensional (1D) configurations, enrich the Bose polaron problem with some peculiar features that are worth investigating. First of all the enhanced role of quantum fluctuations capable to destroy the off-diagonal long-range order responsible for Bose-Einstein condensation even at zero temperature. Secondly, the possibility to achieve strongly correlated regimes for the quantum bath, where the bosons approach the so called Tonks-Girardeau (TG) limit of fermion-

like impenetrable particles [73, 80, 75, 76]. The use of confinement induced resonances of the s-wave scattering amplitude represents for these 1D systems a powerful tool, allowing for a wide tunability of both the interactions within the bath and between the bath and the impurity [77, 76, 65, 79]. For example, in Ref. [65] a 1D mixture of K impurities in a gas of Rb atoms was realized and different values of the impurity-bath interaction, obtained by varying the magnetic field, were probed. Similarly, in Ref. [79], two different hyperfine states of Cs atoms have been used to realize arrays of 1D tubes in the strongly interacting regime with approximately one impurity per tube at variable coupling between the impurity and the bath. The gas parameter in the bath can also be tuned by changing the density or the effective mass of the atoms by means of a lattice potential [80, 75].

The results show that the polaron energy reaches a constant value for large repulsive impurity-boson interaction, whereas in the opposite limit of large attraction the impurity gets deeply bound to the bath. Unless the bosons are impenetrable particles, this binding energy is found to be much larger than the one of the dimer state, the solution to the two-body problem in vacuum. The tendency of bosons attracted by the impurity to form large clusters involving many particles is also evident from the density profile of the medium around the impurity. The size of these clusters, as well as their binding energy, increases with decreasing interaction strength within the bath, indicating an instability of the weakly interacting Lieb–Liniger gas towards collapse around an attractive impurity. The effective mass of the polaron moving in a weakly interacting medium exhibits a sharp increase as a function of the coupling, both on the repulsive and on the attractive side of the impurity-bath interaction. Already for a moderate coupling strength the impurity gets very heavy, thus realizing the so-called "self-localization" regime predicted by Landau and Pekar for polarons in crystals [81]. This picture was also proposed for Bose polarons in three dimensions (3D) on the basis of a Fröhlich-type model [82, 83, 84, 85] which, however, does not capture the relevant physics at strong coupling [68, 86]. On approaching the TG limit, instead, the effective mass increases sizeably only for large values of the coupling on the repulsive side and saturates at twice the bare mass on the attractive side.

It is worth pointing out that the results mentioned above are directly relevant for experiments on few impurities in a quantum bath where the binding energy can be measured using spectroscopic techniques [87, 88, 89, 90, 63, 91] and the effective mass from the study of collective modes in harmonic traps [92, 65], as well as from radiofrequency measurements at finite impurity concentration [87, 91].

We characterize the Bose polaron by calculating its binding energy, effective

mass, and contact parameter.

The binding energy

The total energy of the system, including the bath and the impurity , is given by

$$\tilde{E} = E_B + \mu \tag{3.1}$$

where E_B is the energy of the bath in absence of the impurity and the $\tilde{E}$ is the energy of the system including the impurity. This equation defines the *polaron energy* or *binding energy* μ. In the polaronic picture the binding energy corresponds to a shift in the energy carried by the particle when at rest.

The effective mass

If the impurity is not at rest , but carries some average momentum different from zero , it will also acquire a kinetic energy. In general the relation $E(p)$ is difficult to compute , but in the limit of $p \to 0$ one gets

$$\tilde{E} = E_B + \mu + \frac{p^2}{2m^*} + o(p^4) \tag{3.2}$$

where we have defined the effective mass m^*. The polaron can still be seen as a free particle but with an effective mass that differs from the bare mass of the impurity.

The contact parameter

Another important feature of the polaron is the contact parameter defined as

$$C = \left\langle \Psi_B^\dagger \Psi_I^\dagger \Psi_B \Psi_I \right\rangle \tag{3.3}$$

The contact parameter represents the probability to find a particle of the bath at the same spatial position of the impurity and is equal to the density of the bath at the impurity position. The contact parameter can be related to the energy of the system through the Helmann-Feynmann theorem [93].

$$C = \frac{\partial}{\partial \tilde{g}} \tilde{E} \tag{3.4}$$

which allows to calculate the contact parameter from the equation of state of the system.
The contact parameter is an especially important quantity as it can be related to many short range properties of the impurity[94, 95]. For instance it defines the high momentum decay of the momentum distribution [94].

3.2 General theory

We consider the following hamiltonian

$$\begin{aligned} H &= -\frac{\hbar^2}{2m_B}\sum_{i=1}^{N}\frac{\partial^2}{\partial x_i^2} + \sum_{i<j} g\delta(x_i - x_j) \\ &- \frac{\hbar^2}{2m_I}\frac{\partial^2}{\partial x_\alpha^2} + \sum_{i=1}^{N}\tilde{g}\delta(x_i - x_\alpha) \ , \end{aligned} \tag{3.5}$$

describing a 1D system of N identical bosons with mass m_B interacting via a repulsive contact potential of strength $g > 0$. A single impurity of mass m_I is coupled to the particles of the bath via another contact potential characterized by the strength $\tilde{g}$. The coordinates of the bosons and the impurity are denoted respectively by x_i $(i = 1, \ldots, N)$ and x_α. We introduce the dimensionless parameters

$$\gamma = \frac{g m_B}{\hbar^2 n} \qquad \eta = \frac{2\tilde{g}}{\hbar^2 n}\frac{m_B m_I}{m_B + m_I} \ , \tag{3.6}$$

where $n = N/L$ is the density of the bath in the 1D box of size L. The first parameter gives the strength of interactions within the bath which can range from the weakly correlated mean-field regime ($\gamma \ll 1$) to the strongly correlated TG regime ($\gamma \gg 1$), where bosons are impenetrable and behave similarly to a gas of spinless fermions. The parameter η is instead related to the coupling between the impurity and the bath and, contrary to γ, can be either positive or negative depending on the sign of $\tilde{g}$. Notice that for equal masses ($m_B = m_I$) and for equal coupling strengths ($\tilde{g} = g$) the equality $\gamma = \eta$ holds.

The above hamiltonian (3.5) of the clean bath , without the impurity , is equivalent to the Lieb-Liniger hamiltonian we saw in the previous chapter. There we saw that the energy can by written in the form

$$E_0 = N\frac{\hbar^2 n^2 \pi^2}{2m_B}\epsilon(\gamma) \ , \tag{3.7}$$

where the dimensionless energy per particle $\epsilon(\gamma)$ is obtained by solving a pair of coupled integral equations. The scale of energy in Eq. (3.7) is chosen as $\epsilon_F = \frac{\hbar^2 k_F^2}{2m_B}$, with $k_F = \pi n$, corresponding to the Fermi energy of a gas of spinless fermions with the same mass and density. Some limits of $\epsilon(\gamma)$ can be derived analytically: if $\gamma \ll 1$, one finds $\epsilon \simeq \frac{\gamma}{\pi^2}(1 - \frac{4}{3\pi}\sqrt{\gamma})$; in the opposite limit, $\gamma \gg 1$, one has instead $\epsilon \simeq \frac{1}{3}(1 - \frac{4}{\gamma})$. As we already mentioned, the

former result holds in the weak-coupling regime and includes the Bogoliubov term and the first beyond mean-field correction whereas, in the latter, the leading term corresponds to the energy of the equivalent non-interacting Fermi gas. The energy of the bath plus the impurity can be written as

$$\tilde{E}_0 = \frac{\hbar^2 n^2 \pi^2}{2m_B} \left[N\epsilon(\gamma) + \mu(\gamma, \eta) \right] , \tag{3.8}$$

allowing one to express the energy difference $\tilde{E}_0 - E_0$ in terms of the dimensionless function $\mu(\gamma, \eta)$ which yields the polaron energy in units of the scale ϵ_F.

3.2.1 Weak interactions

In the limit of small γ and small η one can determine the energy and the effective mass of the polaron by using the perturbation approach based on the Bogolubov approximation as it is outlined in Ref. [86]. By introducing the mass ratio $w = \frac{m_B}{m_I}$ of the bosonic to the impurity mass, the result for the polaron energy reads:

$$\begin{aligned} \mu(\gamma, \eta) &\simeq \frac{\eta(1+w)}{\pi^2} \left(1 - \frac{\eta}{\sqrt{8\gamma}} \frac{1+w}{\pi} \right. \\ &\times \left. \int_0^\infty \frac{dx}{\sqrt{x+2}} \frac{1}{\sqrt{x^2+2x} + wx} \right) , \end{aligned} \tag{3.9}$$

and for the effective mass one finds

$$\begin{aligned} \frac{m_I^*}{m_I} &\simeq 1 + \frac{\eta^2}{\gamma^{3/2}} \frac{w(1+w)^2}{\sqrt{2}\pi} \\ &\times \int_0^\infty \frac{dx}{\sqrt{x+2}} \frac{x}{(\sqrt{x^2+2x} + wx)^3} . \end{aligned} \tag{3.10}$$

The first term in Eq. 3.9 is the mean-field contribution proportional to $\tilde{g}$, whereas next-to-leading order corrections to both μ and the effective mass are proportional to $\tilde{g}^2$ and are independent of the sign of the impurity-boson interaction. We also notice that in the limit $\gamma \to 0$, for a fixed value of η, both these corrections diverge, signalling an instability of the medium surrounding the impurity when boson-boson interactions are suppressed. The situation is different in the 3D case where, in the same limit, only the effective mass exhibits a divergent behavior [86]. We consider explicitly two particular values of the mass ratio w: the case of equal masses ($w = 1$) and the case of

a static impurity with infinite mass ($w = 0$). For the former case, Eqs. (3.9) and (3.10) give

$$\mu(\gamma,\eta) \simeq \frac{2\eta}{\pi^2}\left(1-\frac{\eta}{\pi\sqrt{\gamma}}\right), \tag{3.11}$$

$$\frac{m^*}{m} \simeq 1+\frac{2}{3\pi}\frac{\eta^2}{\gamma^{3/2}}, \tag{3.12}$$

where we have set $m_B = m_I = m$. The binding energy of a static impurity, instead, is found to be:

$$\mu(\gamma,\eta) \simeq \frac{\eta}{\pi^2}\left(1-\frac{\eta}{4\sqrt{\gamma}}\right). \tag{3.13}$$

An asymptotically exact result for a static impurity ($w = 0$) is obtained when interactions within the bath are weak ($\gamma \ll 1$) and there is a strong impurity-boson repulsion ($\eta \to +\infty$). In this case, the polaron energy coincides with the excitation energy of a dark soliton [31]

$$\mu = \frac{8}{3\pi^2}\sqrt{\gamma}\,. \tag{3.14}$$

This excited state of the gas is indeed stationary and is characterized by a zero in the density profile. In the case of equal masses ($w = 1$) the contact parameter can be derived analytically in the weak-coupling limit, where Eq. (3.11) together with Eq. (3.4) yields

$$C = 1-\frac{2\eta}{\pi\sqrt{\gamma}} \tag{3.15}$$

3.2.2 TG bath

An exact solution is available when the bath is in the TG limit ($\gamma = \infty$). The binding energy and the effective mass of the equal mass case ($w = 1$) were calculated by McGuire [20, 21] with the result

$$\mu = \frac{2}{\pi}\left[\frac{\eta}{2\pi}+\arctan\frac{\eta}{2\pi}-\frac{\eta^2}{4\pi^2}\left(\frac{\pi}{2}-\arctan\frac{\eta}{2\pi}\right)\right] \tag{3.16}$$

and the two results

$$\frac{m^*}{m} = \frac{2}{\pi}\frac{\left(\arctan\frac{2\pi}{\eta}\right)^2}{\arctan\frac{2\pi}{\eta}-\frac{2\pi/\eta}{1+\frac{4\pi^2}{\eta^2}}}, \tag{3.17}$$

$$\frac{m^*}{m} = \frac{2\left(1-\frac{1}{\pi}\arctan\frac{2\pi}{|\eta|}\right)^2}{1-\frac{1}{\pi}\left(\arctan\frac{2\pi}{|\eta|}-\frac{2\pi/|\eta|}{1+\frac{4\pi^2}{\eta^2}}\right)}, \tag{3.18}$$

holding, respectively, for positive and negative values of the coupling constant $\tilde{g}$. Some limits of the above Eqs. (3.16)-(3.18) are worth discussing: i) If $\eta \to +\infty$ one finds $\mu \simeq 1$, yielding a polaron energy equal to the chemical potential of the surrounding Fermi gas, whereas the effective mass diverges as $\frac{m^*}{m} \simeq \frac{3\eta}{2\pi^2}$. ii) If $\eta \to -\infty$, then $\mu \simeq -\frac{\eta^2}{2\pi^2}$ and $\frac{m^*}{m} \simeq 2$, corresponding to the binding energy and the mass of a dimer in vacuum.

In the case of a TG gas with a static impurity ($w = 0$) one proceeds by considering the impurity in the center of a large box of size L with impenetrable walls and by calculating the phase shift of each single-particle state generated by the impurity contact potential with strength $\tilde{g}$. The ground-state energy difference $\tilde{E}_0 - E_0$ is readily calculated yielding the result

$$\begin{aligned} \mu &= \frac{1}{\pi}\left[\left(1+\frac{\eta^2}{4\pi^2}\right)\arctan\frac{\eta}{2\pi} + \frac{\eta}{2\pi} - \frac{\eta|\eta|}{8\pi}\right] \\ &- [1-\theta(\eta)]\frac{\eta^2}{4\pi^2}\,. \end{aligned} \tag{3.19}$$

The term involving the Heaviside function $\theta(x)$, where $\theta(x) = 1$ if $x > 0$ and zero otherwise, accounts for the binding energy of the dimer when $\tilde{g} < 0$. Also in this case we can easily extract the following limiting behaviors: i) if $\eta \to +\infty$, then $\mu \simeq \frac{1}{2}$ and ii) if $\eta \to -\infty$ one finds the result $\mu \simeq -\frac{\eta^2}{4\pi^2} - \frac{1}{2}$. Notice that the energy of the mobile impurity (3.16) in the limit of infinite repulsion is twice the corresponding energy of the static impurity (3.19), even though the effective mass (3.17) diverges in the same limit. This is due to the kinetic energy contribution of the mobile impurity within the region of space delimited by the two nearest neighbour particles of the bath acting as impenetrable barriers. In the TG limit, the contact parameter can readily be evaluated from Eq. (3.19) together with Eq. (3.4) as

$$C = 1 - \frac{\eta}{4} + \frac{\eta}{2\pi}\arctan\frac{\eta}{2\pi}\,. \tag{3.20}$$

From the above result we see that $C \simeq \frac{4\pi^2}{3\eta^2}$ when η is large and positive and $C \simeq \frac{|\eta|}{2}$ in the opposite limit of large and negative values of η.

3.3 The Wavefunction

We perform DMC simulations using a a wavefunction that takes the Jastrow form definied in the previous chapter. For a bath with an impurity it takes the form

$$\Psi = \prod_{i<j} f_{BB}(x_i - x_j) \prod_i f_{BI}(x_i - x_\alpha) \tag{3.21}$$

where i, j range from one to the number of bosons N in the bath and x_α is the position of the impurity. The function f_{BB} takes the form 2.130 while the function f_{BI} takes the form 2.130 for a repulsive impurity and 2.132 for an attractive impurity.

3.4 The Binding Energy

We first discuss the results on the binding energy for the mobile ($w = 1$) and the static ($w = 0$) impurity.

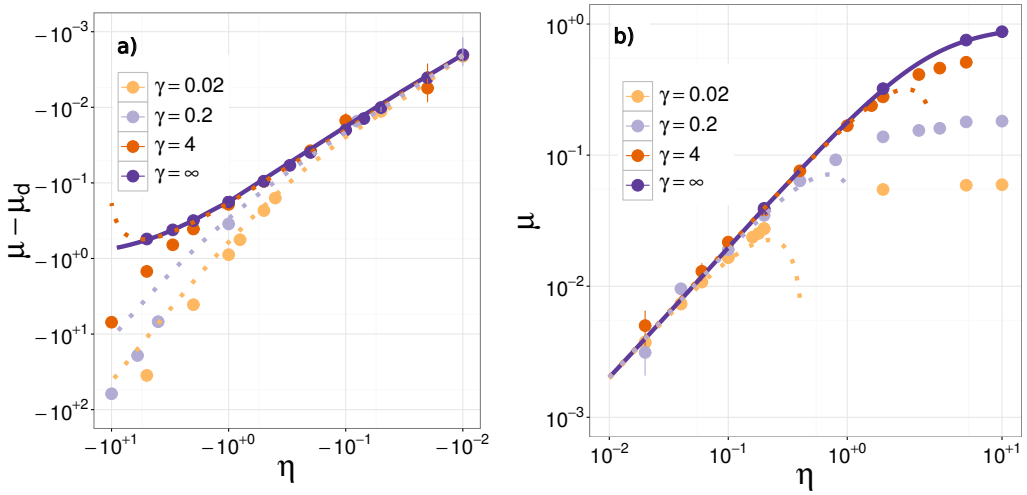

Figure 3.1: Binding energy of the mobile impurity with mass ratio $w = 1$ as a function of the impurity-boson interaction parameter η and for different values of the coupling strength γ within the bath. Panel (a) and (b) refers respectively to negative and positive values of $\tilde{g}$ and in panel (a) we have subtracted from μ the trivial contribution from the dimer state. The $\gamma = \infty$ curve corresponds to the exact result by McGuire [Eq. (3.19)]. Dashed lines refer instead to the perturbation result in Eq. (3.11).

In Fig. 3.1 we show the energy of the mobile impurity as a function of the coupling strength η, ranging from large negative to large positive values, when the interaction parameter γ in the bath is kept fixed. For this latter we consider values varying from the weakly coupled regime, $\gamma \ll 1$, to the TG regime where $\gamma = \infty$. The corresponding results for the static impurity are presented in Fig 3.2. Notice that for $\eta < 0$ we subtract from the binding energy μ the contribution from the two-body bound state given by $\mu_d = -\eta^2 \frac{1+w}{4\pi^2}$. The exact polaron energies corresponding to the TG regime

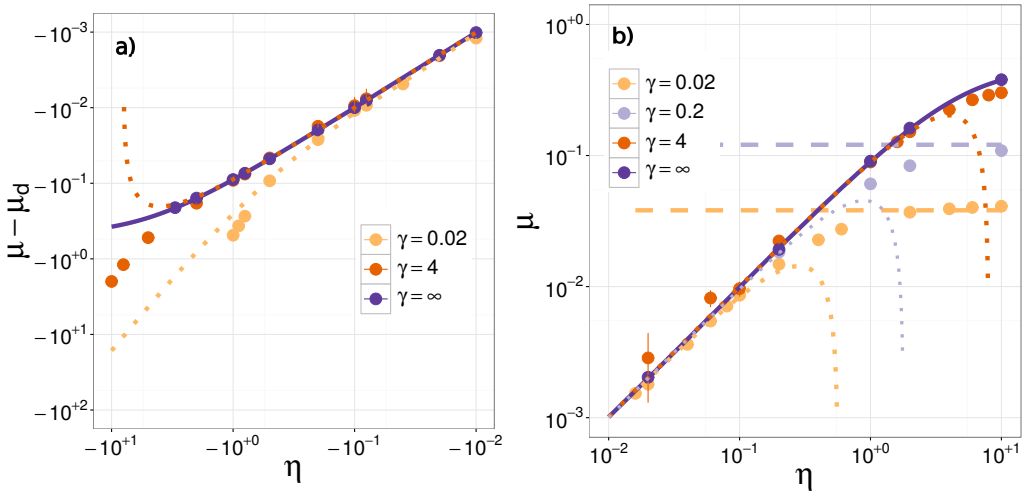

Figure 3.2: Binding energy for the static impurity with mass ratio $w = 0$ as a function of the impurity-boson interaction parameter η and for different values of the coupling strength γ within the bath. Panel (a) and (b) refers respectively to negative and positive values of $\tilde{g}$ and in panel (a) we have subtracted from μ the trivial contribution from the dimer state. The $\gamma = \infty$ curve corresponds to the exact result in Eq. (3.16). Dashed lines refer instead to the perturbation result in Eq. (3.13).

and given by Eqs. (3.16) and (3.19) are shown as solid lines in Fig. 3.1 and Fig. 3.2, respectively for $w = 1$ and for $w = 0$. As an important benchmark test we find that the values of μ obtained from our QMC simulations with $\gamma = \infty$ perfectly reproduce these results. In the regime of small values of $|\eta|$, our results also recover the expansions from perturbation theory given by Eqs. (3.11) and (3.13). In particular, both for $w = 1$ and for $w = 0$, we find that the range of values of $|\eta|$ where the perturbation expansion agrees well with the calculated polaron energy becomes larger as γ increases. In fact we notice that, when γ is large, from Eq. (3.9) one finds $\mu \simeq \frac{\eta(1+w)}{\pi^2}$. Remarkably this result agrees with the expansion of Eq. (3.16) and (3.19), respectively for the mobile and static impurity, up to values of the impurity-boson coupling constant on the order of $|\eta| \simeq 1$. For smaller values of γ, typically $\gamma < 1$, the applicability of perturbation theory is instead limited to the region where $|\eta| \lesssim \sqrt{\gamma}$.

If η is large and positive the energy of both the mobile and the static impurity tends to saturate to a value that becomes smaller with decreasing γ [see panel (b) of Fig. 3.1 and Fig. 3.2]. In the TG regime ($\gamma = \infty$) this asymptotic energy coincides with the energy ϵ_F of adding an extra particle

to the bath in the mobile case and with $\epsilon_F/2$ in the static case. As already discussed in Sec. II, this energy difference arises from the kinetic energy contribution of the mobile impurity. A similar difference persists also for smaller values of γ: for example, at $\gamma = 0.02$ and $\eta = 10$, we find $\mu = 0.059(1)$ and $\mu = 0.041(1)$ respectively for the $w = 1$ and $w = 0$ case. We notice that, in this latter limit of large η and small γ, the energy of the static impurity is expected to coincide with the excitation energy (3.14) of a dark soliton as determined using the mean-field Gross-Pitaevskii equation. Indeed, in panel b) of Fig. 3.2, good agreement between the two energies is found for $\gamma = 0.02$ and also for $\gamma = 0.2$.

In the opposite regime of large and negative values of η, the energy difference $\mu - \mu_d$ tends, when $\gamma = \infty$, respectively to -1 and to $-1/2$ in the mobile and in the static case. Here, the impurity forms a two-body bound state with one of the particles of the medium which is then missing from the Fermi sea of the TG gas. Notice that, similarly to the case of $\eta > 0$, the binding energy μ of the mobile impurity is larger by a factor of two compared to the energy of the static one. For smaller values of γ our results indicate that $\mu - \mu_d$ is always negative and grows unbounded as $\eta \to -\infty$ [see panel (a) of Fig. 3.1 and Fig. 3.2]. This behavior arises because, for attractive interactions between the impurity and the bath and for not too strong repulsion within the bath, many particles of the medium tend to cluster around the impurity producing a large negative binding energy for the polaron.

An interesting question concerns the value of the polaron energy when η is fixed and the interaction strength within the bath gets weaker and weaker ($\gamma \to 0$). At the level of perturbation theory [see Eq. (3.9)] the answer to this question is that μ becomes large and negative irrespective of the sign of η. This result differs from the corresponding situation in 3D where perturbation theory predicts that, when interactions within the bath vanish, the polaron energy reduces to the mean-field value, proportional to the interspecies coupling constant [86]. For positive values of η, a proper answer to the question, going beyond the result of perturbation theory, is provided by panel (b) of Fig. 3.1 and Fig. 3.2: when $\gamma \ll \eta$ the polaron energy decreases to zero and for the static impurity the behavior of μ is correctly described by the dark-soliton excitation energy given in Eq. (3.14).

In the case of $\eta < 0$, panel (a) of Fig. 3.1 and Fig. 3.2 shows that the binding energy of the impurity grows large and negative as γ decreases for a fixed value of η. However, in this limit, one can expect that either i) $\mu \to -\infty$, indicating the instability of the non-interacting bath in the presence of the impurity, or ii) μ saturates to a finite energy, indicating that even a tiny repulsion in the bath is enough to stabilize the polaron. We notice that the value of $\mu(\gamma, \eta)$ refers to the polaron energy in the thermodynamic limit and

that the $\gamma \to 0$ limit is intended to be taken after the one of $N \to \infty$. Of course, in the opposite case of a strictly non-interacting bath with a finite number of particles, the polaron energy would trivially diverge when the number N increases. We address the question for the mobile impurity with mass ratio $w = 1$, when the interaction between the impurity and the bath is attractive and kept fixed at the value $\eta = -1$. The results of the inverse energy $1/\mu$ are shown in Fig. 3.3 as a function of decreasing values of γ. We find that $1/\mu$ decreases in absolute value as γ decreases, even though the result (3.11) of perturbation theory fails completely in describing the trend of the calculated binding energies. A simple linear fit to the data extrapolates to a value compatible with $1/\mu = 0$ when $\gamma = 0$, given that error bars are significantly large. Our findings are thus compatible with the above case i), showing an instability of the weakly repulsive bath towards a collapse around the impurity. A similar behavior is expected for the static impurity with $w = 0$. This latter result is in contrast with the binding energy of a static impurity in 3D and resonantly interacting with the medium which was found to approach a finite value in the limit of a vanishing repulsion within the bath [96].

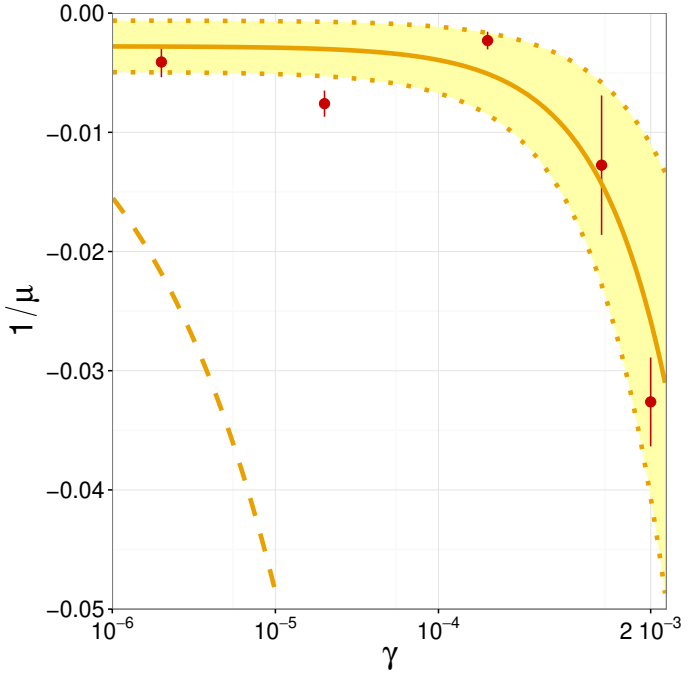

Figure 3.3: Inverse binding energy (in units of the scale ϵ_F) of the mobile impurity with $w = 1$ as a function of the parameter γ and for the fixed value $\eta = -1$ of the impurity-boson coupling constant. The line is a linear fit to the data and the shadow region shows the statistical uncertainty of the fit. The dashed line is the prediction from perturbation theory given in Eq. (3.11).

3.5 The effective Mass

In Fig. 3.4 we show the results of the polaron effective mass in the case of the mobile impurity with mass ratio $w = 1$. We find that, for a given value of γ, the inverse effective mass decreases as $|\eta|$ increases both for repulsive and attractive interactions. We also notice that, in the TG limit of $\gamma = \infty$, we recover the exact results obtained by McGuire and given in Eqs. (3.17) and (3.18). Furthermore, the comparison with the prediction (3.10) of perturbation theory shows that, similarly to the case of the energy μ, the range of values of $|\eta|$ where agreement is found gets larger as γ increases. On the attractive side of impurity-bath interactions, the exact TG-gas result in Eq. (3.18) yields $m^* \to 2m$ in the limit of η large and negative. For the strongly interacting medium with $\gamma = 4$ we find in the same limit that the

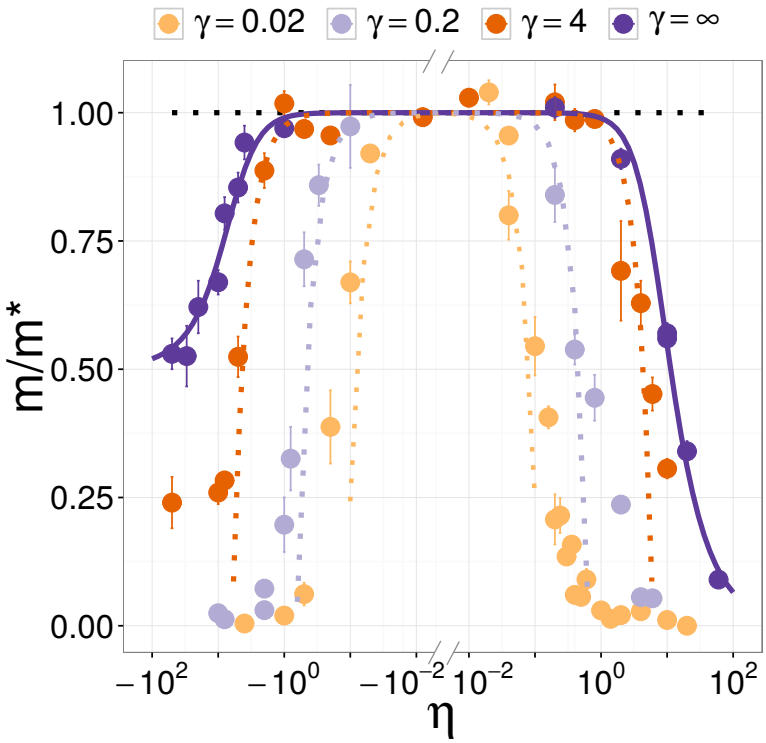

Figure 3.4: Inverse effective mass of the mobile impurity with mass ratio $w = 1$ as a function of the impurity-boson interaction parameter η and for different values of the coupling strength γ within the bath. Both values corresponding to η positive and negative are shown in the same graph. The $\gamma = \infty$ curve corresponds to the exact results by McGuire of Eqs. (3.17) and (3.18) in the TG limit. Dotted lines refer to the result of perturbation theory given in Eq. (3.12).

effective mass seems to saturate to $m^* \simeq 4m$. One should stress here that for large attractions the calculation of the effective mass requires increasingly longer simulation times resulting in larger error bars. For smaller values of γ, both on the attractive and on the repulsive side, the value of m^*/m becomes very large for $|\eta| \gtrsim 10$, if $\gamma = 0.2$, and already for $|\eta| \gtrsim 1$ if $\gamma = 0.02$. It is worth noticing that this rapid increase of the effective mass as a function of the impurity-bath coupling does not occur in the 3D counterpart of the Bose polaron problem, where in the limit of resonant interaction between the impurity and the bath one finds $m^*/m \lesssim 2$ (see Ref. [86]).

An increase of the effective mass as a function of the impurity-bath cou-

pling has been reported in the experiment of Ref. [65] both for attractive and repulsive interactions. In this experiment a cloud of K impurities immersed in a 1D bath of Rb atoms is suddenly released after compression with an optical potential and the rate of increase of its axial size is measured for different fixed values of the interaction strength between the impurities and the bath. The connection with the effective mass of the impurities is provided by interpreting the normalized width of the cloud with $\sqrt{m_I/m_I^*}$. The coupling constant of the bath was $\gamma \simeq 1$ and values of η as large as $|\eta| \simeq 10$ were produced, resulting in a maximum measured decrease of the normalized width by a factor of roughly 0.6.
In experiments , which are tipically carried by averaging over many elongated tubes, the number of particles per tube is also very small , ranging from just a few to several tens of particles. With so few particles, deviations from the LDA predictions have been observed. In the Thomas Fermi limit , where LDA can be applied, collective modes depend on the number of particles only trough the parameters Λ and $\tilde{\Lambda}$.

3.6 Density Profiles

In Fig. 3.5 and Fig. 3.6 we show the density profiles of the bath as a function of the distance from the mobile impurity with mass ratio $w = 1$ and for different values of both the impurity-boson and the boson-boson coupling constant. Fig. 3.5 refers to repulsive interactions between the impurity and the bath, whereas Fig. 3.6 refers to attractive interactions. By increasing the value of η in the case of repulsive interactions, the density of bosons in the close vicinity of the impurity decreases until a hole, completely empty of particles, is created for very large η. The size of the hole strongly depends on the interaction parameter within the bath: it is on the order of the interparticle distance for the largest value ($\gamma = \infty$) and it extends to up to ~ 10 interparticle distances for the smallest one ($\gamma = 0.02$) [see panels (a)-(c) in Fig. 3.5]. In particular, in this last case, the density of the gas reaches its bulk value at distances $xn \sim 100$ not shown in the figure. We also notice that, for $\gamma = \infty$ and for the largest value of η, Friedel-type oscillations, typical of the fermionic nature of the TG gas, are visible in the density profile. The results of Fig. 3.6, instead, feature a peak of the boson density around the position of the impurity which becomes higher as the strength of the attraction increases. Also in this case the size of the peak gets larger as γ decreases. For the largest γ [see panel (a) in Fig. 3.6] the size of the peak is smaller than the interparticle distance and at large values of $|\eta|$ only one particle of the bath is, on average, close to the impurity forming a bound dimer with energy

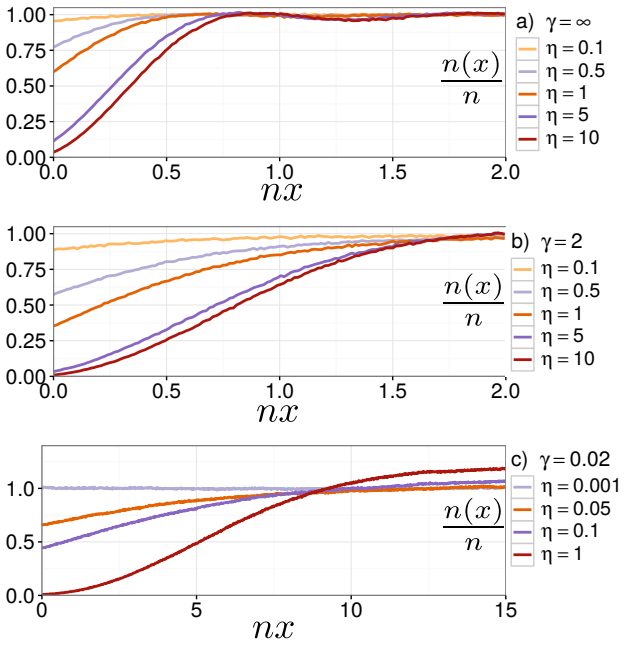

Figure 3.5: Normalized density profile $\frac{n(x)}{n}$ of the bath as a function of the distance from the repulsive mobile impurity with mass ratio $w = 1$. Distances are in units of the inverse 1D density $1/n$. The different curves correspond to different values of the parameter η characterizing the strength of impurity-bath repulsive interactions. The various panels refer to different values of the coupling constant within the bath: panel (a) $\gamma = \infty$, panel (b) $\gamma = 2$ and panel (c) $\gamma = 0.02$.

μ_d. Indeed, as already mentioned when discussing panel (a) of Fig. 3.1, the energy of a polaron in a TG gas tends to μ_d when η is large and negative. On the contrary, as the value of γ decreases, the density peak becomes wider and involves more and more particles of the bath [see panels (b) and (c) in Fig. 3.6]. As a consequence, the binding energy of the impurity increases in absolute value and one is approaching the situation of an unstable weakly interacting gas as shown in Fig. 3.3. Finally, in Fig 3.7, we show the results on the contact parameter C defined in Eq. (3.4). As explained in the previous section, the value of C is determined from the boson density $n(x)$ at the impurity position normalized by the bulk density n. We notice that we reproduce the exact result of Eq. (3.20) in the TG regime. Furthermore, as compared to the $\gamma = \infty$ case, we see that for smaller values of γ the contact parameter drops faster with increasing positive η and diverges faster with increasing negative η. Qualitatively similar results for the density profiles

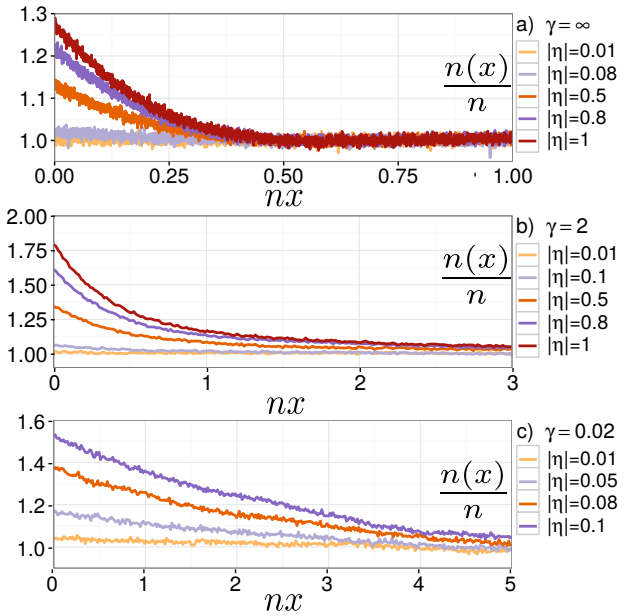

Figure 3.6: Normalized density profile $\frac{n(x)}{n}$ of the bath as a function of the distance from the attractive mobile impurity with mass ratio $w = 1$. Distances are in units of the inverse 1D density $1/n$. The different curves correspond to different values of the parameter $|\eta|$ characterizing the strength of impurity-bath attractive interactions. The various panels refer to different values of the coupling constant within the bath: panel (a) $\gamma = \infty$, panel (b) $\gamma = 2$ and panel (c) $\gamma = 0.02$.

and the contact parameter are obtained in the case of the static impurity with mass ratio $w = 0$.

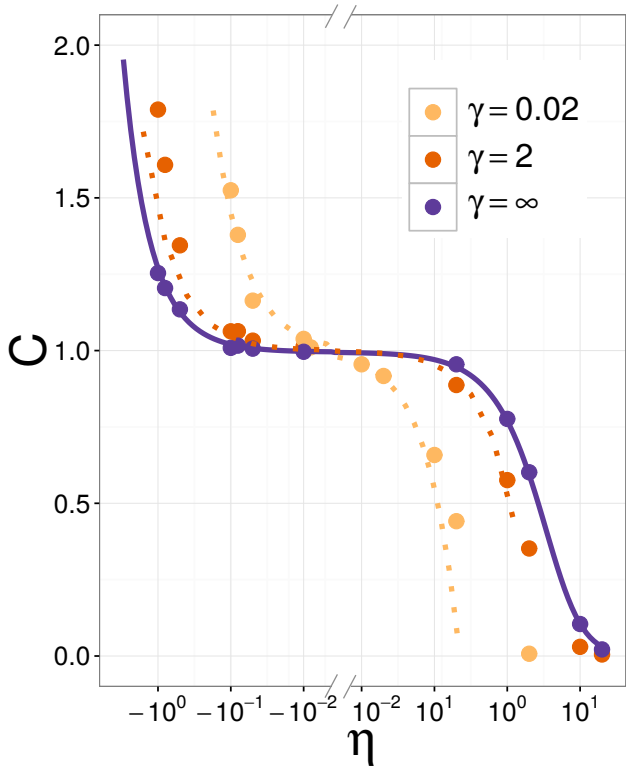

Figure 3.7: Contact parameter C [see Eq. (3.4)] of a mobile impurity with mass ratio $w = 1$ as a function of the impurity-boson interaction parameter η and for different values of the coupling strength γ within the bath. Both values corresponding to η positive and negative are shown in the same graph. The solid line corresponds to the exact result (3.20) holding in the TG limit. Dotted lines refer to the perturbative result holding for small values of η.

3.7 Conclusions

By using “exact" QMC numerical methods we investigated the properties of a Bose polaron in 1D as a function of both the coupling strength between the impurity and the bath and within the bath. For a given impurity-bath interaction strength we find that the repulsive polaron can never exceed the energy reached when the bath is in the TG regime. On the contrary, the binding energy of the attractive polaron lies always below the energy of a dimer in vacuum and becomes increasingly large as the repulsion within the medium is reduced, thereby signaling an instability of the weakly interacting gas to-

wards collapse around the impurity position. Furthermore, in the regime of a weakly repulsive medium, the polaron effective mass is found to increase sharply with the strength of the impurity-bath coupling. Such a heavy impurity, practically immobile within the medium, realizes the long-sought after regime of “self-localization" of the strongly coupled Landau-Pekar polaron. The impurity study may be a basis to study the effective interactions between impurities. The problem of effective interactions between impurities have been studied in three dimensions [97], where a theory for the effective interaction was introduced and validated with quantum Monte Carlo simulations. Effective interactions between bosonic and fermionic impurities immersed in a bosonic bath were also investigated in [98] using diagrammatic techniques. In one dimension the effective interactions have also been studied for a weakly interacting bath in presence of an harmonic trap [99]. There it was found that the interaction with the bath create an effective attraction between impurities. However the regime of a strongly interacting bath remains yet unexplored. It could be interesting to characterize the properties of two impurities immersed in a bosonic bath using Quantum Monte Carlo methods, which are also able to describe the regime of a strongly interacting bath, where fermionization becomes important.

Chapter 4

Repulsive Uniform Mixtures

This chapter is based on the article [28].

4.1 Introduction

The problem of dissipationless spin transport is a widely studied topic in condensed matter physics with important applications to electron-hole superfluidity, superfluid ^{3}He and spintronic devices [100]. Ultracold gases, with the possibility they offer to realize quantum degenerate mixtures, open new interesting perspectives for the investigation of spin dynamics. Spin diffusion in a strongly interacting two-component Fermi gas has been observed and characterized in a series of recent experiments [101, 102, 103], whereas the existence of spin supercurrents in Bose mixtures has been demonstrated both at very low temperatures [104, 105, 106, 107, 108, 109] and in the presence of a large thermal component [110]. In this respect one-dimensional (1D) mixtures are particularly interesting for several reasons: i) the low-energy dynamics is universal and described by the Luttinger liquid model [111]; ii) spin and charge degrees of freedom are expected to be completely decoupled at low energy [112, 113]; and, finally, iii) regimes of strong interactions can be achieved in long-lived samples [73, 80, 75, 76]. The undamped propagation of spin waves is an important signature of spin superfluidity and an unbiased determination of the spin-sound velocity is a crucial element to understand the dynamics of two-component Bose mixtures at ultralow temperatures. Notably, for such mixtures, the propagation of sound in the spin channel depends not only on the static magnetic susceptibility, but also on a purely dynamic quantity known as the Andreev-Bashkin non-dissipative drag [114]. This intriguing effect, never observed so far, involves two coupled superfluids and entails that a superflow in one component can induce

a supercurrent in the second component which is dragged without energy dissipation. In its original form, the Andreev-Bashkin effect was discussed in connection with possible superfluid mixtures of ^{3}He in ^{4}He. However, due to the limited solubility of the two isotopes [115], such superfluid mixtures have never been realized. In the context of ultracold atoms the Andreev-Bashkin effect was studied in the continuum using a perturbative approach based on the Bogoliubov theory [116] as well as in lattice systems [117]. More recently, its consequences on the propagation of spin waves were analyzed using the hydrodynamic theory [118]. In this chapter we investigate spin dynamics and the effect of the Andreev-Bashkin superfluid drag in 1D repulsive mixtures of Bose gases. To this aim we use quantum Monte-Carlo (QMC) methods first to establish the critical condition for the miscibility of the two gases, which is a preliminary requisite to investigate the regime of homogeneous mixtures. Second we calculate the entrainment effect from the coupled superfluid response and the spin-wave velocity by means of hydrodynamic theory and of a sum-rule approach. On the basis of simulations performed by varying both the intra-species and the inter-species coupling strength, we find that the superfluid drag can be large if the inter-species coupling is strong, and it contributes to the softening of spin waves on approaching the critical point of phase separation.

We consider Bose-Bose mixtures in a 1D geometry described by the following hamiltonian

$$\begin{aligned} H &= -\frac{\hbar^2}{2m}\sum_{i=1}^{N_a}\frac{\partial^2}{\partial x_i^2} + g\sum_{i<j}\delta(x_i - x_j) \\ &- \frac{\hbar^2}{2m}\sum_{\alpha=1}^{N_b}\frac{\partial^2}{\partial x_\alpha^2} + g\sum_{\alpha<\beta}\delta(x_\alpha - x_\beta) + \tilde{g}\sum_{i,\alpha}\delta(x_i - x_\alpha)\ , \end{aligned} \tag{4.1}$$

which includes, in addition to the kinetic energy terms of the two components with N_a and N_b particles, equal intra-species interactions modeled by the contact coupling constant $g > 0$ and a contact inter-species repulsive potential of strength $\tilde{g} > 0$. Here x_i with $i = 1, \ldots, N_a$ and x_α with $\alpha = 1, \ldots, N_b$ denote, respectively, the positions of particles belonging to component a and b of the mixture. We also consider mass balanced mixtures, m being the mass of particles of both components. In the absence of inter-species interactions, the above hamiltonian for each component separately yields the well-known Lieb-Liniger (LL) model [35], which can be solved exactly via Bethe ansatz for any value of the coupling constant g. In particular, for very strong repulsion ($g \to \infty$) corresponding to the so-called Tonks-Girardeau (TG) regime, the LL model describes a gas of impenetrable bosons which is equivalent to

a gas of non-interacting spinless fermions [36]. The full hamiltonian (4.1) consists of two LL gases, with the same interaction strength g, coupled via a contact repulsive force. One should point out that this full hamiltonian also admits exact solutions, but only when it enjoys SU(2) symmetry, *i.e.* if $\tilde{g} = g$ or when both components are in the TG regime ($g = \infty$). In the first case the ground-state is ferromagnetic [119, 120] and the equation of state can be calculated using the LL model of a single-component gas. In the latter case, the system corresponds to a mixture of interacting Fermi gases and the solution is provided by the Yang-Gaudin model [8, 9] yielding a paramagnetic ground-state for any value of the repulsive coupling $\tilde{g}$. In all other cases, for which the Bethe ansatz approach is no longer applicable, only numerical solutions are available by means, for example, of QMC methods.

A population balanced system, where $N_a = N_b = N/2$, can be fully characterized in the thermodynamic limit by the following two dimensionless parameters

$$\gamma = \frac{gm}{\hbar^2 n} \qquad \eta = \frac{\tilde{g}m}{\hbar^2 n} \,. \tag{4.2}$$

These are fixed by the values of interaction strength and by the total density $n = n_a + n_b$ of the gas, where $n_a = N_a/L$ and $n_b = N_b/L$ are the densities of the two components in terms of the size L of the 1D box. In unbalanced configurations, an additional parameter is needed to describe the polarization: $P = (n_a - n_b)/n$. In the previous section we studied the extreme case of one impurity immersed in a LL gas ($N_b = 1$). Here we make use of a similar diffusion Monte-Carlo method extended to any configuration $N_b \leq N_a$ with periodic boundary conditions. The relevance of finite-size effects is estimated by repeating the simulations with increasing numbers of particles (typically ranging from $N = 50$ to $N = 200$), thereby ensuring a well-controlled approach to the thermodynamic limit.

4.2 The Wavefunction

We perform DMC simulations using a a wavefunction that takes the Jastrow form definied in the previous chapter. For a bath with an impurity it takes the form

$$\Psi = \prod_{i<j=1}^{N_a} f_{aa}(x_i - x_j) \prod_{\alpha<\beta=1}^{N_b} f_{bb}(x_\alpha - x_\beta) \prod_{i=1}^{N_B} \prod_{\alpha=1}^{N_b} f_{ab}(x_i - x_\alpha) \tag{4.3}$$

The functions f_{aa},f_{bb},f_{ab} all takes the form 2.130 and satisfy the Bethe-Beierls conditions with coupling g and $\tilde{g}$ respectively for intraparticle jastrows (f_{aa} and f_{bb}) and the inter particle jastrow (f_{ab}).

4.3 Phase separation

The first question we address concerns the condition of miscibility of the mixture at $T = 0$ and of its eventual phase separation. This latter is signaled by the divergence of the magnetic susceptibility χ, whose inverse is related to the curvature of the energy increase as the system is polarized away from the $P = 0$ balanced configuration: $\frac{1}{\chi} = \frac{\partial^2 E/L}{n^2 \partial P^2}$. In the weak-coupling regime, corresponding to $\gamma \ll 1$ and $\eta \ll 1$, one can use the mean-field theory yielding the analytical result $\frac{1}{\chi} = \frac{g-\tilde{g}}{2}$ [121]. Based on this approach the mixture is miscible for $\tilde{g} < g$ and phase separation occurs as soon as $\tilde{g} > g$. Furthermore, in the Yang-Gaudin model where both components are in the fermionic TG limit, the homogenous mixture is known to be stable for any value of the inter-species coupling strength $\tilde{g}$. A question worth addressing concerns the determination of the critical parameter for phase separation in the regime of intermediate values of the coupling strength γ. To this purpose we calculate the ground-state energy for fixed values of γ and η with varying polarization P. The characteristic dependencies, obtained for $\gamma = 2$ and $\gamma = 20$, are shown in Fig. 4.1.

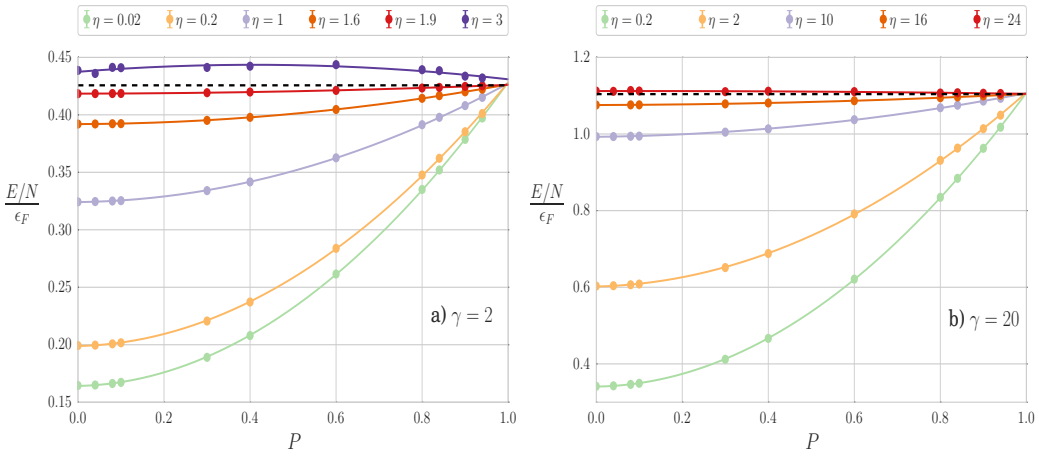

Figure 4.1: Energy per particle of the homogeneous mixture as a function of the polarization P for different values of the coupling strengths η. Panel (a) refers to $\gamma = 2$ and panel (b) to $\gamma = 20$. Energies are shown in units of $\epsilon_F = \frac{\hbar^2 \pi^2 n^2}{8m}$ corresponding to the Fermi energy of the mixture when $\gamma = \infty$. The solid lines are best fits quadratic in P and the dashed horizontal lines indicate the energy of the fully polarized ($P = 1$) states. Statistical error bars are smaller than the symbol size.

We find that the energy of the $P = 0$ state is lower than the one of the

fully polarized ($P = 1$) state provided that $\eta < \gamma$. For η slightly larger than γ the energy lies above the $P = 1$ threshold signalling the instability against the formation of two fully polarized domains [122].

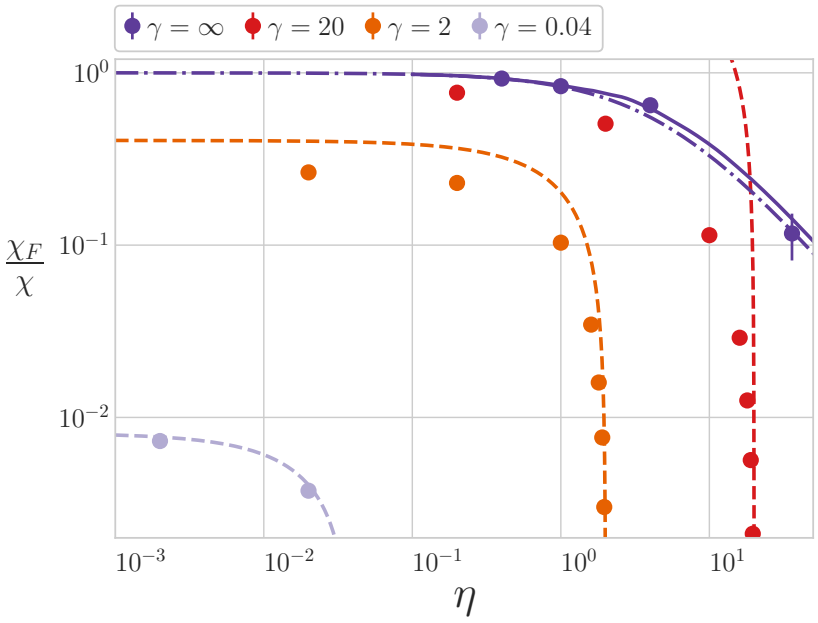

Figure 4.2: Inverse susceptibility $1/\chi$ as a function of η for various values of γ ranging from the weak-coupling regime ($\gamma = 0.04$) to the TG limit ($\gamma = \infty$). Here $\chi_F = \frac{4m}{\hbar^2\pi^2 n}$ is the susceptibility of the non-interacting mixture when $\gamma = \infty$. Dashed lines correspond to the mean-field result $1/\chi = (g - \tilde{g})/2$, whereas the dash-dotted line to the perturbation expansion $\frac{\chi_F}{\chi} = 1 - \frac{2\eta}{\pi^2}$ holding in the TG limit. The solid line is obtained from the exact solution of the Yang-Gaudin model at finite polarization.

From the equation of state as a function of the polarization P we extract the inverse magnetic susceptibility $1/\chi$ which we report in Fig. 4.2 for various values of γ. We see that for $\gamma = 0.04$ the results of $1/\chi$ are well reproduced by the mean-field prediction whereas, for larger values of γ, deviations are visible away from the critical point. Close to the point of phase separation, however, we notice that the susceptibility of both $\gamma = 2$ and $\gamma = 20$ is well described by the linear dependence $1/\chi \propto (\gamma - \eta)$ of the mean-field prediction. Finally, for $\gamma = \infty$, our results reproduce the η-dependence of $1/\chi$ obtained from the exact solution [123, 129, 124] of the Yang-Gaudin model at finite polarization [125]. From this analysis we conclude that, for the reported values of $\gamma < \infty$, the critical parameter for phase separation is $\eta = \gamma$. At this

value of the inter-species interaction strength the system jumps from being paramagnetic with $P = 0$ to fully ferromagnetic. These results are consistent with the known findings of the Yang-Gaudin model ($\gamma = \infty$) where phase separation never occurs [8], and of the SU(2) symmetric case ($\gamma = \eta$) where the stable phase is ferromagnetic [119, 120].

4.4 Hydrodynamic theory

We have already described the hydrodynamic theory for a single species. Let us now generalize the hydrodynamic theory to the case of interacting mixtures. We can write the superfluid velocity as a two component vector

$$v = \begin{pmatrix} \partial_x \phi_1(x) \\ \partial_x \phi_2(x) \end{pmatrix} \tag{4.4}$$

where $\phi_a(x)$ is the phase of the a component. The classical hamiltonian can than be generalized to

$$H = \int dx \frac{1}{2} \left[v^T \rho v + e(\rho) \right] \tag{4.5}$$

where the superfluid density of the single component case has been replaced by a matrix.

$$\rho = \begin{pmatrix} \rho_{11} & \rho_{12} \\ \rho_{12} & \rho_{22} \end{pmatrix} \tag{4.6}$$

The first term in the hamiltonian represents the kinetic energy arising from the fluid flow and must always be positive, for any velocity vector v. This condition can only be satisfied when the matrix is definite positive or equivalently its determinant must be positive.

$$\rho_{12}^2 <= \rho_{11}\rho_{22} \tag{4.7}$$

The corresponding current takes the form

$$\begin{pmatrix} j_1 \\ j_2 \end{pmatrix} = \begin{pmatrix} \rho_{11} & \rho_D \\ \rho_D & \rho_{22} \end{pmatrix} \begin{pmatrix} v_1 \\ v_2 \end{pmatrix} \tag{4.8}$$

Notice that one can obtain a current in one component even if its superfluid velocity is zero, as long as the superfluid velocity of the second component is different from zero. Imprinting a superfluid velocity in one component will also trigger a motion of the second component. This effect can be seen as a

form of dissipation-less drag between the two components.
The total current is given by

$$J = j_1 + j_2 \tag{4.9}$$

$$= (\rho_{11} + \rho_D)v_1 + (\rho_{22} + \rho_D)v_2 \tag{4.10}$$

$$= \rho_1 v_1 + \rho_2 v_2 \tag{4.11}$$

where ρ_1 and ρ_2 are the superfluid fraction of the two different components.

$$\rho_1 = \rho_{11} + \rho_D \tag{4.12}$$

$$\rho_2 = \rho_{22} + \rho_D \tag{4.13}$$

Together with the positiveness condition , one gets an upper bound for the superfluid drag

$$\rho_D \leq \frac{\rho_1 \rho_2}{\rho_1 + \rho_2} \tag{4.14}$$

In our case the two components are symmetric and the superfluid densities of the two components must be the same. Setting $\rho_1 = \rho_2 = \rho_T/2$ one gets

$$\rho_D \leq \frac{\rho_T}{4} \tag{4.15}$$

As we did for the single-component, we now can promote ρ and ϕ to operators. We then expand the hamiltonian around the ground-state average ρ_T up to second order in the fluctuations. After some algebra one arrives to the hamiltonian

$$H = \frac{1}{2}\left[\partial_x \hat{\phi} \rho \partial_x \hat{\phi} + \delta\hat{\rho} K \delta\hat{\rho}\right] \tag{4.16}$$

with

$$K = \begin{pmatrix} \frac{\partial^2}{\partial^2_{\rho_1}} e & \frac{\partial^2}{\partial_{\rho_1}\partial_{\rho_2}} e \\ \frac{\partial^2}{\partial_{\rho_1}\partial_{\rho_2}} e & \frac{\partial^2}{\partial^2_{\rho_2}} e \end{pmatrix} \tag{4.17}$$

and

$$\delta\hat{\rho} = \begin{pmatrix} \hat{\rho}_1 - \rho_T/2 \\ \hat{\rho}_2 - \rho_T/2 \end{pmatrix} \tag{4.18}$$

In order to decouple the hamiltonian we can perform the change of variables

$$\phi_{d,s} = \phi_1 \pm \phi_2 \tag{4.19}$$

$$\delta\rho_{d,s} = \delta\rho_1 \pm \delta\rho_2 \tag{4.20}$$

The hamiltonian in terms of these new variables decouples in two channels, the density and spin channel.

$$H = H_d + H_s \tag{4.21}$$

$$H_d = \frac{1}{2}\int dx \left[\partial_x\phi_d\rho_d\partial_x\phi_d + c^2(\delta\rho_d)^2\right] \tag{4.22}$$

where $\rho_d = \rho_T$ and c is the speed of sound

$$\frac{m^2c^2}{\rho_T} = \rho_T\frac{\partial\mu}{\partial_{\rho_T}} = \frac{1}{\kappa} \tag{4.23}$$

The excited states of the hamiltonian are phonons, with a linear dispersion relation whose slope is given by the speed of sound c. Notice that the dependence on the drag coefficient in the density channel disappears entirely.
The spin part of the hamiltonian takes instead the form

$$H_s = \frac{1}{2}\int dx \left[\partial_x\phi_s\rho_s\partial_x\phi_s + v_s^2(\delta\rho_s)^2\right] \tag{4.24}$$

where $\rho_s = \rho_T - 4\rho_D$ and

$$v_s^2 = \frac{\rho - 4\rho_D}{m^2\chi} \tag{4.25}$$

and χ is the magnetic susceptibility. The excitations in the spin channel still have a linear dispersion, but with a different slope given by v_s, which we call the speed of spin waves.
As phonons correspond to excitations in the total density , spin waves correspond to excitations in the magnetization. They depend both on the spin susceptibility and on the drag coefficient ρ_D.

4.5 Superfluid drag

For 1D mixtures with $\rho_1 = \rho_2 = \rho/2$, one can calculate ρ_D to lowest order in $\tilde{g}$ by using the Bogoliubov approach of Ref. [116] which yields the result

$$\frac{\rho_D}{\rho} \simeq \frac{4\eta^2}{3\pi}\frac{1}{\left(\sqrt{2(\gamma+\eta)} + \sqrt{2(\gamma-\eta)}\right)^3} . \tag{4.26}$$

This shows that the drag effect is quadratic in the inter-species coupling η and is maximum at the critical point $\eta = \gamma$ where it takes the value $\frac{\rho_D}{\rho} = \frac{\sqrt{\gamma}}{6\pi}$. For arbitrary coupling strengths, we calculate ρ_D by means of the exact relation

$$4\frac{\rho_D}{\rho} = 1 - \lim_{\tau\to\infty}\frac{\langle(W_a(\tau) - W_b(\tau))^2\rangle}{4ND\tau} , \tag{4.27}$$

based on the paired superfluid response of the two components which in QMC simulations is provided by the statistics of winding numbers [118]. Here, $D = \hbar^2/2m$ is the diffusion constant of a free particle in imaginary time $\tau = it/\hbar$, whereas the winding number $W_a(\tau) = \sum_{i=1}^{N_a} \int_0^\tau d\tau' \frac{dx_i(\tau')}{d\tau'}$ of the first component and, analogously, $W_b(\tau)$ of the second component are obtained by integrating the corresponding particle trajectories. In the absence of inter-species coupling, the winding numbers W_a and W_b are independent and, being normalized as $N_{a(b)} = \lim_{\tau\to\infty} \frac{\langle W^2_{a(b)}(\tau)\rangle}{4D\tau}$, result in $\rho_D = 0$. In the opposite case of fully paired motion of the two components, the relative winding number $(W_a - W_b)$ vanishes and the drag takes its maximum value $4\rho_D/\rho = 1$. In Fig. 4.3 we report the results of ρ_D calculated as a function of η for different values of the interaction parameter γ. We find that $4\rho_D/\rho$ approaches unity in the simultaneous limit $\gamma = \infty$ and $\eta = \infty$. However, already for $\gamma = 20$, ρ_D reaches ~ 0.7 of its maximum value in the vicinity of the critical point $\eta = \gamma$.

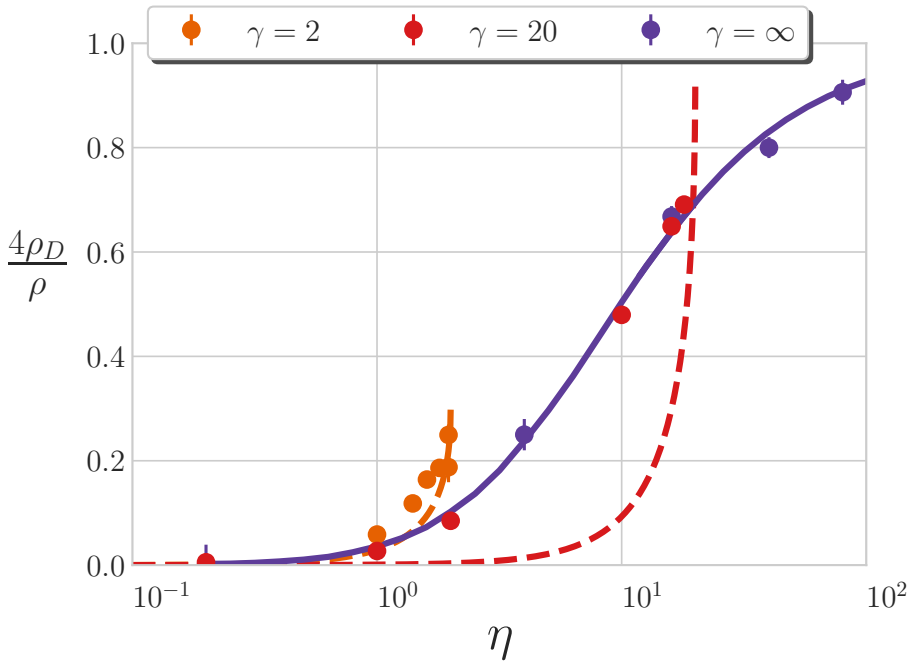

Figure 4.3: Superfluid drag as a function of η for different values of γ. Dashed lines correspond to the weak-coupling result (4.26) for $\gamma = 2$ and $\gamma = 20$. The solid line refers to $\gamma = \infty$ and is obtained by inverting Eq. (4.28) with both χ and v_s from the exact solution of the Yang-Gaudin model.

4.6 Velocity of spin waves

Within the mean-field approach the long-wavelength elementary excitations in the spin channel consist of waves propagating with the velocity $v_s = \sqrt{\frac{n(g-\tilde{g})}{2m}}$ [121], such that $v_s^2 = \frac{\rho}{m^2\chi}$ in terms of the magnetic susceptibility and of the mass density $\rho = mn$. This result, however, holds only if one neglects the drag effect exerted by one component as it moves with respect to the other. Within the hydrodynamic theory , the speed of sound can be written as

$$v_s^2 = \frac{\rho - 4\rho_D}{m^2\chi} \, , \tag{4.28}$$

and can be obtained from the magnetic susceptibility and the superfluid drag.

In order to determine the spin-wave velocity v_s, we follow two independent approaches. The first is based on the hydrodynamic theory of superfluids entailed by Eq. (4.28), where we determine v_s from the knowledge of the magnetic susceptibility χ and of the superfluid drag ρ_D calculated above. The second, instead, is based on linear response theory and is conveniently discussed in terms of the frequency-weighted moments $m_k = \int d\omega \, (\hbar\omega)^k S_s(\mathbf{q},\omega)$ of the spin-dependent dynamic structure factor $S_s(\mathbf{q},\omega)$. In particular, for the following two moments one finds

$$m_{-1} = N\frac{\chi_s(q)}{2n} \underset{q\to 0}{\to} N\frac{\chi}{2n} \, , \tag{4.29}$$

$$m_0 = S_s(q) \, . \tag{4.30}$$

Here, Eq. (4.29) is the susceptibility sum rule involving the static spin-spin response function $\chi_s(q)$, which reduces to χ in the long-wavelength limit, and Eq. (4.30) defines the static spin-spin structure factor. One can show that in the $q \to 0$ limit both the m_{-1} and m_0 sum rules are exhausted by the spin-wave excitation with energy $\epsilon_s(q) = v_s\hbar q$, because multi-mode excitations contribute to the two sum rules with higher powers of q [126, 127, 128]. From this analysis it follows that the energy of the low-lying spin-wave excitations can be obtained from the ratio of sum rules calculated in the $q \to 0$ limit

$$\hbar q v_s = \lim_{q\to 0} \frac{m_0}{m_{-1}} \, . \tag{4.31}$$

A direct calculation of the static spin-spin structure factor $S_s(q)$ allows one to extract the coefficient of its low-q linear dependence $S_s(q)/N = \frac{v_s\chi}{2n}\hbar q$. Once divided by the magnetic susceptibility χ obtained above, this result gives the spin velocity v_s.

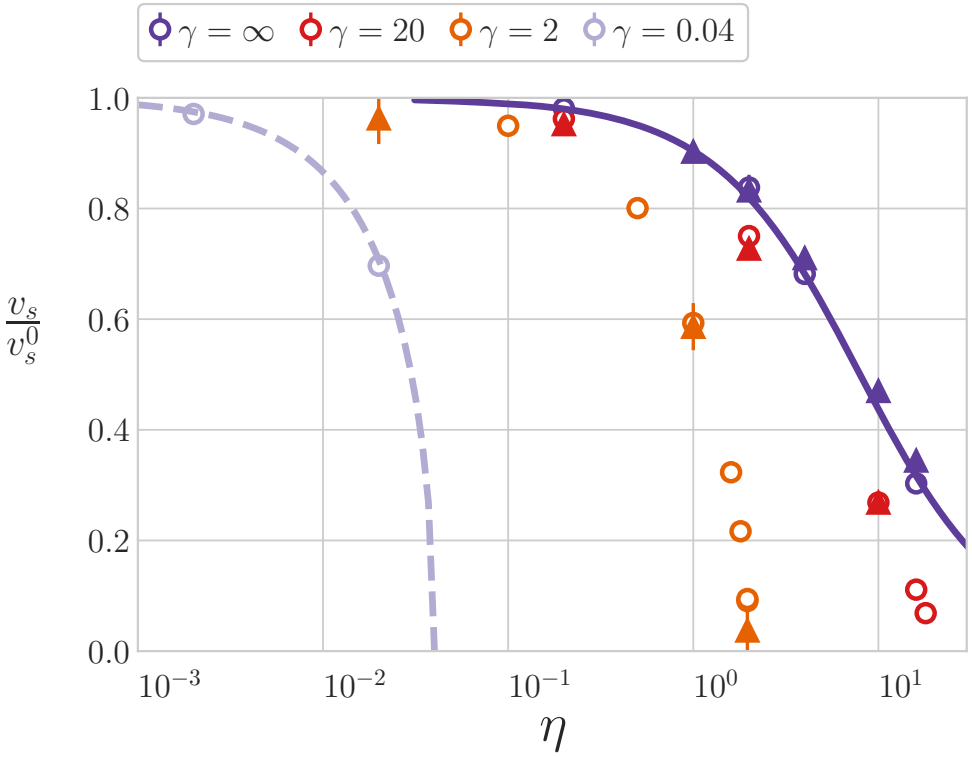

Figure 4.4: Spin-wave velocity v_s as a function of η for different values of γ. The units are provided by the spin-wave velocity in the absence of inter-species interactions, $v_s^0 = \sqrt{\rho/m^2\chi_0}$. Open symbols refer to Eq. (4.28) and solid symbols to Eq. (4.31). The dashed line corresponds to the mean-field prediction $v_s = \sqrt{n(g-\tilde{g})/2m}$ and the solid line to the exact solution in the Yang-Gaudin model [129].

Both the hydrodynamic and the more microscopic estimate of v_s are shown in Fig. 4.4 and are found to agree within statistical errors providing a very strong evidence of the reliability of our results. When $\gamma = \infty$ we also find agreement with the exact result of v_s from the Yang-Gaudin model [38, 129]. By increasing the inter-species interaction strength, the spin-wave velocity decreases due to the combined effect of the susceptibility, which rises from the non-interacting value χ_0, and of the drag density ρ_D until it vanishes at the critical point of phase separation. For example, for $\eta = 10$ and $\gamma = 20$ the spin-wave velocity is reduced to $v_s \simeq 0.3 v_s^0$ of the value corresponding to $\eta = 0$ (see Fig. 4.4). The reduction is caused by an approximate five-fold increase of χ/χ_0 shown in Fig. 4.2 and by an additional factor of about 0.5 deriving from the term $1 - 4\rho_D/\rho$ shown in Fig. 4.3.

4.7 Conclusions

In conclusion, we investigated balanced repulsive one-dimensional mixtures. We have shown that the miscibility phase diagram predicted by mean-field theories remains valid even at strong interactions, where mean-field theories cannot be reliably applied. We compute the drag between two components of the mixtures, and found that the drag becomes high when both inter-species and intra-species interactions become important.
Finally we computed the speed of the sound waves using linear response theory and using quantum hydrodynamics theory by combining calculations of the magnetic susceptibility and of the drag coefficient. The velocity of the spin waves can be measured experimentally using spectroscopic techniques. The magnetic susceptibility can also be observed in experiments. Thus one may use equation 4.28 to indirectly measure the superfluid drag in an experiment by measuring both the magnetic susceptibility and the speed of sound waves.

Chapter 5

Trapped Mixtures

5.1 Introduction

While recently it has become possible to realize Bose-Einstein condensation in arbitrary potentials[130], most experiments are still performed in harmonic traps. Moreover, collective modes of atoms in traps are characteristic features of the many-body system[131] and are experimentally accessible. For instance, in one dimension, the breathing mode of a one dimensional Bose gas has been experimentally investigated[50]. In mixtures, the simplest modes to excite are the breathing mode, i.e. the response to a small change in the radius of the cloud and the spin-dipole mode, the response to a small relative displacement between the center of mass of the two components. The local density approximation (LDA), holding in the limit of a large number of trapped atoms[31], can be used to link the properties of the uniform systems to the ones of the system in a trap. The spin-dipole mode has been computed [132] in the weakly interacting regime and has been observed experimentally in three dimensions [133] . In one dimension the LDA theory has been successfully applied to predict the breathing mode in strongly correlated systems . For instance the frequency of the breathing mode of a trapped Lieb-Liniger gas [134] and of a trapped Yang-Gaudin gas [135] have been calculated. For a trapped Yang-Gaudin gas , the LDA approximation yields a diverging result for the spin-dipole mode and one needs to go beyond the LDA approximation to obtain the frequency of the spin-dipole mode beyond logarithmic accuracy[136].
We will first review some general theory of quantum systems trapped by a harmonic potential and define the different regimes of interest. Then we will turn to the description of our DMC results. In particular we calculate the frequency of the spin-dipole mode for several values of inter-species and

intra-species interaction strength.

5.2 General theory

We will be considering a Bose mixture of two components in the presence of contact interactions in presence of an external trapping potential

$$\begin{aligned} H &= -\frac{\hbar^2}{2m}\sum_{i=1}^{N_a}\frac{\partial^2}{\partial x_i^2} + g\sum_{i<j}\delta(x_i - x_j) - \frac{\hbar^2}{2m}\sum_{\alpha=1}^{N_b}\frac{\partial^2}{\partial x_\alpha^2} \\ &+ g\sum_{\alpha<\beta}\delta(x_\alpha - x_\beta) + \tilde{g}\sum_{i,\alpha}\delta(x_i - x_\alpha) \qquad (5.1) \\ &+ \sum_i V_a(x_i) + \sum_\alpha V_b(x_\alpha) \qquad (5.2) \end{aligned}$$

where $V_{a(b)}$ is an external single particle potential,N_a is the number of particles of the a component and b is the number of particles of the b component . We will consider a harmonic trapping potential

$$V_{a(b)}(x) = \frac{1}{2}m\omega^2\left(x \pm \frac{d}{2}\right)^2 \qquad (5.3)$$

where the + sign stands for the a component and the − sign for the b component, while d represents the distance between the minimums of the two harmonic potentials.

5.2.1 The local density approximation (LDA)

The properties of the trapped system can be related to the properties of the homogenous system trough the local density approximation [31] (LDA).The LDA approximation consists in writing the chemical potential of the system as the sum of the chemical potential at density n and the external potential. In a two component system we may write

$$\mu_{0,a} = \mu_a(n_a, n_b) + V_a(x) \qquad (5.4)$$

$$\mu_{0,b} = \mu_b(n_a, n_b) + V_b(x) \qquad (5.5)$$

In equilibrium the chemical potential of each component $\mu_{0,a(b)}$ must be a constant. Thus one may invert equations 5.4 and 5.5 to obtain the spatial dependence of the density profile of the two components of the mixture. The unkown values of the chemical potentials $\mu_{0,b(a)}$ are determined by requiring

that the integral of the density profiles $n_{a(b)}(x)$ sums to $N_{a(b)}$, the number of particles for each component.
For the sake of simplicity, let us consider the balanced case with vanishing trap displacement: $d = 0$ and $N_a = N_b = N/2$ and $V_a = V_b$. Summing 5.4 and 5.5 one gets

$$\mu_0 = \mu(n) + V(x) \tag{5.6}$$

where $\mu_0 = (\mu_{0,a} + \mu_{0,b})/2$ and $\mu = (\mu_a + \mu_b)/2$. The local density approximation is expected to be valid when the radius of the cloud is much larger than the harmonic oscillator length $a_h = \sqrt{\hbar/m\omega}$.

TG gas

In the limit of $g \to \infty$ and $\tilde{g} \to \infty$ the uniform system is equivalent to a single gas of N particles with energy per particle

$$\frac{E}{N} = \frac{\hbar^2\pi^2 n^2}{6m} \tag{5.7}$$

where the chemical potential is equal to the Fermi energy

$$\mu = \frac{\hbar^2\pi^2 n^2}{2m} \tag{5.8}$$

Using 5.6 one gets the total density profile

$$n(x) = n_0\sqrt{1 - \left(\frac{x}{R}\right)^2} \tag{5.9}$$

where n_0 is the density profile at the center of the trap and R is the radius of the trap

$$n_0 = \frac{R}{\pi a_h^2} \tag{5.10}$$

$$R = \sqrt{2N}a_h \tag{5.11}$$

Mean-field

In the regime of weak coupling $g \ll 1$ and $\tilde{g} \ll 1$ the energy takes the form

$$\frac{E}{N} = \frac{1}{4}gn + \frac{1}{4}\tilde{g}n \tag{5.12}$$

where E/N is the energy per particle. Using equation 5.6 one gets

$$n(x) = n_0\left(1 - \left(\frac{x}{R}\right)^2\right) \tag{5.13}$$

$$n_0 = \frac{m\omega^2 R^2}{2g} \tag{5.14}$$

$$R = \left(\frac{3gN}{2m\omega^2}\right)^{1/3} \tag{5.15}$$

Notice that in the two regimes the scaling of the radius R with the number of particles is very different. In the mean-field case the radius scales as $N^{1/3}$ while in the TG regime it scales as $N^{1/2}$.

5.2.2 GP theory

In the weakly interacting regime , non homogenous systems can be described by the GP equation generalized to two components.
For a two-component gas the GP theory takes the form of two coupled equation2 for the order parameters of the two components Ψ_a and Ψ_b.

$$\left\{-\frac{\hbar^2}{2m}\frac{\partial_x^2}{\partial_x^2} + g|\Psi_a(x)|^2 + \tilde{g}|\Psi_b(x)|^2\right\}\Psi_a(x) = \mu_a\Psi_a \tag{5.16}$$

$$\left\{-\frac{\hbar^2}{2m}\frac{\partial_x^2}{\partial_x^2} + g|\Psi_b(x)|^2 + \tilde{g}|\Psi_a(x)|^2\right\}\Psi_b(x) = \mu_b\Psi_b \tag{5.17}$$

The advantage of equations 5.16 and 5.17 is that they are always valid in the weakly interacting regime, even when the LDA approximation is not valid. The GP equation depends on the number of particles trough the normalization of the wavefunctions

$$\int |\Psi_a(x)|^2 = N_a \tag{5.18}$$

$$\int |\Psi_b(x)|^2 = N_b \tag{5.19}$$

One can rewrite the GP equations in term of the dimensionless quantities

$$x' = x/a_h \qquad t' = t\omega \tag{5.20}$$

$$\psi'_{a(b)}(x) = \frac{\psi_{a,b}(x)}{\sqrt{N_{a,b}}} \quad a_h = \sqrt{\tfrac{\hbar}{m\omega}} \tag{5.21}$$

$$\mu'_a = \frac{\mu_a}{\hbar\omega} \qquad \mu'_b = \tfrac{\mu_b}{\hbar\omega} \tag{5.22}$$

obtaining

$$\left\{-\frac{1}{2}\frac{\partial^2}{\partial_{x'}^2}+\frac{\lambda}{2}|\Psi_a'|^2+\frac{\tilde{\lambda}}{2}|\Psi_b'|^2+\frac{1}{2}x^2\right\}\Psi_a'=\mu_a'\Psi_a' \tag{5.23}$$

$$\left\{-\frac{1}{2}\frac{\partial^2}{\partial_{x'}^2}+\frac{\lambda}{2}|\Psi_b'|^2+\frac{\tilde{\lambda}}{2}|\Psi_a'|^2+\frac{1}{2}x^2\right\}\Psi_b'=\mu_b'\Psi_b' \tag{5.24}$$

where the N dependance is explicity contained in the parameters

$$\lambda=\frac{N_a a_h}{a} \tag{5.25}$$

$$\tilde{\lambda}=\frac{N_b a_h}{\tilde{a}} \tag{5.26}$$

where a_h is the harmonic oscillator length and $a(\tilde{a})$ is the intra-species(inter-species) scattering length. Note that in the large N limit $\lambda,\tilde{\lambda}\to\infty$. In this regime the kinetic term can be neglected and one recovers the LDA equations and the inverted parabola density profile. In the limit $\lambda,\tilde{\lambda}\to 0$ one recovers the equations for a single particle in a harmonic oscillator whose solution is a gaussian.

5.2.3 Interaction regimes in 1D

The parameters λ and $\tilde{\lambda}$ are able to capture the crossover from a gaussian profile to the Thomas-Fermi profile, where the local density approximation is valid. This is not only true in the weakly interacting regime, but in the strongly interacting regime as well[31][137]. For a trapped Lieb-Liniger gas it was found that the parameter that characterizes the strength of the interactions is proportional to $N(a/a_h)^2$[137]. Not only it determines the crossover from a MF density profile to a TG density profile, but it can be shown that the breathing mode depends only on this parameter in the limit $\lambda\to\infty$[137]. In a single component Lieb-Liniger gas in an harmonic potential the two parameters that entirely determine the system are

$$\Lambda=\frac{1}{N}\left(\frac{a_h}{a}\right)^2 \quad \lambda=\tfrac{Na_h}{a} \tag{5.27}$$

The two parameters Λ and λ are related by $\Lambda=\lambda^2N^{-3}$. The condition for the validity of the LDA approximation , $\lambda\gg 1$,implies $\Lambda\gg N^{-3}$. Thus when $\Lambda\ll N^{-3}$ the system is found in the gaussian regime where the LDA approximation does not hold. When $N^{-3}\ll\Lambda\ll 1$ the system is well described by the LDA mean-field theory and the density profile takes the form of an inverted parabola. Finally when $\Lambda\gg 1$ the system is in

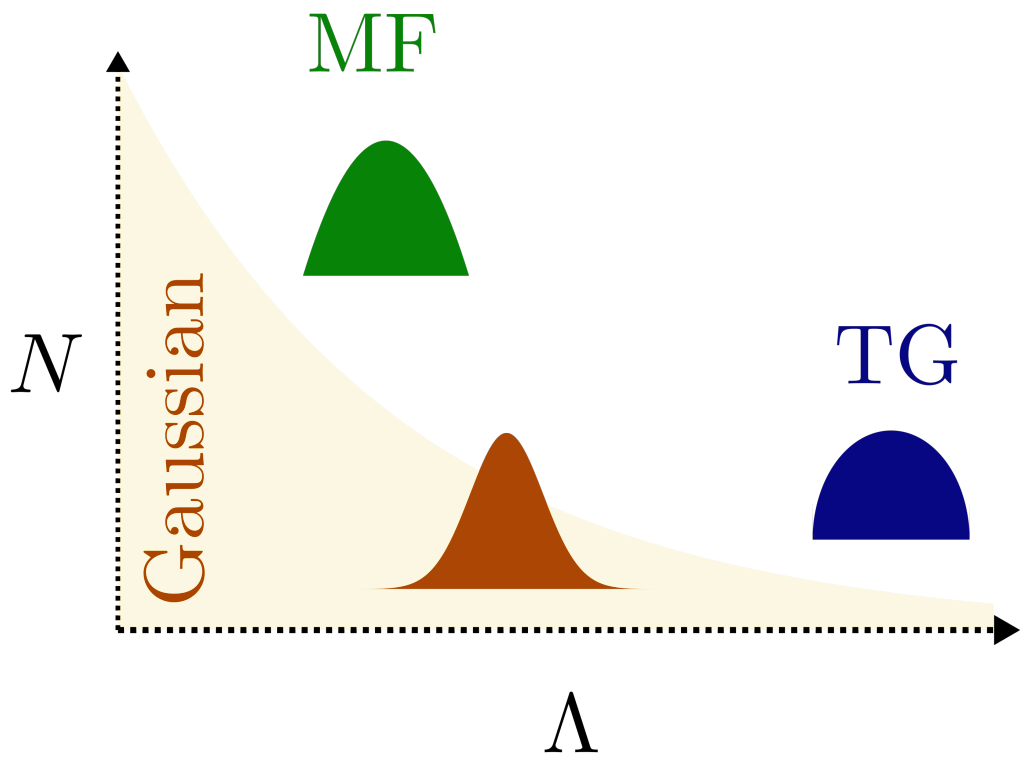

Figure 5.1: Illustration of the different regimes for a single component one dimensional gas in a harmonic trap in function of the parameter Λ and the number of particles N. The region where the condition for the validity of the LDA approximation $\Lambda \ll N^{-3}$ is not satisfied is colored in yellow. On can clearly see that a large number of particles is required to apply LDA in the weakly interacting regime while just a few particles are required to obtain the Thomas-Fermi profile in the strongly interacting limit.

the regime described by the Thomas Fermi profile of a trapped TG gas. The different regimes are illustrated in figure 5.1. Notice that the condition $\Lambda \gg N^{-3}$ for the LDA approximation to hold can be reached already at very small particle number. For instance, when $\Lambda = 0.01$ and $N = 20$ one gets $\Lambda = 10^{-2} \gg N^{-3} = 20^{-3} = 1.25 \cdot 10^{-4}$. However, in experiments where the 1D confinement is obtained with an optical lattice producing a large number of tubes, the average number of atoms per tube can be as small as a few tens of particles [138][79] . In this case deviations from LDA are siginificant [138]. Much larger condensates can however be obtained using micro-traps [139].
In a one dimensional mixture, on can easily generalize by defining the pa-

rameters

$$\Lambda = \frac{1}{N}\left(\frac{a_h}{a}\right)^2 \quad \lambda = \frac{Na_h}{a} \tag{5.28}$$

$$\tilde{\Lambda} = \frac{1}{N}\left(\frac{a_h}{\tilde{a}}\right)^2 \quad \tilde{\lambda} = \frac{Na_h}{\tilde{a}} \tag{5.29}$$

where N is the total number of particles in the mixture.

5.3 The trial wavefunction

The guiding wavefunction we use in our simulations can be written as

$$\begin{array}{rl} \Psi = & \prod_{i<j=1}^{N_a} f_{aa}(x_i - x_j) \prod_{\alpha<\beta=1}^{N_b} f_{bb}(x_\alpha - x_\beta) \\ & \prod_{i=1}^{N_B} \prod_{\alpha=1}^{N_b} f_{ab}(x_i - x_\alpha) \\ & \prod_{i=1}^{N_a} \phi(x_i - a) \prod_{\alpha=1}^{N_b} \phi(x_\alpha - b) \end{array} \tag{5.30}$$

where $f_{aa} = f_{bb}$ and f_{ab} take the form 2.133 respectively with the scattering lengths a and $\tilde{a}$. The one body term $\phi(x) = e^{-\alpha x^2}$ is written as a simple gaussian whose width is treated as a variational parameter. Both a and b are variational parameters and are required in the case of non zero displacement d between the two harmonic traps.

5.4 Density Profiles

We performed several simulations for different values of $\Lambda, \tilde{\Lambda}$. In this section we show several profiles of the total density in the case of zero displacement and balanced number of particles. In figure 5.2 we show the density profiles in units of the harmonic oscillator length a_h for infinite intra-species repulsion $\Lambda = \infty$ and 40 particles.
In absence of interactions between the two species, the system is equivalent to two trapped non-increcting TG gases with $N = 20$ particles each. The corresponding density profile is shown in blue in figure 5.2 . For comparison we also plot the corresponding Thomas-Fermi profile. We see that our profile is in good agreement with the Thomas-Fermi prediction, except at the boundaries of the cloud, where the Local Density approximation can be reliably applied. Our simulations also show the presence of oscillations. These oscillations are called Friedel oscillations[33] and cannot be obtained by the local density approximation.

Increasing the role of intra-particle interactions, the density profiles broadens. As the normalization is conserved, it follows that the peak density must

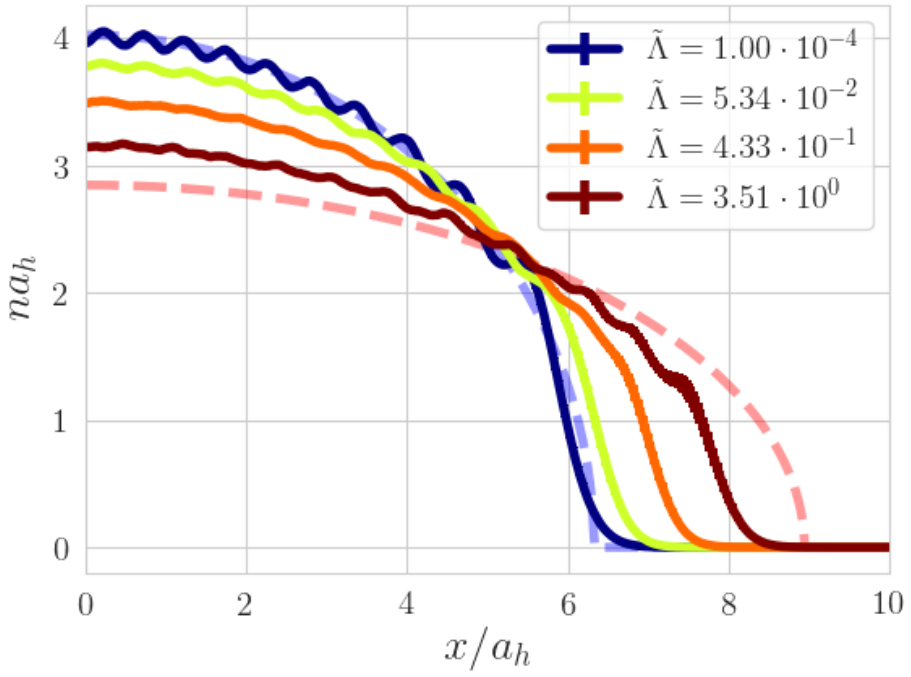

Figure 5.2: Density profiles for N=40 particles with $\Lambda = 1$ for various values of $\tilde{\Lambda}$ in units of the oscillator harmonic length.Solid lines are QMC results while dashed lines are the LDA predictions for two non interacting components in th TG regime (blue dashed line) and one single component with N=40 in the TG regime(dashed red line).

decrease.
In figure 5.3 we also plot the density profiles for $\Lambda = 1$ and $N = 20$ particles. For these values of Λ and N one gets $\lambda = 20^{3/2} \approx 100$). Such an high value indicates that in this regime the local density regime should be valid. We can observe a trend similar to the $\Lambda = 0$ case. As one increases the inter particle interactions the radius of the cloud increases and the central density decreases. We also compare our results with the mean field Thomas-Fermi profile, which is not expected to be valid in the regime of interactions. Indeed, we clearly see that mean-field theory is not able to describe the system and the Thomas-Fermi profile is much broader than the density profile we obtained in our simulations. The over-estimation of the radius of the cloud is due to the over-estimation of the interaction energy of the mean field theory.

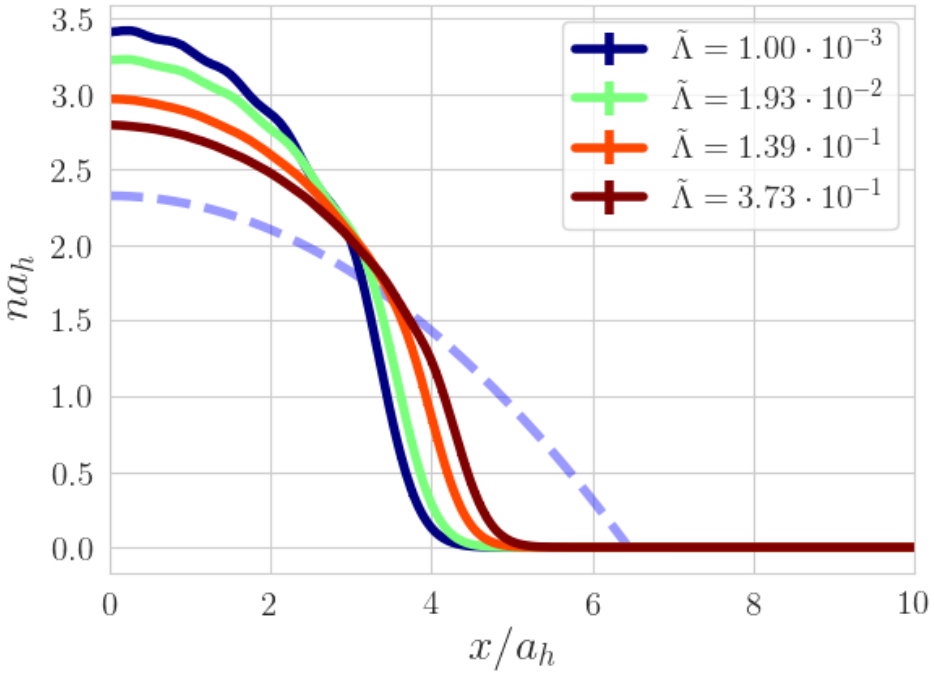

Figure 5.3: Density profiles for N=20 particles with $\Lambda = 1$ for various values of $\tilde{\Lambda}$ in units of the oscillator harmonic length.Solid lines are QMC results while dashed lines are the LDA predictions from the mean mield equation of state.

5.5 Polarization

Let us assume one displaces the minimums of the two traps by an amount d. In absence of interactions between different components this will lead to a displacement of the center of mass of the two components by an amount d. If we turn on the interactions the two clouds will push apart and the distance between the center of mass of the two components will be larger than the trap displacement d. For small displacements, one expects the system to respond linearly , obtaining $\langle x_a \rangle - \langle x_b \rangle \propto d$. We can define the polarization as

$$\mathcal{P} = \lim_{d \to 0} \frac{\langle x_a \rangle - \langle x_b \rangle}{d} \tag{5.31}$$

We performed several DMC simulations and computed the difference between the center of mass of the two components in several regimes.

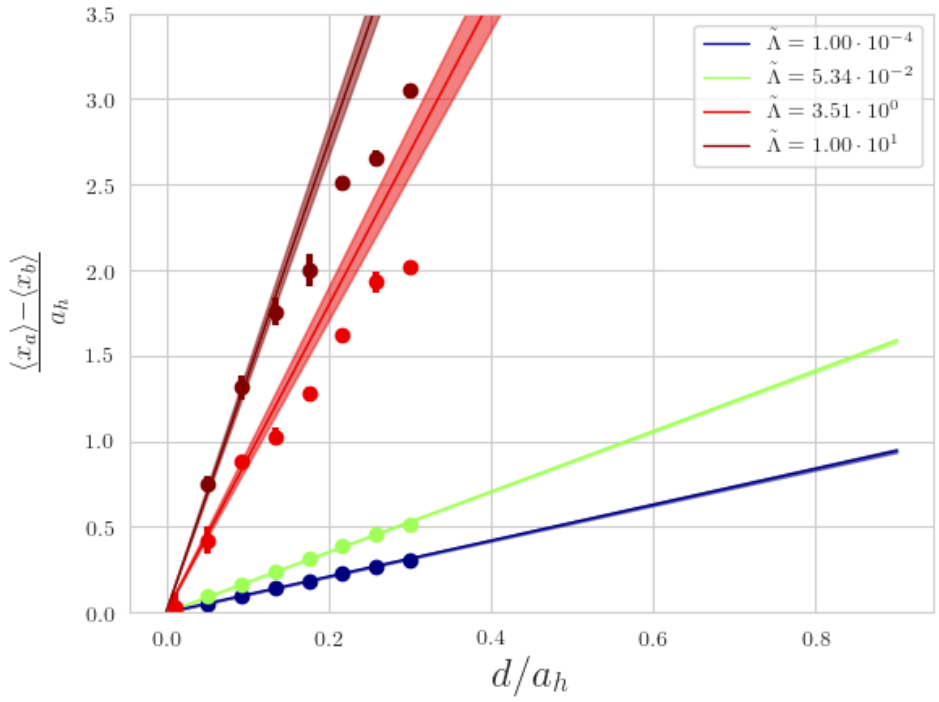

Figure 5.4: Distance between the center of masses of each component in function of trap separation d for several values of $\tilde{\Lambda}$ and $\Lambda = \infty$, in units of the harmonic oscillator length. Linear fits have all been performed with at least three data points.

In figure 5.4 we report the average center of mass displacement versus trap separation in the case $\Lambda = \infty$ and several values of $\tilde{\Lambda}$ for $N = 40$. When $\tilde{\Lambda}$ is very small one recovers the non interacting case $\langle x_a \rangle - \langle x_b \rangle = d$. As one increases the inter-species interaction the average inter-species separation increases and the linear behaviour is lost. However we still observe a linear dependence for a sufficiently small trap displacement. For $\tilde{\lambda} = 10$ the linear dependence is retained up to $d \approx 0.1 a_h$. The polarization can then be obtained by a linear fit at sufficiently small trap displacements. A similar trend can be seen in figure 5.5, where we report on our results for $\Lambda = 1$ and several values of $\tilde{\Lambda}$. The polarization can be extracted from the slope of the linear fit at small displacements.
In figure 5.6 we show a typical profile of the magnetization density for differ-

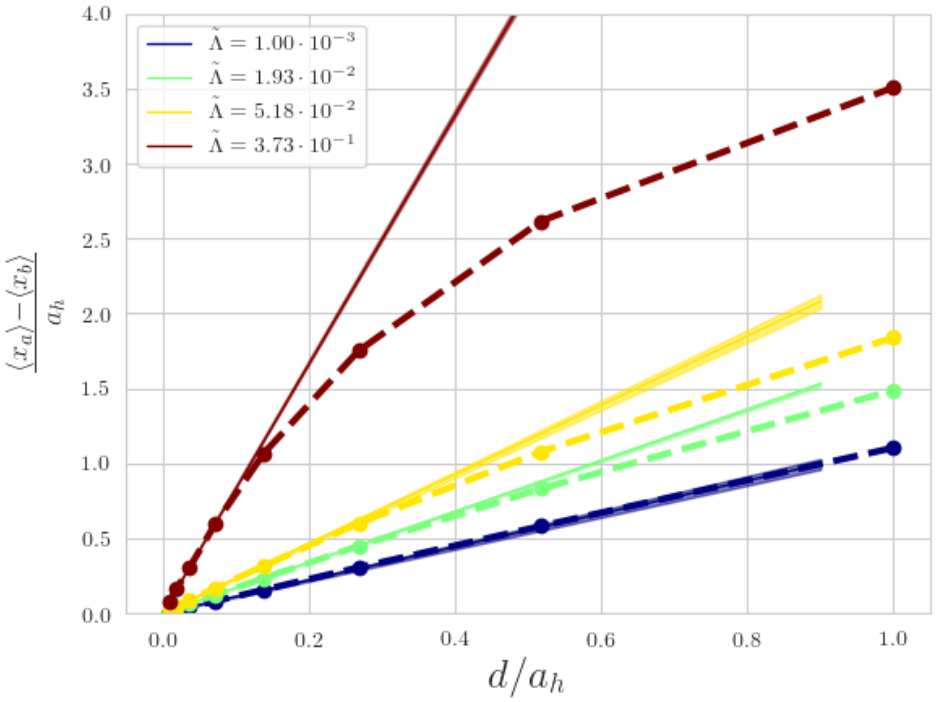

Figure 5.5: Distance between the center of masses of each component in function of trap separation d for several values of λ_{tilde} and $\lambda = 1$, in units of the harmonic oscillator length.

ent trap displacements. The local imbalance is zero at the midpoint between the center of the two traps, where both components feel the same potential. The magnetization is an odd function of the displacement around the midpoint. By increasing the distance from the midpoint the imbalance increases. As one approaches the edges of the traps, the densities of both components vanish. The profile of the net imbalance is thus non monotonous, first increasing until reaching a maximum at a certain distance and then decreasing to zero.

5.5.1 Spin-Dipole Mode

We can compute the spin-dipole mode using sum rules[132]. A general discussion on sum rules can be found in section B.0.2 or in [31]. Let us consider the excitation operator $F = \sum_{i=1}^{N_a} x_i - \sum_{\alpha}^{N_b} x_\alpha$ where we sum respectively

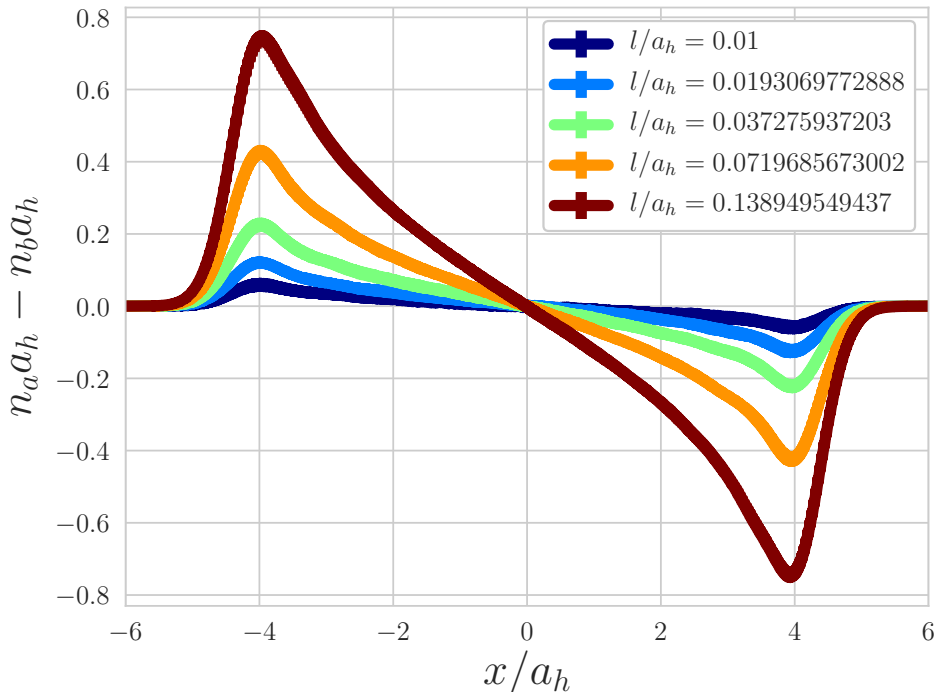

Figure 5.6: Difference between the density profile of the two components $n_a(x)$ and $n_b(x)$ for N=20 and $\lambda = 1$ and $\tilde{\lambda} = 3.73$

over all particles of components a and b. The m_1 sum rule reads

$$m_1 = N\frac{\hbar^2}{2m} \tag{5.32}$$

independent of particle interactions. The m_{-1} sum rule can also be calculated and yields.

$$m_{-1} = \frac{N}{2m\omega^2}\mathcal{P} \tag{5.33}$$

Finally the m_0 moment can be written as

$$m_0 = \hbar\left\langle F^2\right\rangle \tag{5.34}$$

proportional to the fluctuations of the center of mass of the two different components for the case of no displacement between the minimums of the two traps. An estimate of the spin-dipole mode can also be obtained trough

the relation[132]

$$\hbar\omega_{SD} \approx \sqrt{\frac{m_1}{m_{-1}}} \tag{5.35}$$

Within mean-field and LDA approximation the spin-dipole mode can be obtained using 5.35 obtaining

$$\frac{\omega_{SD}}{\omega} = \sqrt{\frac{g-\tilde{g}}{g+\tilde{g}}} \tag{5.36}$$

Notice that for $\tilde{g} \to g$ the frequency of the spin-dipole mode vanishes. This result is consistent with the behavior of the uniform system where miscibility requires $\tilde{g} < g$. A second estimate can be obtained trough

$$\hbar\omega_{SD} \approx m_1/m_0 \tag{5.37}$$

As the m_1 sum rule is not expected to be exhausted by the spin-dipole mode, the two estimates may differ because of the Andreev-Bashkin effect between the two trapped components. In figure 5.7 we show our results for the spin-dipole mode frequency obtained from 5.37 and 5.35. Within statistical accuracy the two expressions yield equivalent results. At small values of $\tilde{\Lambda}$, where interactions are also negligible correlations between the two spin components are negligible and the fluctuations of the spin center of mass are equal to the fluctuations of the center of mass of the total system. Moreover the center of mass displacement of one component will be equal to the displacement of the trap and will be unaffected by the other component. Thus in the limit $\tilde{\Lambda} \to 0$ the excitation of the spin-dipole mode is equivalent to the excitation of the dipole mode for each component . In this case it does not depend on interactions and is equal to the trapping frequency. When inter-species and intra-species interactions become similar one approaches the unmiscible phase. Close to the transition point , the cost of creating excitations in the magnetization becomes small and the response to a local imbalance between the two components is large.Moreover correlations between the two components become very large. Thus both the polarization and the fluctuations of the spin center of mass increases and the spin-dipole mode is suppressed. Our results are compatible with a vanishing spin-dipole mode close to the phase transition. In the weakly interacting regime $\Lambda = 10^{-2}$ we recover the LDA prediction for a weakly interacting gas. For $\Lambda = 1$ one can see significant deviations from the mean-field LDA predictions. For $\Lambda = 0$ the spin-dipole mode frequency decays much more slowly, with the spin-dipole mode being $\approx 1/4$ at $\tilde{\Lambda} \approx 3.5$.

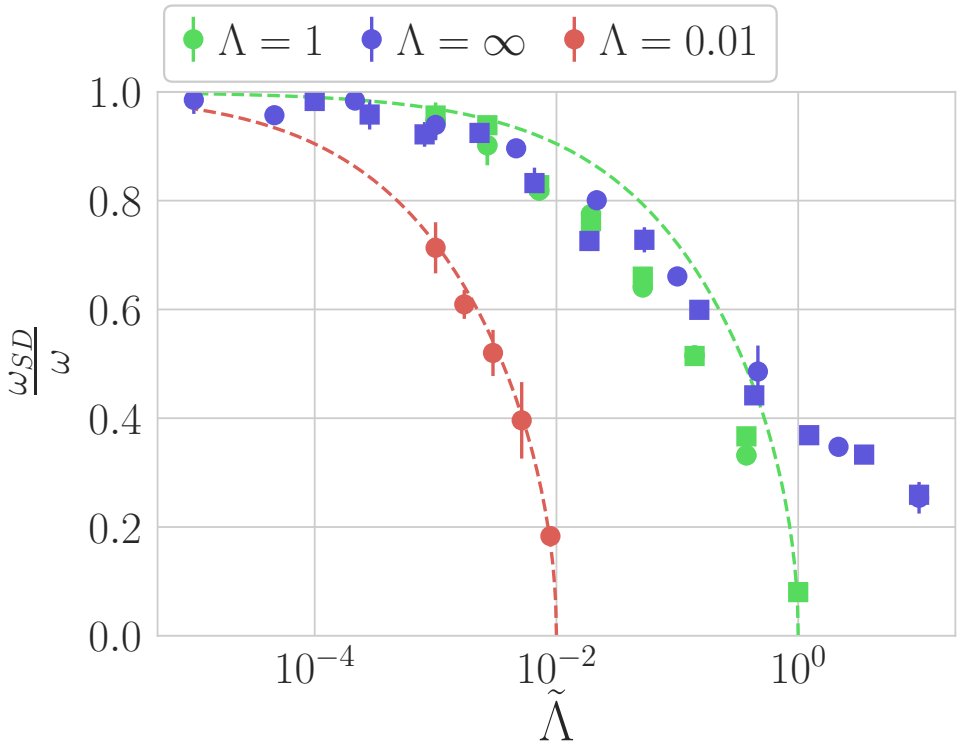

Figure 5.7: spin-dipole mode computed using the sum rules $\sqrt{m_1/m_{-1}}$ (squares) and m_1/m_0 (circles). Dashed lines are mean-field predictions in the LDA approximation.

5.6 Conclusions

In conclusion we have investigated repulsive mixtures in a trap.
We computed the spin-dipole mode within several regimes of inter and intra species interactions. As the LDA theory yields a diverging solution, we computed for the first time the spin-dipole mode beyond LDA in the regime where finite-size effects are negligible.
We found no signature of the spin drag effect in the spin-dipole mode, which is likely smaller than our numerical resolution.

Chapter 6

Quantum liquids

This chapted is baed on the article [30].

6.1 Introduction

The mixtures we studied in the previous chapters all have repulsive interactions. For these systems the ground-state is a gas. A system is defined to be a gas when it prefers to occupy the whole volume of the container it is placed in. This statement at zero temperature , is equivalent to requiring that the mimimum of the energy versus density, is equal to zero. Self-bound liquid droplets were generated as a result of quantum fluctuations in samples interacting via anisotropic dipolar forces [140, 141, 142, 143, 144] as well as via contact interparticle potentials [145, 146, 147].

In three and two dimensions such droplets would collapse according to mean-field theory and are stabilized, for large enough numbers of particles, by repulsive correlations beyond the mean-field description. Dipolar droplets were characterized theoretically by means of a generalized nonlocal, nonlinear Schrödinger equation [148] and also by exact quantum Monte-Carlo (QMC) methods, employing a model two-body potential with hard-core repulsion [149]. Droplets in a two-component Bose gas with short-range interactions have been first predicted and studied using a generalized Gross-Pitaevskii (GGP) equation in Ref. [150]. QMC simulations of these latter systems have also been carried out, even though only for limited numbers of particles [151].

In one spatial dimension (1D), quantum droplets of Bose mixtures with contact interactions have been predicted to occur as a result of a different mechanism. Here, beyond mean-field fluctuations are attractive and one needs a net mean-field repulsion in order to stabilize the droplet, which there-

fore are expected to form in the region where, according to mean-field theory, the homogeneous gas mixture is still stable [152]. The approach based on the GGP equation is valid in the weak-coupling limit and provides a full description of the ground-state energetics of the bulk liquid phase as well as of the density profiles in droplets with a finite number of particles [152].

Droplets in 1D are also particularly interesting because of the enhanced role of quantum fluctuations and because stable regimes of strong correlations are experimentally achievable [73, 80, 75, 76] and enjoy enhanced stability. This opens the intriguing perspective of investigating the 1D liquid phase when interactions are strong and can not be accounted for by the GGP approach. In this thesis we address theoretically the regime of strongly correlated liquids by means of exact QMC methods applied to a 1D mixture of Bose gases with contact interactions. We determine the phase diagram of the homogeneous liquid in terms of density and coupling strengths. Furthermore, in bulk systems at equilibrium a number of relevant thermodynamic quantities is calculated, such as chemical potential and compressibility, as well as the behaviour of correlation functions which provides a clear indication of the presence of strong interactions.

We consider the following hamiltonian

$$\begin{aligned} H &= -\frac{\hbar^2}{2m}\sum_{i=1}^{N_a}\frac{\partial^2}{\partial x_i^2} + g\sum_{i<j}\delta(x_i - x_j) - \frac{\hbar^2}{2m}\sum_{\alpha=1}^{N_b}\frac{\partial^2}{\partial x_\alpha^2} \\ &+ g\sum_{\alpha<\beta}\delta(x_\alpha - x_\beta) + \tilde{g}\sum_{i,\alpha}\delta(x_i - x_\alpha)\,, \end{aligned} \tag{6.1}$$

composed of the kinetic energy of the two components with the same mass m and atom numbers N_a and N_b, of the repulsive intra-species potentials modelled by the same coupling constant $g > 0$ and by the attractive inter-species potential of strength $\tilde{g} < 0$. Here x_i with $i = 1, \ldots, N_a$ and x_α with $\alpha = 1, \ldots, N_b$ denote, respectively, the positions of particles belonging to component a and b of the mixture. In a box of size L the homogeneous densities of the two components are given by $n_a = N_a/L$ and $n_b = N_b/L$. We consider balanced systems where $N_a = N_b = N/2$, such that the relevant dimensionless coupling parameters are given by $\gamma = \frac{gm}{n\hbar^2}$ and $\eta = \frac{|\tilde{g}|m}{n\hbar^2}$ in terms of the total density $n = N/L$. An important energy scale is fixed by the binding energy of dimers in vacuum, $\epsilon_b = -\frac{\hbar^2}{m\tilde{a}^2}$, where $\tilde{a} = \frac{2\hbar^2}{m|\tilde{g}|}$ is the 1D scattering length associated with the attractive inter-species contact potential.

Let us first discuss the ground-state of the hamiltonian in Eq. (6.1) in the weak-coupling limit, corresponding to $\gamma \ll 1$ and $\eta \ll 1$. The energy density

in terms of the total density n is given by

$$\begin{aligned}\frac{E_{\rm GGP}}{L} &= \frac{n^2}{4}\left(g-|\tilde{g}|\right) \\ &- \frac{\sqrt{m}n^{3/2}}{3\sqrt{2}\pi\hbar}\left[\left(g-|\tilde{g}|\right)^{3/2}+\left(g+|\tilde{g}|\right)^{3/2}\right] . \end{aligned} \tag{6.2}$$

This represents the local energy to which the GGP functional adds the kinetic energy contribution $\frac{\hbar^2}{2m}(\nabla\sqrt{n})^2$ [152]. From the ground-state energy E of the mixture one can extract all relevant thermodynamic quantities: the extremum condition $\frac{dE/N}{dn}=0$ yields the equilibrium density $n_{\rm eq}$ of the liquid and the relations $\mu=\frac{dE}{dN}$ and $mc^2=n\frac{d\mu}{dn}$ calculated at the density $n_{\rm eq}$ give, respectively, the chemical potential $\mu_{\rm eq}$ and the speed of sound $c_{\rm eq}$ at equilibrium. In the GGP approach these quantities are obtained using $E_{\rm GGP}$ of Eq. (6.2) as a perturbative approximation to the energy E.

6.2 The Phase Diagram

We study the ground-state properties of the hamiltonian in Eq. (6.1) in a box of size L with periodic boundary conditions by means of QMC techniques. More specifically, the diffusion Monte-Carlo (DMC) method solves the many-body Schrödinger equation in imaginary time, thereby obtaining the exact ground-state energy through a large-time projection [153]. Importance sampling is implemented via a guiding function, which also encodes the contact boundary conditions imposed by the interactions in the hamiltonian. The guiding wave function is constructed as a product of pairwise correlation terms which, at short interparticle distance, reproduce the exact solution of the two-body problem with the contact potential and at longer distances account for many-body correlations. Finite-size effects are considered by performing calculations with different N and are found to be smaller than the typical statistical uncertainty.

The results for the ground-state energy per particle E/N are shown in Fig. 6.1 for fixed values of the ratio of coupling constants $|\tilde{g}|/g$ and as a function of the dimensionless gas parameter $n|a|$. Here, $a=-\frac{2\hbar^2}{mg}$ is the scattering length associated with collision processes of the repulsive intra-species potential with strength g. Two distinct behaviours are clearly visible: if the ratio $|\tilde{g}|/g$ is sufficiently small the energy is a monotonously increasing function of the density signalling a gas phase where the minimum of energy is reached at a vanishing density and corresponds to half of the binding energy ϵ_b. On the contrary, if the ratio is larger than a critical value, a minimum shows up in E/N and the density at the minimum corresponds to the equilibrium density

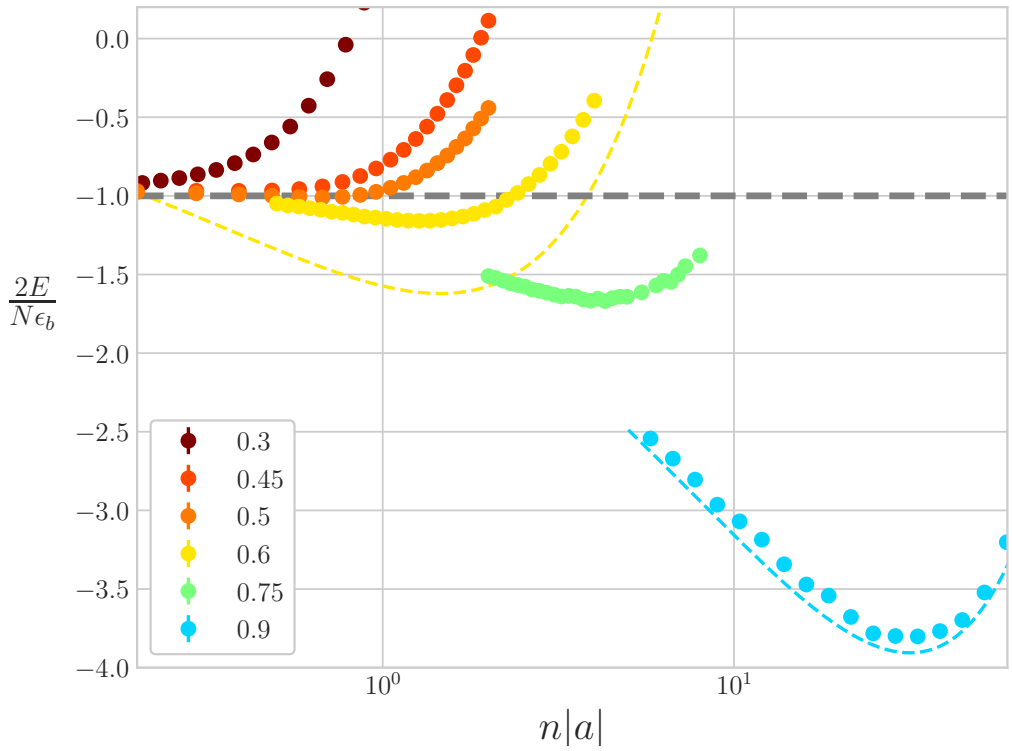

Figure 6.1: Energy per particle, in units of half of the binding energy, as a function of the density for different values of the ratio $|\tilde{g}|/g$ of coupling constants. Error bars are smaller than the symbol sizes. The dashed line is the result of the GGP approach at $|\tilde{g}|/g = 0.9$ (cyan) and at $|\tilde{g}|/g = 0.6$ (yellow).

of the liquid phase. The critical ratio of coupling strengths is found to be $(|\tilde{g}|/g)_{\rm crit} = 0.47(2)$. This value is in close agreement with the result of the four-body scattering problem where the effective interaction between dimers crosses from repulsive to attractive [154]. Simultaneous effective three-dimer repulsion [155] provides a microscopic scenario for the formation of the liquid which is consistent with our many-body calculations. Fig. 6.1 reports also the result of the GGP theory based on the energy functional of Eq. (6.2). At high density, where the weak-coupling theory is applicable, we find good agreement, but large deviations both in the energy of the minimum and in the shape of curve are visible at small density. Similar results for the 3D homogeneous liquid phase have been obtained in Ref. [156] using a variational approach.

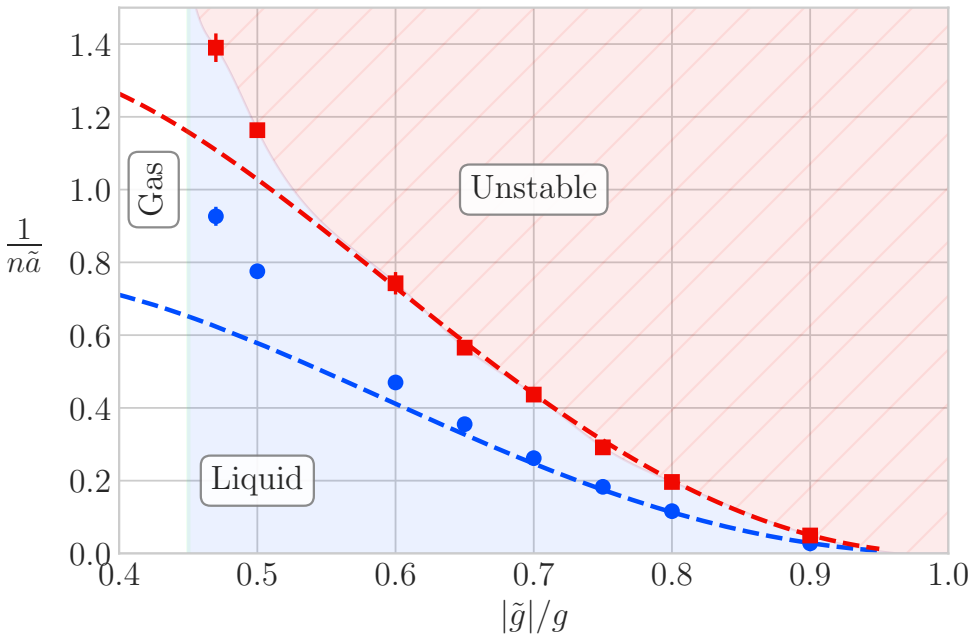

Figure 6.2: Phase diagram of the homogeneous liquid phase: (blue) circles correspond to the equilibrium density of the liquid and (red) squares to the spinodal point where the compressibility diverges. Dashed lines refer to the predictions of the GGP theory.

The curves shown in Fig. 6.1 allow us to determine the phase diagram of the homogeneous liquid in the region of ratios $(|\tilde{g}|/g)_{\rm crit} < |\tilde{g}|/g < 1$ where this state can exist. The phase diagram is shown in Fig. 6.2, where we report the values of the equilibrium density $n_{\rm eq}$ and of the spinodal density, defined as the point where $\frac{d^2E/L}{dn^2} = 0$. At density n below the spinodal line the homogeneous system is mechanically unstable and breaks into droplets. For larger values of n the homogeneous phase is stable with a positive or negative pressure depending on whether n is larger or smaller than $n_{\rm eq}$. We also find that the GGP approach is quite reliable in predicting both the equilibrium and the spinodal line. Deviations start to appear for $|\tilde{g}|/g \lesssim 0.6$.

6.3 The liquid Phase

6.3.1 Energetics

Various ground-state properties of the liquid state at the equilibrium density $n_{\rm eq}$ are shown in Fig. 6.3 as a function of the ratio $|\tilde{g}|/g$. In particular, we provide results for the chemical potential $\mu_{\rm eq}$, which determines the rate of evaporation of particles from a droplet due to thermal effects, and the speed of sound $c_{\rm eq}$, fixing the low-lying collective modes of the droplet. Significant deviations compared to the GGP approach are found for $\mu_{\rm eq}$ at small ratios, where the weak-coupling theory fails to recover the physics of bound dimers. On the other hand, we find that $c_{\rm eq}$ is well described by the GGP energy functional down to the smallest values of $|\tilde{g}|/g$ considered in Fig. 6.3. Notice, however, that the speed of sound is reported here in units of the Fermi velocity $v_F = \frac{\hbar\pi n_{\rm eq}}{2m}$ which itself depends on the equilibrium density $n_{\rm eq}$.

6.3.2 Pair Correlations

Relevant information about the structure of the liquid state at equilibrium are obtained from the study of correlation functions. The pair correlation functions of parallel and anti-parallel spins are defined as expectation values $\langle \dots \rangle$ over the ground-state

$$\begin{aligned} g_{aa}(s) &= 1 + \frac{4}{n^2}\left(\langle \delta n_a(x+s)\delta n_a(x)\rangle - \frac{n}{2}\delta(s)\right) \\ g_{ab}(s) &= 1 + \frac{4}{n^2}\langle \delta n_a(x+s)\delta n_b(x)\rangle \,, \end{aligned} \tag{6.3}$$

of the density fluctuations $\delta n_a(x) = \sum_{i=1}^{N_a}\delta(x-x_i) - \frac{n}{2}$ and $\delta n_b(x) = \sum_{\alpha=1}^{N_b}\delta(x-x_\alpha) - \frac{n}{2}$ of the two components measured with respect to the average density. These functions are shown in Fig. 6.4 for different values of the ratio $|\tilde{g}|/g$. At large distances correlations vanish yielding the result $g_{aa} = g_{ab} = 1$. The anti-parallel spin correlation function g_{ab} shows a long-range suppression and a peak for $s \lesssim \tilde{a}$. This behaviour arises from the short-range pairing between opposite spins occurring on length scales of the order of the size $\tilde{a}$ of a dimer and from the phononic long-range tail. By reducing the ratio $|\tilde{g}|/g$ both the minimum and the height of the peak become more prominent. On the contrary, the behaviour of g_{aa} is fully determined by the repulsive intra-species correlations and it exhibits a monotonously decreasing behaviour as the distance is reduced. Also in this case, for smaller values of $|\tilde{g}|/g$, correlation effects are stronger and close to the critical ratio the repulsion between like particles produces a large suppression of g_{aa}.

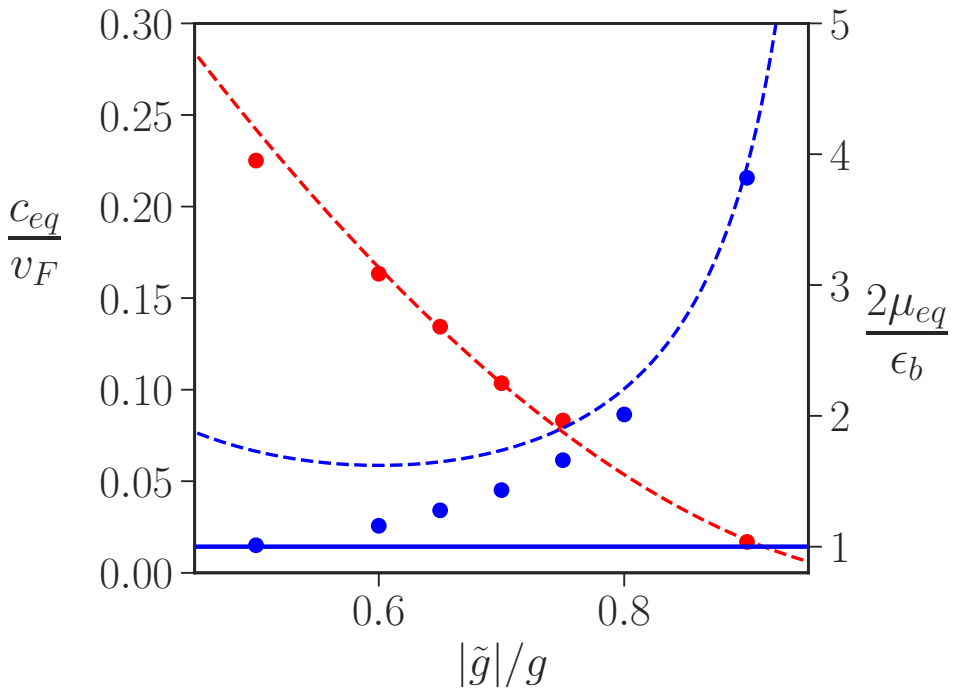

Figure 6.3: Chemical potential $\mu_{\rm eq}$ in units of half of the dimer binding energy: (blue) circles and right vertical axis. Speed of sound $c_{\rm eq}$ in units of the Fermi velocity: (red) squares and left vertical axis. The dashed lines correspond to the results of the GGP theory.

We notice that the density pair correlation function, defined as the average $g_D(s) = \frac{1}{2}[g_{aa}(s) + g_{ab}(s)]$, is peaked at short distances signalling the dominant role of attractive interactions characteristic of a liquid. Conversely, the magnetic pair correlation function defined as $g_M(s) = 1 + \frac{1}{2}[g_{aa}(s) - g_{ab}(s)]$ is suppressed at short distances as a consequence of the repulsion between dimers.

6.3.3 Structure Factor

From the Fourier transforms of the pair correlation functions $g_{D(M)}(s)$ one obtains the density and magnetic static structure factors defined as $S_{D(M)}(q) = 1 + n \int ds\, e^{iqs} \left(g_{D(M)}(s) - 1\right)$. Both structure factors are shown in Fig. 6.5. At large momenta $S_D(q)$ and $S_M(q)$ tend to unity, while for small values of

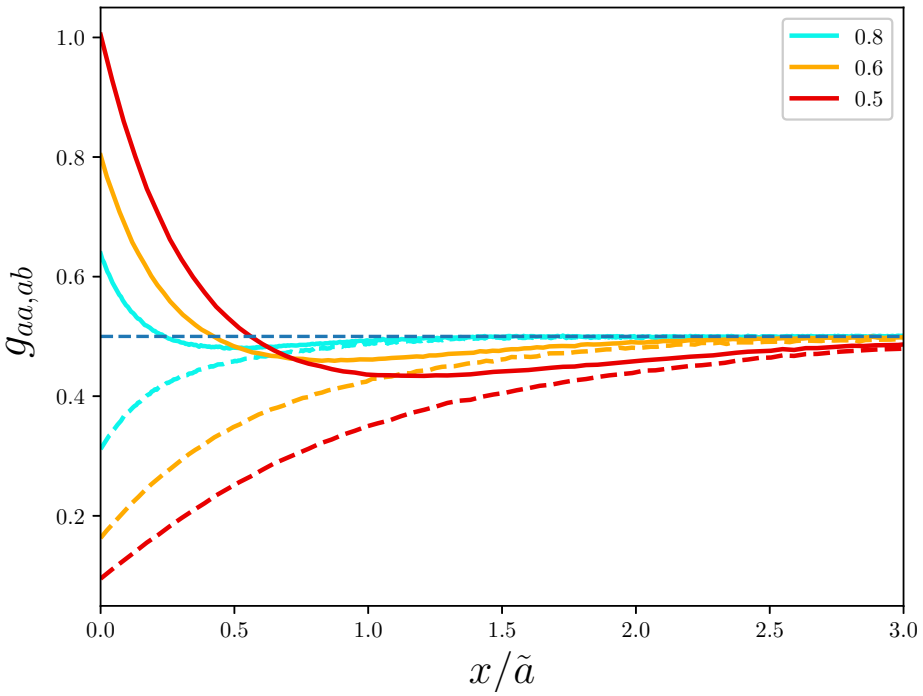

Figure 6.4: Pair correlation function of parallel spins g_{aa} (dashed lines) and anti-parallel spins g_{ab} (solid lines) in the liquid for different values of the ratio $|\tilde{g}|/g$ of coupling constants.

q we find in both cases a linear dependence. This is expected in the case of the density structure factor which should obey the law $S_D(q) = \frac{\hbar q}{2mc_{\rm eq}}$ fixed by the speed of sound $c_{\rm eq}$. In the case of $S_M(q)$, instead, one might expect a quadratic dependence as $q \to 0$ caused by the presence of a pairing gap in the spin sector [157]. However, as evident from Fig. 6.3, we are in the regime $|\epsilon_b| \lesssim |\mu_{\rm eq}|$ where the pairing gap is exponentially suppressed [157]. This implies that the q^2 dependence of the magnetic structure factor should take over only at vanishingly small values of q not reachable in our simulations. In Fig. 6.5 we compare the low-q behaviour of both structure factors with the linear slope fixed by $S_{D(M)}(q) = \frac{\hbar q}{2}\sqrt{\frac{\chi_{D(M)}}{mn_{\rm eq}}}$ where $\chi_D = \frac{n_{\rm eq}}{mc_{\rm eq}^2}$ is the isothermal compressibility and $\chi_M = \frac{2}{g+|\tilde{g}|}$ is the estimate of the magnetic susceptibility assuming the spin sector gapless [158].

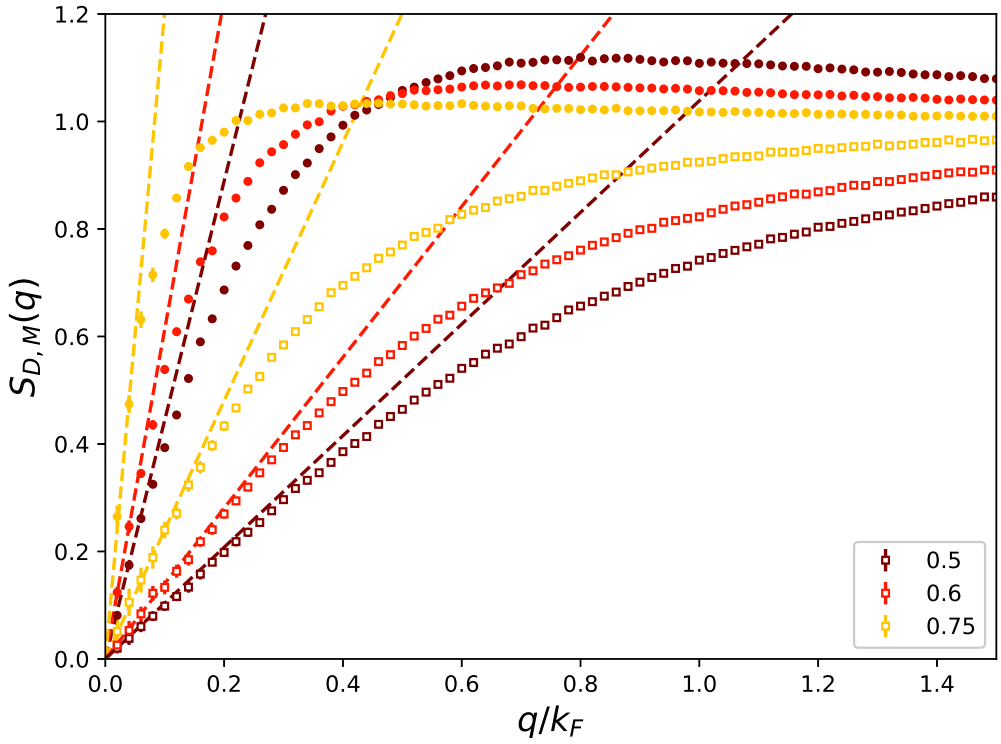

Figure 6.5: Density (full symbols) and magnetic (open symbols) static structure factor in the liquid as a function of q/k_F for different values of the ratio $|\tilde{g}|/g$. Here $k_F = \frac{\hbar\pi n}{2}$ is the Fermi wave vector. Dashed lines correspond to the low-q linear dependence fixed by the compressibility and by the magnetic susceptibility respectively for $S_D(q)$ and $S_M(q)$.

6.3.4 One-body density matrix

Coherence properties in the liquid state at equilibrium are characterised by the behaviour of the one-body density matrix (OBDM). This is invariant under the exchange of the two species and is defined as

$$\rho(s) = \langle \psi^\dagger_{a(b)}(x+s)\psi_{a(b)}(x)\rangle \ , \tag{6.4}$$

in terms of the field operators giving the density of each component: $n_{a(b)}(x) = \psi^\dagger_{a(b)}(x)\psi_{a(b)}(x)$. In systems exhibiting off-diagonal long-range order the OBDM at large distance s reaches a constant value identified with the condensate density. However, Bose-Einstein condensation does not exist in 1D and at $T = 0$ the OBDM is expected to decay with a power law. In Fig. 6.6 we show

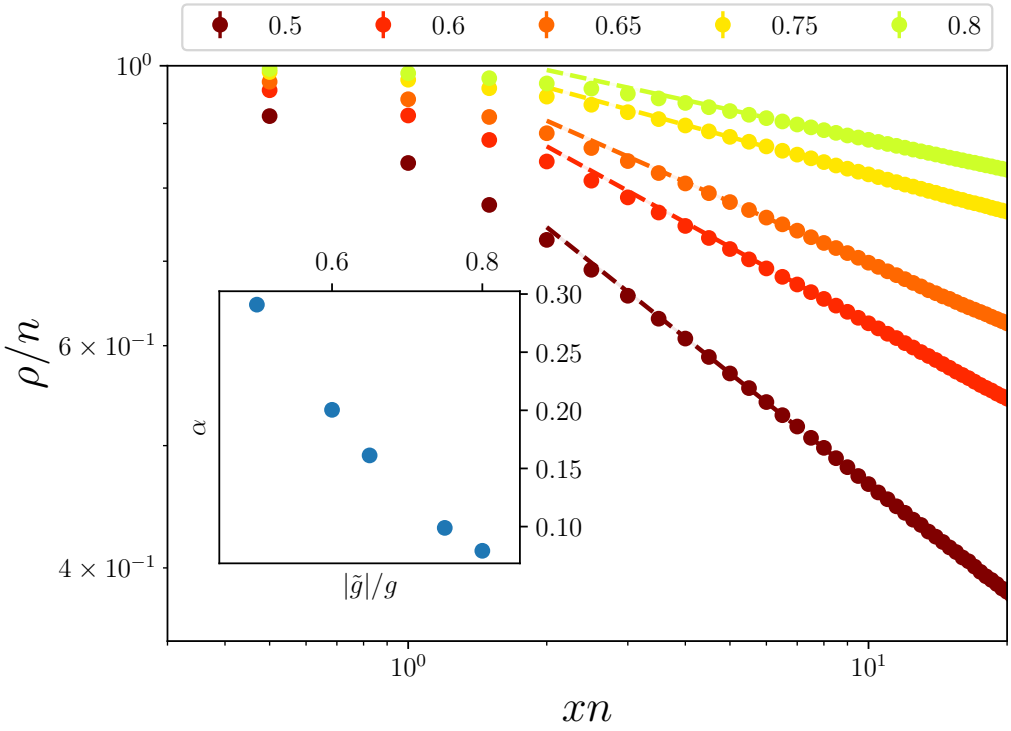

Figure 6.6: Spatial dependence of the OBDM for different values of the ratio $|\tilde{g}|/g$ of coupling constants. Dashed lines are power-law fits $1/x^{\alpha}$ to the long-range behaviour. In the inset we report the values of the exponent α obtained from the fit.

the results of $\rho(s)$ by varying the ratio $|\tilde{g}|/g$ and we find a clear algebraic decay with the distance: $\rho(s) \propto 1/|s|^{\alpha}$, which sets in at sufficiently large values of s. The value of the exponent α is reported in the inset of Fig. 6.6 as a function of the ratio $|\tilde{g}/g|$. The exponent ranges from very small values at $|\tilde{g}|/g \simeq 1$, where the GGP theory is applicable, to values as large as $\alpha \simeq 0.3$ close to the critical ratio of coupling constants. We emphasise that in the Tonks-Girardeau regime of a single-component Bose gas, corresponding to particles being impenetrable and behaving like fermions, the OBDM decays as $\rho(s) \propto 1/\sqrt{|s|}$ [159]. The values of α found moving towards the critical ratio $(|\tilde{g}|/g)_{\text{crit}}$ arise from very strong correlations acting between particles of the same species, which result in a suppression of the momentum distribution peak at low wave vectors $n(q) \propto 1/|q|^{1-\alpha}$ as entailed by the relation between $n(q)$ and the OBDM via the Fourier transform $n(q) = \int ds\, e^{iqs}\rho(s)$.

6.4 Conclusions

In conclusion, we have investigated the properties of the bulk liquid state in attractive 1D Bose-Bose mixtures by using exact QMC methods. We find that the liquid state can exist only if the ratio of coupling constants exceeds a critical value. The thermodynamic properties of the equilibrium state derived from our simulations are crucial ingredients when studying the stability and the collective modes of the liquid droplets realized in experiments. In particular, we find that regimes of strongly correlated liquid states are achievable in 1D well beyond the conditions of applicability of the weak-coupling GGP theory.

In this work we studied homogeneous mixtures , but did not investigate finite size systems. In a finite size system , the liquid will not be homogeneous but will form a droplet. The properties of these droplets would be interesting to compute as they can be directly probed in experiments. In particular it would be interesting to obtain the density profiles , the surface energy and the collective modes of these quantum liquid droplets.

A similar study was realized in three dimensions using Quantum Monte Carlo techniques[160] , but has not yet been carried out in one-dimensional systems.

Quantum droplets in one-dimensional mixtures where characterized in the weakly interacting regime[161] using the GGP theory but the strongly interacting regime remains unexplored.

Chapter 7

Conclusions

In conclusions in this thesis I presented the results I have obtained in the last three years. I have used quantum Monte-Carlo methods to investigate bosonic one-dimensional mixtures. I have studied the problem of an extremely imbalanced mixture, composed of just one impurity immersed in a Bose gas and studied the main properties of the impurity. In particular I have showed that the increase of the effective mass of the impurity with the interactions with the bath is enhanced in a gas with weak interactions.
Then I turned to the study of imbalanced uniform mixtures. In particular I considered the Andreev-Bashkin effect and proposed to observe signatures of the drag effect by measuring the speed of sound waves.
In trapped systems I computed the frequency of the spin-dipole mode and showed that it is not much affected by the presence of a drag between the two components of the mixtures.
Finally I have investigated the liquid phase in mixtures with attractive inter-species interactions. In particular I have found evidence of a liquid-gas phase transition at a critical ratio of the inter-species and intra-species coupling. I have characterized the liquid phase, where I have found deviations from predictions based on the generalized Gross-Pitaevsky theory.
Future directions could be the investigation of mixtures in artificial gauge potentials, which allow to implement an effective hamiltonian with Spin Orbit Coupling. These hamiltonians have been implemented using ultracold quantum gases[162]. The systems have been attracted much attention recently [163] and have been instigated theoretically at the mean field level, where they exhibit multiple non-trivial phases [164]. However , these systems have not so far been investigated in the regime of strong correlations. Quantum Monte Carlo techniques may be able to shed some light on the fate of these phases in the strongly correlated regime.
These hamiltonians have been realized with one-dimensional couplings [162]

and reaching the strongly correlated regime in one dimension should be experimentally achievable. On the theoretical side, accounting for an effective spin-orbit coupling introduces a sign problem which causes an exponentially small signal to noise ratio in Quantum Monte Carlo [55]. However this problem can partly be overcome using the fixed phase approximation, which has already proven to be successful in other systems [165, 166].

Appendix A

The effective mass estimator

An estimator for the effective mass can easily be obtained from imaginary time correlations within a QMC simulation. Let use consider an impurity immersed in a bath of atoms. The Energy of the system can then be written as

$$E = E_B + \mu + \frac{p^2}{2m^*} \tag{A.1}$$

where μ is the binding energy of the impurity and m^* is the impurity effective mass. Let us denote a spacial configuration of the system as $|X, x\rangle$. We are interested in the long time evolution of the distribution $f(X, X')$ of the impurity

$$\frac{\int dX f(X, x, \tau)}{\int dX dx f(X, x, \tau)} = f_I(x, \tau) \tag{A.2}$$

In the long time evolution, assuming that the energy assumes the form A.1 in the long time evolution the distribution can be written as

$$f_i(x, \tau) = \frac{e^{-(E_B+\mu)(\tau-\tau_0)}}{e^{-(E_B+\mu)(\tau-\tau_0)}} \left\langle x(\tau) \left| e^{-\left(D* \frac{\partial^2}{\partial_x^2}\right)} \right| x(\tau_0) \right\rangle \tag{A.3}$$

$$= \frac{1}{\sqrt{4\pi D^*}} e^{-\frac{(x-x_0)^2}{4Dm^*}} \tag{A.4}$$

where $D^* = \frac{\hbar^2}{2m^*}$ is the diffusion constant of the impurity. Thus we see that the long time evolution distribution of an impurity is given by a Gaussian with width $2D*$. Then one can record the path $x(\tau)$ of an impurity during a regular simulation of the full system. The distribution of the differance of the tails of the paths, for long enough evolutions, will be distributed according to a gaussian distribution. The effective mass can than be extracted from

the variance of that distribution. The effective mass can than be estimated from a DMC calculations as

$$\frac{m}{m^*} = \lim_{\tau\to\infty} \frac{1}{D\tau} \left\langle W_i^2(\tau) \right\rangle \tag{A.5}$$

where $D = \hbar^2/2m$ is the number of walkers at time τ and

$$W_i(\tau) = x(\tau) - x(\tau_0) \tag{A.6}$$

is the impurity winding number.

Appendix B

Linear response theory

In this section we give a brief overview of linear response theory[31]. Let us suppose to have the hamiltonian

$$H = H_0 + H_{\text{pert}} \tag{B.1}$$

where H_0 is the hamiltonian we want to study. H_{pert} is an additional perturbaion hamiltonian term that takes the form

$$H_{\text{pert}} = -\lambda G e^{-i\omega t} e^{\eta t} - \lambda^* G^\dagger e^{i\omega t} e^{\eta t} \tag{B.2}$$

where λ is the coupling strength which we assume to be much smaller compared with the typical energy scale of the hamiltonian H. The exponential term $e^{\eta t}$ allows one to switch on the perturbation in the distant past at a rate given by the small parameter η , which is chosen to be very small. This form is chosen in order that for $t = -\infty$ the perturbation disappears. Our goal is to evaluate the change in the average value of some operator $\hat{F}$ due to the inclusion of the perturbation. We can write the response to a small perturbation as

$$\delta \langle F \rangle = \lambda e^{-i\omega t} e^{\eta t} \chi_{F^\dagger, G} + \lambda^* e^{i\omega t} e^{\eta t} \chi_{F^\dagger, G^\dagger}(-\omega) \tag{B.3}$$

which defines the response function $\chi_{F,G}$

B.0.1 Structure factor and response function

At T=0 the response function can be written as

$$\chi_{F,G}(\omega) = -\sum_n \left[\frac{\langle 0 \,|\, F \,|\, n \rangle \langle n \,|\, G \,|\, 0 \rangle}{\hbar\omega - (E_n - E_0) + i\eta} - \frac{\langle 0 \,|\, G \,|\, n \rangle \langle 0 \,|\, F \,|\, n \rangle}{\hbar\omega + E_n - E_0} \right] \tag{B.4}$$

where the sum runs over all eigen-states $|n\rangle$ with energy E_n of the unperturbed hamiltonian H_0. Another useful quantity is the dynamic structure factor

$$S_F(\omega) = \sum_n |\langle n \,|\, F \,|\, 0\rangle|^2 \delta(\hbar\omega - (E_n - E_0)) \tag{B.5}$$

The dynamic structure factor is a sum of delta functions centered on the excited states of the unperturbed hamiltonian and strength equal to the linear coupling between the ground-state and the excited state trough the operator $\hat{F}$. The dynamic structure factor contains all the information on the excited states which can be excited trough the operator $\hat{F}$.
The dynamic structure factor and the response function are not independent. In the common case in which $\hat{F} = \hat{G}$ the response function can be written as

$$\chi_R(\omega) = -\int_{-\infty}^{\infty} d\omega' \left[S_F(\omega) P \frac{1}{\omega - \omega'} - S_F^\dagger(\omega) P \frac{1}{\omega + \omega'} \right] \tag{B.6}$$

$$\chi_I(\omega) = \pi S_F(\omega) \tag{B.7}$$

where P indicates that one should take the principal value of the integral and $\chi_{R(I)}$ stands for the real (imaginary) part of the response function.

B.0.2 Sum rules

Unfortunately the dynamic structure factor is hard to calculate in most cases. However one may still obtain informations on the dynamic structure factors from the evaluation of its moments

$$m_p(F) = \hbar \int_{-\infty}^{\infty} (\hbar\omega)^p S_F(\omega) d\omega \tag{B.8}$$

which can also be written as[31]

$$m_p(F) = \sum_n (E_n - E_0)^p |\langle n \,|\, F \,|\, 0\rangle|^2 \tag{B.9}$$

Sum of these moments can be linked to other many-body properties of interest. Particular cases are the m_0 moment , also called static structure factor

$$m_0(F) = \int d\omega S_F(\omega) \tag{B.10}$$

Also from the relation linking the static response function and the dynamic response function one can write the low frequency limit of the static response function

$$\lim_{\omega \to 0} \chi_F(\omega) = m_{-1}(F) + m_{-1}(F^\dagger) \tag{B.11}$$

The moments can be more easily calculated as they can be related to properties of the ground-state. In fact one can prove the relations

$$m_0(F) + m_0(F^\dagger) = \left\langle \{F^\dagger, F\} \right\rangle \tag{B.12}$$

$$m_0(F) - m_0(F^\dagger) = \left\langle [F^\dagger, F] \right\rangle \tag{B.13}$$

$$m_1(F) + m_1(F^\dagger) = \left\langle [F^\dagger, [H, F]] \right\rangle \tag{B.14}$$

$$m_1(F) - m_1(F^\dagger) = \left\langle \{F^\dagger, [H, F]\} \right\rangle \tag{B.15}$$

where $\langle . \rangle$ indicates an average on the ground-state of the unperturbed hamiltonian.
Moments satisfy some general inequalities. Different moments of the same dynamic stricture factor must obey the inequality

$$\frac{m_{p+1}(F)}{m_p(F)} \geq \frac{m_p(F)}{m_{p-1}(F)} \tag{B.16}$$

another useful inequality is

$$\hbar\omega_{\min} \leq \frac{m_{p+1}(F)}{m_p(F)} \tag{B.17}$$

where $\hbar\omega_{\min}$ is the lowest energy mode excited by the operator F. The inequality allows us to place an upper bound on the energy the lower state excited by the perturbation.
In the case that the perturbation excites just one state , the inequalities transform into equalities. In general if only one state between the low energy states gives a significant contribution to the dynamic structure factor the upper bound will give a very good approximation to the excited state energy

$$\hbar\omega_{\min} \approx \frac{m_{p+1}(F)}{m_p(F)} \tag{B.18}$$

B.0.3 Density response

Let us apply the linear response theory to the operator

$$F(k) = \rho_k = \sum_i e^{-ikx_i} = \int n(x) e^{-ikx} dx \tag{B.19}$$

where $n(x)$ is the density operator

$$n(x) = \sum_{i=1}^{N} \delta(x - x_i) \tag{B.20}$$

$F(k)$ is proportional to the k component of the dynamic structure factor and can be seen as an operator exciting spatial density oscillations with wavenumber k. In a homogeneous system the average value $\langle F \rangle$ is zero. However its fluctuations are finite and , exploiting the relation B.12 one obtains

$$m_0(F) = NS(q) = \left\langle \left| \rho_k \right|^2 \right\rangle \tag{B.21}$$

where $S(q)$ is the static structure factor 1.18. another interesting moment is the m_1 moment. By using relation B.14 one can easily derive the formula

$$m_1(k) = N\frac{\hbar^2 k^2}{2m} \tag{B.22}$$

also known as the *f-sum* rule , which no longer depends on the hamiltonian of the system, but just on the momentum of the excitation operator. We can use the disequalities above to place an upper bound on the dispersion of the static structure factor S(q). Using the disequalities

$$\frac{m_0}{m_{-1}} \leq \frac{m_1}{m_0} \tag{B.23}$$

one gets the condition

$$S(q) \leq \sqrt{\frac{\hbar^2 q^2 \chi(q)}{4m}} \tag{B.24}$$

which puts an upper limit on the dispersion of the static structure factor. In the limit $q \to 0$ the response function tends to the compressibility and one obtains the low-q behaviour

$$S(q) \leq \frac{\hbar q}{2}\sqrt{\frac{K}{m}} \tag{B.25}$$

One may estimate the energy of the excitation $\hbar\omega(q)$ using the inequality

$$\hbar\omega(k) \leq \frac{m_1(k)}{m_0(k)} = cq \tag{B.26}$$

where

$$c = \sqrt{\frac{1}{mK}} \tag{B.27}$$

When the inequality becomes an equality, c can be interpreted as the speed of sound. In this case the speed of phonons is entirely determined from the compressibility of the system.

Bibliography

[1] Belén Paredes et al , Nature volume 429, pages 277–281 (20 May 2004)

[2] J. Catani at al, Quantum dynamics of impurities in a 1D Bose gas, Phys. Rev. A 85, 023623 (2012)

[3] Quantum liquid droplets in a mixture of Bose-Einstein condensates, Science 359, 301 (2018)

[4] Self-Bound Quantum Droplets of Atomic Mixtures in Free Space,G. Semeghini et al, Phys. Rev. Lett. 120, 235301 – Published 7 June 2018

[5] Lieb, E. H. , Liniger, W. Exact analysis of an interacting Bose gas. The general solution and the ground state. Phys. Rev. 130, 1605–1616 (1963)

[6] X.-W. Guan, M. T. Batchelor, and C. Lee, Reviews of Modern Physics 85, 1633 (2013).

[7] Girardeau, M. Relationship between systems of impenetrable bosons and fermions in one dimension. J. Math. Phys. 1, 516–523 (1960)

[8] C. N. Yang, Phys. Rev. Lett. **19**, 1312 (1967).

[9] M. Gaudin, Phys. Lett. **24A**, 55 (1967).

[10] L. D. Landau and S. I. Pekar, Effective mass of a polaron, Zh. Eksp. Teor. Fiz. 18, 419–423 (1948)

[11] L. A. Peña Ardila, S. Giorgini Phys. Rev. A 92, 033612 (2015)

[12] Rasmus Søgaard Christensen, Jesper Levinsen, and Georg M. Bruun. Quasiparticle properties of a mobile impurity in a bose-einstein condensate. *Phys. Rev. Lett.*, 115:160401, Oct 2015.

[13] Steffen Patrick Rath and Richard Schmidt. Field-theoretical study of the bose polaron. *Phys. Rev. A*, 88:053632, Nov 2013.

[14] Yulia E. Shchadilova, Richard Schmidt, Fabian Grusdt, and Eugene Demler. Quantum dynamics of ultracold bose polarons. *Phys. Rev. Lett.*, 117:113002, Sep 2016.

[15] Jesper Levinsen, Meera M. Parish, and Georg M. Bruun. Impurity in a bose-einstein condensate and the efimov effect. *Phys. Rev. Lett.*, 115:125302, Sep 2015.

[16] Ming-Guang Hu, Michael J. Van de Graaff, Dhruv Kedar, John P. Corson, Eric A. Cornell, and Deborah S. Jin. Bose polarons in the strongly interacting regime. *Phys. Rev. Lett.*, 117:055301, Jul 2016.

[17] Nils B. Jørgensen, Lars Wacker, Kristoffer T. Skalmstang, Meera M. Parish, Jesper Levinsen, Rasmus S. Christensen, Georg M. Bruun, and Jan J. Arlt. Observation of attractive and repulsive polarons in a bose-einstein condensate. *Phys. Rev. Lett.*, 117:055302, Jul 2016.

[18] L. A. Peña Ardila and S. Giorgini. Bose polaron problem: Effect of mass imbalance on binding energy. *Phys. Rev. A*, 94:063640, Dec 2016.

[19] S. Ospelkaus, C. Ospelkaus, O. Wille, M. Succo, P. Ernst, K. Sengstock, and K. Bongs. Localization of bosonic atoms by fermionic impurities in a three-dimensional optical lattice. *Phys. Rev. Lett.*, 96:180403, May 2006.

[20] J. B. McGuire, J. Math. Phys. **6**, 432 (1965).

[21] J. B. McGuire, J. Math. Phys. **7**, 123 (1966).

[22] J. Catani, G. Lamporesi, D. Naik, M. Gring, M. Inguscio, F. Minardi, A. Kantian, and T. Giamarchi, Phys. Rev. A **85**, 023623 (2012).

[23] Axel Freyn and Serge Florens. Numerical renormalization group at marginal spectral density: Application to tunneling in luttinger liquids. *Phys. Rev. Lett.*, 107:017201, Jun 2011.

[24] V. Meden, W. Metzner, U. Schollwöck, and K. Schönhammer. Scaling behavior of impurities in mesoscopic luttinger liquids. *Phys. Rev. B*, 65:045318, Jan 2002.

[25] A. Kantian, U. Schollwöck, and T. Giamarchi. Competing regimes of motion of 1d mobile impurities. *Phys. Rev. Lett.*, 113:070601, Aug 2014.

[26] L. Parisi and S. Giorgini. Quantum monte carlo study of the bose-polaron problem in a one-dimensional gas with contact interactions. *Phys. Rev. A*, 95:023619, Feb 2017.

[27] A. F. Andreev and E. P. Bashkin, "Three velocity hydrodynamics of superfluid solutions," Sov. Phys.-JETP 42, 164–167 (1976).

[28] L. Parisi, G. E. Astrakharchik, and S. Giorgini. Spin dynamics and andreev-bashkin effect in mixtures of one-dimensional bose gases. *Phys. Rev. Lett.*, 121:025302, Jul 2018.

[29] D. S. Petrov, G. E. Astrakharchik, Phys. Rev. Lett. 117, 100401 (2016)

[30] L. Parisi, G. E. Astrakharchik, and S. Giorgini. Liquid state of one-dimensional bose mixtures: A quantum monte carlo study. *Phys. Rev. Lett.*, 122:105302, Mar 2019.

[31] Bose-Einstein Condensation,Lev. P. Pitaevskii and Sandro Stringari, International Series of Monographs on Physics,ISBN: 9780198507192

[32] J. J. Sakurai and Jim Napolitano. *Modern Quantum Mechanics*. Cambridge University Press, 2 edition, 2017.

[33] G. D. Mahan. *Many Particle Physics, Third Edition*. Plenum, New York, 2000.

[34] Thierry Giamarchi. *Quantum Physics in One Dimension*. Oxford University Press, New York, 2003.

[35] E. H. Lieb and W. Liniger, Phys. Rev. **130**, 1605 (1963).

[36] M. Girardeau, J. Math. Phys. (N. Y.) **1**, 516 (1960).

[37] G E Astrakharchik and S Giorgini. Correlation functions of a lieb–liniger bose gas. *Journal of Physics B: Atomic, Molecular and Optical Physics*, 39(10):S1–S12, may 2006.

[38] C. F. Coll, Phys. Rev. B **9**, 2150 (1974).

[39] M. T. Batchelor, M. Bortz, X.-W. Guan, and N. Oelkers, J. Phys.: Conf. Ser. **42**, 5 (2006).

[40] P. KAPITZA. Viscosity of liquid helium below the λ-point. *Nature*, 74, 1938.

[41] K.B. Davis, M.-O. Mewes, M.R. Andrews, N.J. van Druten, D.S. Durfee, D.M. Kurn, and W. Ketterle ,"Bose-Einstein condensation in a gas of sodium atoms", Phys. Rev. Lett. 75, 3969 (1995)

[42] Observation of Bose-Einstein Condensation in a Dilute Atomic Vapor,M. H. Anderson1, J. R. Ensher1, M. R. Matthews1, C. E. Wieman1, E. A. Cornell

[43] A.L. Migdall, J.V. Prodan, W.D. Philips, T.H. Bergeman, H.J. Metcalf, Phys. Rev. Lett., 54

[44] Ketterle, Wolfgang; Van Druten, N. J. (1996). "Evaporative cooling of trapped atoms". Advances in atomic, molecular, and optical physics. 37: 181–236.

[45] Three-Body Recombination at Large Scattering Lengths in an Ultracold Atomic Gas ,Weber, Tino and Herbig, Jens and Mark, Michael and N' agerl, Hanns-Christoph and Grimm, Rudolf, PhysRevLett.91.123201

[46] Chin, Cheng; Grimm, Rudolf; Julienne, Paul; Tiesinga, Eite (2010-04-29). "Feshbach resonances in ultracold gases"

[47] M. Olshanii. Atomic scattering in the presence of an external confinement and a gas of impenetrable bosons. *Phys. Rev. Lett.*, 81:938–941, Aug 1998.

[48] Tonks–Girardeau gas of ultracold atoms in an optical lattice; Belén Paredes, Artur Widera, Valentin Murg, Olaf Mandel, Simon Fölling, Ignacio Cirac, Gora V. Shlyapnikov, Theodor W. Hänsch , Immanuel Bloch; Tonks–Girardeau gas of ultracold atoms in an optical lattice, Nature volume 429, pages 277–281 (20 May 2004)

[49] F. Meinert, M. Panfil, M. J. Mark, K. Lauber, J.-S. Caux, and H.-C. Nägerl. Probing the excitations of a lieb-liniger gas from weak to strong coupling. *Phys. Rev. Lett.*, 115:085301, Aug 2015.

[50] Elmar Haller, Mattias Gustavsson, Manfred J. Mark, Johann G. Danzl, Russell Hart, Guido Pupillo, and Hanns-Christoph Nägerl. Realization of an excited, strongly correlated quantum gas phase. *Science*, 325(5945):1224–1227, 2009.

[51] Toshiya Kinoshita, Trevor Wenger, and David S. Weiss. Observation of a one-dimensional tonks-girardeau gas. *Science*, 305(5687):1125–1128, 2004.

[52] Federico Becca and Sandro Sorella. *Quantum Monte Carlo Approaches for Correlated Systems*. Cambridge University Press, 2017.

[53] David Landau and Kurt Binder. *A Guide to Monte Carlo Simulations in Statistical Physics*. Cambridge University Press, New York, NY, USA, 2005.

[54] Robert Jastrow. Many-body problem with strong forces. *Phys. Rev.*, 98:1479–1484, Jun 1955.

[55] W. M. C. Foulkes, L. Mitas, R. J. Needs, and G. Rajagopal. Quantum monte carlo simulations of solids. *Rev. Mod. Phys.*, 73:33–83, Jan 2001.

[56] Giuseppe Carleo, Lorenzo Cevolani, Laurent Sanchez-Palencia, and Markus Holzmann. Unitary dynamics of strongly interacting bose gases with the time-dependent variational monte carlo method in continuous space. *Phys. Rev. X*, 7:031026, Aug 2017.

[57] M. Holzmann, D. M. Ceperley, C. Pierleoni, and K. Esler. Backflow correlations for the electron gas and metallic hydrogen. *Phys. Rev. E*, 68:046707, Oct 2003.

[58] Optimization of quantum Monte Carlo wave functions by energy minimization , Julien Toulouse, and C. J. Umrigar, J. Chem. Phys. 126, 084102 (2007);

[59] Sandro Sorella. Generalized lanczos algorithm for variational quantum monte carlo. *Phys. Rev. B*, 64:024512, Jun 2001.

[60] Julien Toulouse and C. J. Umrigar. Optimization of quantum monte carlo wave functions by energy minimization. *The Journal of Chemical Physics*, 126(8):084102, 2007.

[61] P. Massignan, M. Zaccanti, and G. M. Bruun, Rep. Prog. Phys. **77**, 034401 (2014).

[62] N. B. Jørgensen, L. Wacker, K. T. Skalmstang, M. M. Parish, J. Levinsen, R. S. Christensen, G. M. Bruun, and J. J. Arlt, Phys. Rev. Lett. **117**, 055302 (2016).

[63] M.G. Hu, M. J. Van de Graaf, D. Kedar, J. P. Corson, E. A. Cornell, and D. S. Jin, Phys. Rev. Lett. **117**, 055301 (2016).

[64] N. Spethmann, F. Kindermann, S. John, C. Weber, D. Meschede, and A. Widera, Phys. Rev. Lett. 109, 235301 (2012).

[65] J. Catani, G. Lamporesi, D. Naik, M. Gring, M. Inguscio, F. Minardi, A. Kantian, and T. Giamarchi, Phys. Rev. A **85**, 023623 (2012).

[66] R. Scelle, T. Rentrop, A. Trautmann, T. Schuster, and M. K. Oberthaler, Phys. Rev. Lett. **111**, 070401 (2013).

[67] S. P. Rath and R. Schmidt, Phys. Rev. A **88**, 053632 (2013).

[68] R. S. Christensen, J. Levinsen, and G. M. Bruun, Phys. Rev. Lett. **115**, 160401 (2015).

[69] Weiran Li and S. Das Sarma, Phys. Rev. A **90**, 013618 (2014).

[70] J. Levinsen, M. M. Parish, and G. M. Bruun, Phys. Rev. Lett. **115**, 125302 (2015).

[71] L. A. Peña Ardila and S. Giorgini, Phys. Rev. A **92**, 033612 (2015).

[72] L. A. Peña Ardila and S. Giorgini, Phys. Rev. A **94**, 063640 (2016).

[73] T. Stöferle, H. Moritz, C. Schori, Michael Köhl, and T. Esslinger, Phys. Rev. Lett. **92**, 130403 (2004).

[74] B. Paredes, A. Widera, V. Murg, O. Mandel, S. Fölling, I. Cirac, G. V. Shlyapnikov, T. W. Hänsch, and I. Bloch, Nature (London) **429**, 277 (2004).

[75] T. Kinoshita, T. Wenger, and D. S. Weiss, Science **305**, 1125 (2004).

[76] E. Haller, M. Gustavsson, M. J. Mark, J. G. Danzl, R. Hart, G. Pupillo, and H.-C. Nägerl, Science **325**, 1224 (2009).

[77] M. Olshanii, Phys. Rev. Lett. **81**, 938 (1998).

[78] Florian Meinert, Michael Knap, Emil Kirilov, Katharina Jag-Lauber, Mikhail B. Zvonarev, Eugene Demler, and Hanns-Christoph Nägerl. Bloch oscillations in the absence of a lattice. *Science*, 356(6341):945–948, 2017.

[79] Florian Meinert, Michael Knap, Emil Kirilov, Katharina Jag-Lauber, Mikhail B. Zvonarev, Eugene Demler, and Hanns-Christoph Nägerl. Bloch oscillations in the absence of a lattice. *Science*, 356(6341):945–948, 2017.

[80] B. Paredes, A. Widera, V. Murg, O. Mandel, S. Fölling, I. Cirac, G. V. Shlyapnikov, T. W. Hänsch, and I. Bloch, Nature (London) **429**, 277 (2004).

[81] L. D. Landau and S. I. Pekar, Zh. Eksp. Teor. Fiz. **18**, 419 (1948).

[82] F. M. Cucchietti and E. Timmermans, Phys. Rev. Lett. **96**, 210401 (2006).

[83] R. M. Kalas and D. Blume, Phys. Rev. A **73**, 043608 (2006).

[84] M. Bruderer, W. Bao, and D. Jaksch, Eur. Phys. Lett. **82**, 30004 (2008).

[85] J.Tempere, W. Casteels, M. K.Oberthaler, S.Knoop, E. Timmermans, and J. T. Devreese, Phys. Rev. B **80**, 184504 (2009).

[86] L. A. Peña Ardila and S. Giorgini, Phys. Rev. A **92**, 033612 (2015).

[87] A. Schirotzek, C.-H. Wu, A. Sommer, and M. W. Zwierlein, Phys. Rev. Lett. **102**, 230402 (2009).

[88] C. Kohstall, M. Zaccanti, M. Jag, A. Trenkwalder, P. Massignan, G. M. Bruun, F. Schreck, and R. Grimm, Nature **485**, 615 (2012).

[89] M. Koschorreck, D. Pertot, E. Vogt, B. Fröhlich, M. Feld, and M. Köhl, Nature **485**, 619 (2012).

[90] N. B. Jørgensen, L. Wacker, K. T. Skalmstang, M. M. Parish, J. Levinsen, R. S. Christensen, G. M. Bruun, and J. J. Arlt, Phys. Rev. Lett. **117**, 055302 (2016).

[91] F. Scazza, G. Valtolina, P. Massignan, A. Recati, A. Amico, A. Burchianti, C. Fort, M. Inguscio, M. Zaccanti, and G. Roati. Repulsive fermi polarons in a resonant mixture of ultracold ^{6}Li atoms. *Phys. Rev. Lett.*, 118:083602, Feb 2017.

[92] S. Nascimbene, N. Navon, K. J. Jiang, L. Tarruell, M. Teichmann, J. McKeever, F. Chevy, and C. Salomon, Phys. Rev. Lett. **103**, 170402 (2009).

[93] See, *e. g.*, D. M. Gangardt and G. V. Shlyapnikov, Phys. Rev. Lett. **90**, 010401 (2003).

[94] Shina Tan. Energetics of a strongly correlated fermi gas. *Annals of Physics*, 323(12):2952 – 2970, 2008.

[95] Edward Taylor and Mohit Randeria. Viscosity of strongly interacting quantum fluids: Spectral functions and sum rules. *Phys. Rev. A*, 81:053610, May 2010.

[96] L. A. Peña Ardila and S. Giorgini, Phys. Rev. A **94**, 063640 (2016).

[97] A. Camacho-Guardian, L. A. Peña Ardila, T. Pohl, and G. M. Bruun. Bipolarons in a bose-einstein condensate. *Phys. Rev. Lett.*, 121:013401, Jul 2018.

[98] A. Camacho-Guardian and Georg M. Bruun. Landau effective interaction between quasiparticles in a bose-einstein condensate. *Phys. Rev. X*, 8:031042, Aug 2018.

[99] A. S. Dehkharghani, A. G. Volosniev, and N. T. Zinner. Coalescence of two impurities in a trapped one-dimensional bose gas. *Phys. Rev. Lett.*, 121:080405, Aug 2018.

[100] E. Sonin, Advances in Physics **59**, 181 (2010).

[101] A. Sommer, M. Ku, G. Roati, and M. W. Zwierlein, Nature **7342**, 201 (2011).

[102] A. B. Bardon, S. Beattie, C. Luciuk, W. Cairncross, D. Fine, N. S. Cheng, G. J. A. Edge, E. Taylor, S. Zhang, S. Trotzky, and J. H. Thywissen, Science **344**, 722 (2014).

[103] G. Valtolina, F. Scazza, A. Amico, A. Burchianti, A. Recati, T. Enss, M. Inguscio, M. Zaccanti, and G. Roati, Nat. Phys. **13**, 704 (2017).

[104] G. Modugno, M. Modugno, F. Riboli, G. Roati, and M. Inguscio, Phys. Rev. Lett. **89**, 190404 (2002).

[105] K. M. Mertes, J. W. Merrill, R. Carretero-González, D. J. Frantzeskakis, P. G. Kevrekidis, and D. S. Hall, Phys. Rev. Lett. **99**, 190402 (2007).

[106] E. Nicklas, H. Strobel, T. Zibold, C. Gross, B. A. Malomed, P. G. Kevrekidis, and M. K. Oberthaler, Phys. Rev. Lett. **107**, 193001 (2011).

[107] Jin-Yi Zhang, Si-Cong Ji, Zhu Chen, Long Zhang, Zhi-Dong Du, Bo Yan, Ge-Sheng Pan, Bo Zhao, You-Jin Deng, Hui Zhai, Shuai Chen, and Jian-Wei Pan, Phys. Rev. Lett. **109**, 115301 (2012).

[108] M. Egorov, B. Opanchuk, P. Drummond, B. V. Hall, P. Hannaford, and A. I. Sidorov, Phys. Rev. A **87**, 053614 (2013).

[109] T. Bienaimé, E. Fava, G. Colzi,C. Mordini, S. Serafini, C. Qu, S. Stringari, G. Lamporesi, and G. Ferrari, Phys. Rev. A **94**, 063652 (2016).

[110] Eleonora Fava, Tom Bienaimé, Carmelo Mordini, Giacomo Colzi, Chunlei Qu, Sandro Stringari, Giacomo Lamporesi, and Gabriele Ferrari. Observation of spin superfluidity in a bose gas mixture. *Phys. Rev. Lett.*, 120:170401, Apr 2018.

[111] See, *e.g.*, J. Voit, Rep. Prog. Phys. **57**, 977 (1994).

[112] A. Recati, P. O. Fedichev, W. Zwerger, and P. Zoller, Phys. Rev. Lett. **90**, 020401 (2003).

[113] A. Recati, P. O. Fedichev, W. Zwerger, and P. Zoller, J. Opt. B **5**, S55 (2003).

[114] A. F. Andreev and E. P. Bashkin, Sov. Phys. JETP **42**, 164 (1975).

[115] See, for instance, G. Ahlers in *The Physics of Liquid and Solid Helium*, Part I, edited by K. H. Benneman and J. B. Ketterson (Wiley, New York, 1976).

[116] D. V. Fil and S. I. Shevchenko, Phys. Rev. A **72**, 013616 (2005).

[117] V. M. Kaurov, A. B. Kuklov, and A. E. Meyerovich, Phys. Rev. Lett. **95**, 090403 (2005).

[118] J. Nespolo, G. E. Astrakharchik, and A. Recati, New J. Phys. **19**, 125005 (2017).

[119] Y.-Q. Li, S.-J. Gu, Z.-J. Ying, and U. Eckern, Europhys. Lett. **61**, 368 (2003).

[120] K. Yang and Y.-Q. Li, Int. J. Mod. Phys. B **17**, 1027 (2003).

[121] L. Pitaevskii and S. Stringari, *Bose-Einstein Condensation and Superfluidity* (Oxford University Press, 2016), Sec. 21.1.

[122] The instability is triggered by long-wavelength fluctuations of the magnetization density which are inhibited in our finite-size simulations. This allows us for a reliable determination of the equation of state in the metastable regime at least when $\tilde{g}$ is only slightly larger than g.

[123] H. Shiba, Phys. Rev. B **6**, 930 (1972).

[124] Xi-Wen Guan and Zhong-Qi Ma, Phys. Rev. B **85**, 033632 (2012).

[125] We solve the coupled integral equations of the Yang-Gaudin model for polarizations $P \gtrsim 10^{-3}$ and we thereby determine the susceptibility χ at small but still finite polarization. Due to logarithmic singularities the calculation of χ at zero polarization would require much smaller values of P which can not be reproduced by our numerical methods and are most likely experimentally irrelevant. We notice that this zero-polarization susceptibility satisfies the exact relation [38] $\chi v_s = \frac{2}{\hbar\pi}$ in terms of the spin velocity v_s and differs from the one shown in Fig. 5.7.

[126] D. Pines and P. Nozieres, *Theory of Quantum Liquids* (Benjamin, New York, 1966), Vol. 1.

[127] F. Dalfovo and S. Stringari, Phys. Rev. Lett. **63**, 532 (1989).

[128] We notice that the energy-weighted moment (f-sum rule) $m_1 = N\frac{\hbar^2 q^2}{2m}$ is not exhausted at low momenta by the spin-wave excitation. In fact, its contribution to the sum rule is suppressed by the drag effect and is given by $(m_1)_{\rm sw} = m_1(1 - \frac{4\rho_D}{\rho})$.

[129] M. T. Batchelor, M. Bortz, X.-W. Guan, and N. Oelkers, J. Phys.: Conf. Ser. **42**, 5 (2006).

[130] Lauriane Chomaz, Laura Corman, Tom Bienaimé, Rémi Desbuquois, Christof Weitenberg, Sylvain Nascimbène, Jérôme Beugnon, and Jean Dalibard. Emergence of coherence via transverse condensation in a uniform quasi-two-dimensional bose gas. *Nature Communications*, 6:6162, 2015.

[131] Giulia De Rosi and Sandro Stringari. Collective oscillations of a trapped quantum gas in low dimensions. *Phys. Rev. A*, 92:053617, Nov 2015.

[132] A Sartori, J Marino, S Stringari, and A Recati. Spin-dipole oscillation and relaxation of coherently coupled bose–einstein condensates. *New Journal of Physics*, 17(9):093036, sep 2015.

[133] Tom Bienaimé, Eleonora Fava, Giacomo Colzi, Carmelo Mordini, Simone Serafini, Chunlei Qu, Sandro Stringari, Giacomo Lamporesi, and Gabriele Ferrari. Spin-dipole oscillation and polarizability of a binary bose-einstein condensate near the miscible-immiscible phase transition. *Phys. Rev. A*, 94:063652, Dec 2016.

[134] Chiara Menotti and Sandro Stringari. Collective oscillations of a one-dimensional trapped bose-einstein gas. *Phys. Rev. A*, 66:043610, Oct 2002.

[135] Liming Guan and Shu Chen. Super-tonks-girardeau gas of spin-1/2 interacting fermions. *Phys. Rev. Lett.*, 105:175301, Oct 2010.

[136] Alessio Recati and Sandro Stringari. Spin fluctuations, susceptibility, and the dipole oscillation of a nearly ferromagnetic fermi gas. *Phys. Rev. Lett.*, 106:080402, Feb 2011.

[137] D. S. Petrov, G. V. Shlyapnikov, and J. T. M. Walraven. Regimes of quantum degeneracy in trapped 1d gases. *Phys. Rev. Lett.*, 85:3745–3749, Oct 2000.

[138] A. Iu. Gudyma, G. E. Astrakharchik, and Mikhail B. Zvonarev. Reentrant behavior of the breathing-mode-oscillation frequency in a one-dimensional bose gas. *Phys. Rev. A*, 92:021601, Aug 2015.

[139] B. Rauer, P. Grišins, I. E. Mazets, T. Schweigler, W. Rohringer, R. Geiger, T. Langen, and J. Schmiedmayer. Cooling of a one-dimensional bose gas. *Phys. Rev. Lett.*, 116:030402, Jan 2016.

[140] I. Ferrier-Barbut, H. Kadau, M. Schmitt, M. Wenzel, and T. Pfau, Phys. Rev. Lett. **116**, 215301 (2016).

[141] M. Schmitt, M. Wenzel, F. Böttcher, I. Ferrier-Barbut, and T. Pfau, Nature **539**, 259 (2016).

[142] I. Ferrier-Barbut, M. Schmitt, M. Wenzel, H. Kadau, and T. Pfau, J. Phys. B **49**, 214004 (2016).

[143] Igor Ferrier-Barbut, Matthias Wenzel, Fabian Böttcher, Tim Langen, Mathieu Isoard, Sandro Stringari, and Tilman Pfau. Scissors mode of dipolar quantum droplets of dysprosium atoms. *Phys. Rev. Lett.*, 120:160402, Apr 2018.

[144] L. Chomaz, S. Baier, D. Petter, M. J. Mark, F. Wächtler, L. Santos, and F. Ferlaino, Phys. Rev. X **6**, 041039 (2016).

[145] C. R. Cabrera, L. Tanzi, J. Sanz, B. Naylor, P. Thomas, P. Cheiney, and L. Tarruell, Science **359**, 301 (2018).

[146] P. Cheiney, C. R. Cabrera, J. Sanz, B. Naylor, L. Tanzi, and L. Tarruell, Phys. Rev. Lett. **120**, 135301 (2018).

[147] G. Semeghini, G. Ferioli, L. Masi, C. Mazzinghi, L. Wolswijk, F. Minardi, M. Modugno, G. Modugno, M. Inguscio, and M. Fattori. Self-bound quantum droplets of atomic mixtures in free space. *Phys. Rev. Lett.*, 120:235301, Jun 2018.

[148] F. Wächtler and L. Santos, Phys. Rev. A **93**, 061603(R) (2016).

[149] A. Macia, J. Sánchez-Baena, J. Boronat, and F. Mazzanti, Phys. Rev. Lett. **117**, 205301 (2016).

[150] D. S. Petrov, Phys. Rev. Lett. **115**, 155302 (2015).

[151] V. Cikojević, K. Dželalija, P. Stipanović, L. Vranješ Markić, and J. Boronat, Phys. Rev. B **97**, 140502 (2018).

[152] D. S. Petrov and G. E. Astrakharchik, Phys. Rev. Lett. **117**, 100401 (2016).

[153] B. L. Hammond, W. A. Lester Jr., and P. J. Reynolds, *Monte Carlo Methods in Ab Initio Quantum Chemistry*, World Scientific (Singapore, 1994).

[154] A. Pricoupenko and D. S. Petrov, Phys. Rev. A **97**, 063616 (2018).

[155] G. Guijarro, A. Pricoupenko, G. E. Astrakharchik, J. Boronat, and D. S. Petrov, Phys. Rev. A **97**, 061605(R) (2018).

[156] Clemens Staudinger, Ferran Mazzanti, and Robert E. Zillich. Self-bound bose mixtures. *Phys. Rev. A*, 98:023633, Aug 2018.

[157] A pairing gap is present in the exactly solvable Yang-Gaudin model corresponding to $\gamma = \infty$, see for example X.-W. Guan, M. T. Batchelor, and C. Lee, Rev. Mod. Phys. **85**, 1633 (2013). A similar physics is expected to occur also for finite values of γ.

[158] Notice that the result for $S_M(q)$ holds at weak coupling where one neglects the renormalization of the velocity of spin waves caused by the superfluid drag density, see L. Parisi, G. E. Astrakharchik, and S. Giorgini, Phys. Rev. Lett. **121**, 025302 (2018).

[159] A. Lenard, J. Math. Phys. **5**, 930 (1964).

[160] V. Cikojević, K. Dželalija, P. Stipanović, L. Vranješ Markić, and J. Boronat. Ultradilute quantum liquid drops. *Phys. Rev. B*, 97:140502, Apr 2018.

[161] G. E. Astrakharchik and B. A. Malomed. Dynamics of one-dimensional quantum droplets. *Phys. Rev. A*, 98:013631, Jul 2018.

[162] Lin Y.-J., Jiménez-García K., and Spielman I. B. A spin-orbit coupled bose-einstein condensate. *Nature*, 471:83, 2011.

[163] Victor Galitski and Ian B. Spielman. Spin–orbit coupling in quantum gases. *Nature*, 494:49, 2016.

[164] Yun Li, Lev P. Pitaevskii, and Sandro Stringari. Quantum tricriticality and phase transitions in spin-orbit coupled bose-einstein condensates. *Phys. Rev. Lett.*, 108:225301, May 2012.

[165] Cody A. Melton, Minyi Zhu, Shi Guo, Alberto Ambrosetti, Francesco Pederiva, and Lubos Mitas. Spin-orbit interactions in electronic structure quantum monte carlo methods. *Phys. Rev. A*, 93:042502, Apr 2016.

[166] J. Sánchez-Baena, J. Boronat, and F. Mazzanti. Diffusion monte carlo methods for spin-orbit-coupled ultracold bose gases. *Phys. Rev. A*, 98:053632, Nov 2018.